Øyvind Borck

Adsorption of organic molecules at surfaces: A first-principles investigtion

Doktoravhandling
for graden doktor ingeniør

Trondheim, mai 2006

Norges teknisk-naturvitenskapelige universitet
Fakultet for naturvitenskap og teknologi
Institutt for fysikk

NTNU
Det skapende universitet

NTNU
Norges teknisk-naturvitenskapelige universitet

Doktoravhandling
for graden doktor ingeniør

Fakultet for naturvitenskap og teknologi
Institutt for fysikk

ISBN 82-471-7914-8 (trykt utg.)
ISBN 82-471-7912-1 (elektr utg.)
ISSN 1503-8181

Doktoravhandlinger ved NTNU, 2006:81

Trykt av Tapir Uttrykk

Adsorption of organic molecules at surfaces: A first-principles investigation

Øyvind Borck

A thesis submitted in the partial fullfilment
of the requirements for the degree

Doktor Ingeniør

Department of Physics
Norwegian University of Science and Technology
Trondheim, Norway

May 2006

Abstract

The adsorption of a molecule at a surface is a fundamental step in a wide variety of industrially relevant phenomena, including adhesion, corrosion, and catalysis. The work presented in this thesis is motivated by the desire to contribute to a better understanding of the factors affecting the adhesion between an organic coating/adhesive and an aluminium alloy surface. A key factor is the nature and strength of the interfacial bonds between the binder polymers of the organic coating/adhesive and the substrate. The size of the polymers and complexity of the polymer-substrate interactions preclude a detailed, atomic-level description. The strategy followed in this thesis is to study the adsorption of small organic molecules, representing fragments of the industrially relevant amine-cured epoxides, with various surfaces, of metal oxides (α-Al_2O_3(0001) and α-Cr_2O_3(0001)), bimetallic alloys (NiAl(110)), and graphite(0001).

This thesis consists of two parts, an introductory text and a collection of five papers. In the included papers we present results from density functional theory (DFT) calculations on the adsorption of methanol and methylamine on α-Al_2O_3(0001) and α-Cr_2O_3(0001), phenol on α-Al_2O_3(0001) and graphite(0001), and methoxy on α-Cr_2O_3(0001) and NiAl(110). We describe in detail the adsorption sites and geometry, and the nature and strength of the bonding at these surfaces.

The majority of adsorption systems considered in this thesis are well described by traditional implementations of DFT. However, the adsorption of phenol on graphite is predominantly governed by van der Waals interactions. These interactions requires approximations beyond traditional DFT. In this thesis a recently presented functional (vdW-DF) is employed, and is found to be of decisive importance for describing the phenol-graphite interactions. We calculate the contribution from vdW interactions to the adsorption of phenol on α-Al_2O_3(0001), and compare their contribution to the adsorption bond to other forces.

Acknowledgements

The work presented in this thesis was carried out at the Department of Physics, NTNU, and the Materials and Surface Theory group of the Department of Applied Physics at Chalmers University of Technology in Gothenburg. The work was partly carried out within *Light Metal Surface Science* (LMSS), a joint project between SINTEF and NTNU, financed by The Norwegian Research Council (NFR), Hydro Aluminium, Profillakkering AS, Norsk Industrilakkering AS, Fundamus AS, Jotun Powder Coatings AS, and DuPont Powder Coating. Additional financial support provided by NorFA (now NordForsk), the Department of Physics, NTNU, and Chalmers University of Technology is gratefully acknowledged.

I would like to thank my supervisor Anne Borg for encouragement, moral support, and good advice during the years spent on this thesis. I have had the good fortune to visit and work in the Materials and Surface Theory group at Chalmers over extended periods of time during these years. I would like to thank all my friends and collaborators in this group. I am especially grateful to my DFT advisors and co-authors Elsebeth Schröder and Bengt I. Lundqvist, co-authors Per Hyldgaard and Svetla D. Chakarova-Käck, and, for social support, Jesper Kleis.

I am grateful to my fellow participants in the LMSS-project for showing genuine interest in my work, even though it seems far removed from the practical problems of the aluminium industry.

I would also like to thank my colleagues in the surface physics group at the Department of physics, NTNU, for creating such a pleasant work environment. Terje Røsten is gratefully acknowledged for constant computer support.

En spesiell takk til mine foreldre og søsken for all støtte, og for (nødvendige) distraksjoner fra arbeidet mitt.

Trondheim, May 2006

Øyvind Borck

List of papers

The papers included in this thesis are:

Paper I First-principles study of the adsorption of methanol at the α-Al_2O_3(0001) surface
Ø. Borck and E. Schröder
J. Phys.: Condens. Matter **18** (2006) 1.

Paper II Adsorption of methanol and methoxy on the α-Cr_2O_3(0001) surface
Ø. Borck and E. Schröder
Preprint 2006

Paper III Adsorption of methylamine on α-Al_2O_3(0001) and α-Cr_2O_3(0001)
Ø. Borck, P. Hyldgaard, and E. Schröder
Preprint 2006

Paper IV Phenol adsorption on graphite and aluminum oxide
S. D. Chakarova-Käck, Ø. Borck, E. Schröder, and B. I. Lundqvist
Preprint 2006

Paper V Density functional theory investigation of methoxy on NiAl(110)
Ø. Borck, H. Dalaker, and K. Mo
Preprint 2006

Specification of my contribution to the included papers:

Papers I-III All calculations were performed by me. The papers were written jointly.

Paper IV I performed the *traditional*, i.e. not including van der Waals interactions, GGA-DFT calculations of phenol on α-Al_2O_3(0001). All other calculations were performed by Svetla D. Chakarova-Käck. The paper was written jointly.

Paper V The calculations were done by me based on earlier work by H. Dalaker and K. Mo. The paper was written by me.

Scientific publication not included in this thesis:

- Adsorption of methanol on aluminium oxide: A density functional study
  Ø. Borck and E. Schröder
  ATB Metallurgie **43** (2003) 342.

Contents

Part I

Introduction

Chapter 1

Introduction

1.1 Motivation

Aluminium alloy products are found everywhere: They are used for food packaging, kitchen utensils, building decorations, bicycle frames, laptop casings, and car components, to give just a few examples. In many applications components of aluminium alloys are adhesively bonded, painted, or lacquered. To achieve a durable result aluminium alloys are usually given some form of surface pre-treatment to enhance adhesion [1, 2].

One commonly used pre-treatment is to make a chromate conversion coating [1]. This is a chemical process where an amorphous passive layer of chromium oxide is formed on the aluminium alloy surface by means of a treatment with an aqueous acidic solution containing chromium salts. The composition of chromate conversion coatings has been reported to be mainly amorphous chromium oxide, but the detailed structure and composition depend on factors such as the chemical composition of the coating solution, preceding chemical treatment, and the composition of the aluminium alloy, see [3, 4] and references therein. The chromate conversion coatings are very effective adhesion promoters and give excellent protection against corrosion. However, the coating solution contain hexavalent chromium (Cr^{6+}), which is known to have adverse health and environmental effects, and this has resulted in increasingly strict regulation regarding its usage, see

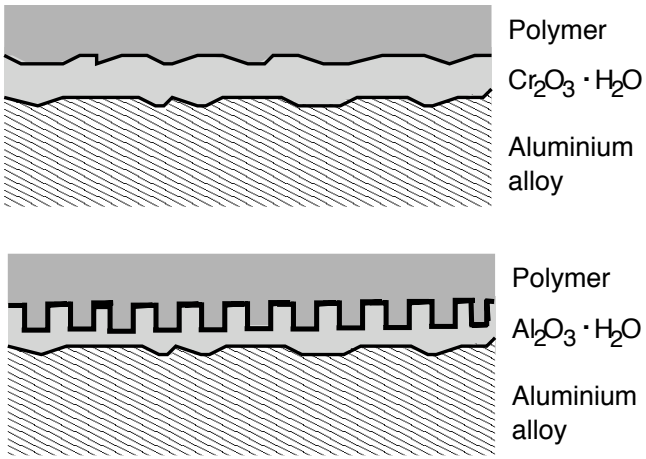

Figure 1.1: Schematic view of the interface region of a polymer-aluminium system with a chromate conversion coating (top) and anodised aluminium (bottom).

e.g. Ref. [5]. For this reason, a lot of effort has been devoted to finding alternative, chromate-free surface pre-treatments [6].

Another commonly used pre-treatment is anodising. Anodising refers to an electrochemical process in which the aluminium is an anode in an electrochemical cell containing an aqueous solution [1]. This process converts aluminium at the surface to aluminium oxide, resulting in a thick, porous oxide film more conducive to adhesive bonding than the naturally occurring aluminium oxide film. The structure (thickness and porosity) of the anodic oxide depends on factors such as the applied voltage, solution temperature, and alloy composition [6].

Figure 1.1 shows a schematic illustrations of the interface region between an organic coating, a polymeric material such as epoxy, and an aluminium alloy substrate with a chromate conversion coating (top panel) or anodised aluminium (bottom panel). To understand and explain the factors that enhance adhesion, it is important to know which interactions occur between the polymer and the pre-treated surface. Such knowledge is difficult to obtain for several reasons: As alluded to above, the pre-treated surfaces are rather complex with varying compositions and

structures depending on factors ranging from the composition of the chemical solutions to the prehistory of the surface (prior chemical treatments). Furthermore, the size of the polymers of the organic coating is such that widely disparate time and length scales come into play. For example, chemical bonding between the polymer and the surface occur at the femto-second time scale and on a length scale of 1 Å, while bulk properties such as hardening of the coating happen at a time-scale of seconds or longer.

Molecular scale interactions between polymers and a substrate are governed by quantum mechanics, and are best described by *ab initio* calculations [7–12]. These are calculations without any experimental input, the only input being the atomic numbers. Such *ab initio* calculations are computationally demanding, typically limited to ~ 100 atoms, so in order to make them feasible one must ignore some of the complications associated with the 'industrial' systems. Simplifications can be achieved by using 'model' surfaces and small molecules to mimic the polymer [7–10].

In our work we model the chromate conversion coating by an α-Cr_2O_3(0001) surface (papers II and III), and the anodised aluminium surface by α-Al_2O_3(0001) (papers I and IV). Although these surfaces are very simplified compared to the amorphous chromate conversion coating and anodised aluminium surface, we believe they provide a good starting point for understanding the physics and chemistry of the industrial surfaces. One further advantage is that *clean* α-Cr_2O_3(0001) and α-Cr_2O_3(0001) surfaces have been extensively studied and characterised both experimentally and theoretically, making it possible to control the quality of our calculations (see paper I-IV).

Amine-cured epoxy polymers are widely used in coatings and adhesives for applications involving aluminium. Amine-groups (NH_2), hydroxyl-groups (OH) and benzene (aromatic ring) are representative functional groups found in this polymer. Rather than studying the interaction of a complete polymer with the chromium and aluminium oxide surfaces, we follow the strategy of 'cutting' the polymer into smaller molecules, each containing one (or more) of the chemically important functional groups of the polymer, see Figure 1.2 for an illustration, and study the interaction of these molecules with the surfaces. The detailed information gained from such *ab initio* calculations can at a later stage be incorporated into models suitable for describing the large-scale interaction between the poly-

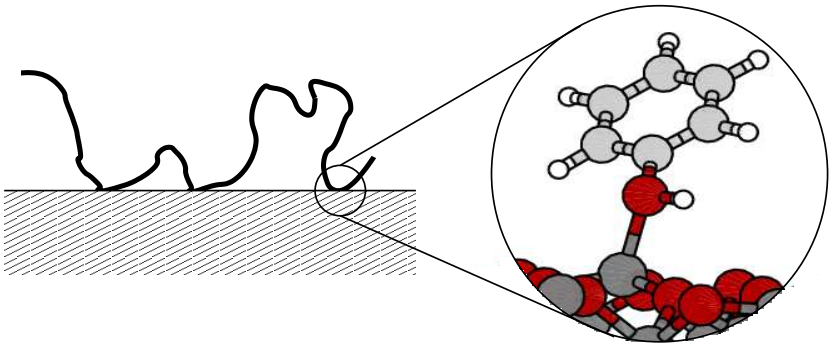

Figure 1.2: Illustrating our strategy. We focus on the interaction of a small organic molecule, in this case phenol, with an model oxide surface.

mer and the substrate [7]. However this is outside the scope of this work. In this thesis we solely focus on the molecule-oxide interactions.

Aluminium alloys generally contain various alloying elements which may influence both the adsorption behaviour of molecular groups as well as the oxide composition. Common alloying elements for the aluminium industry includes among other Mg and Si. In the present work we have chosen a different route, namely investigating the adsorption behaviour at surfaces of an ordered, bimetallic aluminium containing alloy, NiAl (paper V). This alloy has weight and strength characteristics which makes it a candidate for structural applications [13]. In addition the NiAl alloy offers electronic and structural properties which are of fundamental interest.

1.2 Thesis outline

The introductory part of this thesis, part I, contains four chapters. Chapter 1 is this introduction. Chapter 2 present the theoretical methods we have used to obtain the results presented in the papers. Chapter 3 contains a short summary of the included papers. Chapter 4 provides an overall conclusions for the work presented

in this thesis, and an outlook.

The main scientific body of this thesis are the papers included in part II:

Paper I First-principles study of the adsorption of methanol at the α-Al_2O_3(0001) surface
Ø. Borck and E. Schröder
J. Phys.: Condens. Matter **18** (2006) 1.

Paper II Adsorption of methanol and methoxy on the α-Cr_2O_3(0001) surface
Ø. Borck and E. Schröder
Preprint 2006

Paper III Adsorption of methylamine on α-Al_2O_3(0001) and α-Cr_2O_3(0001)
Ø. Borck, P. Hyldgaard, and E. Schröder
Preprint 2006

Paper IV Phenol adsorption on graphite and aluminum oxide
S. D. Chakarova-Käck, Ø. Borck, E. Schröder, and B. I. Lundqvist
Preprint 2006

Paper V Density functional theory investigation of methoxy on NiAl(110)
Ø. Borck, H. Dalaker, and K. Mo
Preprint 2006

Chapter 2

Theoretical methods

In this chapter we present the theoretical methods used to obtain the results presented in the accompanying papers. This chapter is divided into three sections. Section 2.1 contains a presentation of the foundations of density functional theory (DFT) leading up to the Kohn-Sham equations. A brief overview of how these equations are solved is given in section 2.2, with the main emphasis on the methods and approximations we have used in our work. In the final section 2.3 we discuss how information can be extracted from the density functional theory calculations.

For a more detailed description of the topics of this chapter, we refer the reader to the books [14–16] and reviews [17, 18].

2.1 The foundations of density functional theory

Shortly after Schrödinger introduced his quantum mechanical wave equation, L. F. Thomas [19] and E. Fermi [20] independently introduced an equation with the purpose of giving an approximative description of the electron density and ground state energy of an atom with a large number of electrons. In the Thomas-Fermi approach, the electron density, $n(\mathbf{r})$, is the basic variable, rather than the wave function $\Psi(\mathbf{r}_1\sigma_1, \ldots, \mathbf{r}_N\sigma_N)$. For a many-electron problem this represents an enormous simplification: rather than facing the problem of solving an equation for

a function Ψ which depend on the coordinates of *all* the electrons in the system and their spin variables, in the Thomas-Fermi approach the desired function $n(\mathbf{r})$ only depends on three variables. Furthermore, unlike the wave functions, the electron density is an observable quantity, which makes it possible to directly compare the basic quantity of the theory with experiments [21].

The Thomas-Fermi approximation has found use in a broad spectrum of physical problems, including in solid-state theory, see Ref. [22] for a review. However, the main failure of the Thomas-Fermi model makes it rather inappropriate for our purposes: There can be no molecular binding within this theory [23, 24].

2.1.1 The Hohenberg-Kohn theorems

The modern era of density functional theory started with a paper by Hohenberg and Kohn [25] where they presented what now is known as the Hohenberg-Kohn theorems. The theorems are easy to prove [14, 15, 25], but in this thesis we will only state them.

Consider a system of N interacting electrons moving under the influence of some given external (time-independent) potential $v_{\mathrm{ext}}(\mathrm{r})$, for example the potential of the nuclei in a crystal. The Hamiltonian for this system is

$$H = -\frac{\hbar^2}{2m}\nabla^2 + \frac{1}{2}\sum_{i\neq j}\frac{e^2}{|\mathbf{r}_i - \mathbf{r}_j|^2} + V_{\mathrm{ext}}(\mathbf{r}) \ , \tag{2.1}$$

We can, in principle, solve the Schödinger equation for the wave functions corresponding to this Hamiltonian, and compute the electron density $n(\mathrm{r})$. Hence, the external potential $v_{\mathrm{ext}}(\mathbf{r})$ determines the electron density. The first theorem of Hohenberg and Kohn states that the opposite is also true: The electron density determines the external potential (to within an additive constant). From this follows that *all* properties of the theory can be determined once the electron density is known, in particular the total ground state energy. This theorem legitimises the use of the electron density as the basic variable in quantum theory.

The second theorem provides a general method for calculating ground state properties. Introducing the energy functional:

$$E[n] = \int \mathrm{d}\mathbf{r}\, n(\mathbf{r}) v_{\mathrm{ext}}(\mathbf{r}) + F[n] \ , \tag{2.2}$$

Hohenberg and Kohn showed that $F[n]$ is a *universal* functional, in the sense that it does not depend on the external potential, and that the ground state energy, $E_{\rm G}$, can be found by minimising $E[n]$:

$$E_{\rm G} = \min_{n \in \mathcal{N}} E[n] \ . \tag{2.3}$$

where the density that minimises $E[n]$ is the exact ground state density $n_{\rm G}(\mathbf{r})$.

2.1.2 The Kohn-Sham equations

Although the second Hohenberg-Kohn theorem provides a variational method for calculating ground state properties, no information is provided on how to construct the universal functional $F[n]$. There are schemes for approximating $F[n]$, see for example [26], however most applications of density functional theory today use the approach proposed by Kohn and Sham [27], where the direct variation of the functional (2.2) is replaced by an intermediate wave function picture.

The central assumption of the Kohn-Sham approach is that the ground state density of the interacting system is equivalent to the ground state density of an auxiliary system of *non-interacting* particles moving in an effective local potential $v_{\rm eff}(\mathbf{r})$.

In other words, there exists a potential $v_{\rm eff}(\mathbf{r})$ such that solving the simple one-electron Schödinger equation for the (Kohn-Sham) wave functions $\phi_i(\mathbf{r})$:

$$\left(-\frac{\hbar^2}{2m}\nabla^2 + v_{\rm eff}(\mathbf{r}) \right) \phi_i(\mathbf{r}) = \varepsilon_i \phi_i(\mathbf{r}) \ . \tag{2.4}$$

and then using these wave functions to calculate the ground state density for this non-interacting system, $n_0(\mathbf{r})$:

$$n_0(\mathbf{r}) = \sum_i^N |\phi_i(\mathbf{r})|^2 \ , \tag{2.5}$$

one has at the same time obtained the electron density of the 'true', interacting system $n_{\rm G}(\mathbf{r}) \equiv n_0(\mathbf{r})$.

The effective potential can be deduced from the Hohenberg-Kohn theory [27, 15], and it is given by

$$v_{\text{eff}}(\mathrm{r}) = v_{\text{ext}}(\mathbf{r}) + \int \mathrm{d}\mathbf{r}' \, \frac{n(\mathbf{r}')}{|\mathbf{r}' - \mathbf{r}|} + v_{\text{xc}}(n(\mathbf{r})) \tag{2.6}$$

where the second term can be recognised as the Hartree-potential. The last term is the exchange-correlation potential, $v_{\text{xc}}(n(\mathbf{r}))$, and it contains all the many-electron effects. It can be expressed as the functional derivative of an exchange-correlation energy:

$$v_{\text{eff}}(\mathrm{r}) = \left. \frac{\delta E[\tilde{n}]}{\delta \tilde{n}(\mathbf{r})} \right|_{\tilde{n}(\mathbf{r})=n(\mathbf{r})} \tag{2.7}$$

The main problem of density functional theory is finding approximations for the exchange-correlation potential, or equivalently the exchange-correlation energy, and we will have more to say about this in the next section.

2.2 Solving the Kohn-Sham equations

In the previous section the foundation of density functional theory was presented and until now the formalism has been exact. We now turn our attention to the problem of solving the Kohn-Sham equations. We will only comment on the salient points, and refer the reader to references [14, 18] for a more complete discussion of these topics.

The effective potential of the Kohn-Sham equations, Eq. 2.6 is a function of the electron density, which implies that the equations 2.4-2.6 must be solved self-consistently. Figure 2.1 shows a simplified flow chart for this procedure.

The Kohn-Sham equations are a mapping of the many-electron problem onto a set of one-electron equations, and solving such equations is essentially a trivial task. However, for large systems it is important to find effective ways of solving them. For example, the use of pseudopotentials and clever algorithms for ensuring (speedy) convergence of the self-consistent loop [28] have been important factors for the practical implementation of Kohn-Sham equations.

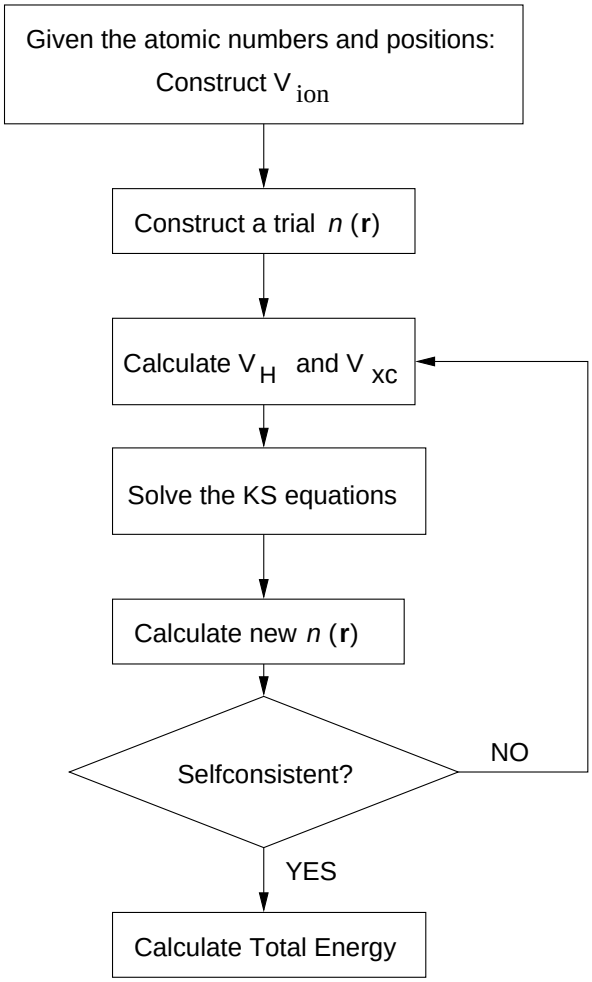

Figure 2.1: Simplified flow chart illustrating the self-consistency loop.

2.2.1 Approximations for the exchange-correlation energy

In the Kohn-Sham formulation of density functional theory, all the many-body effects are hidden in the exchange-correlation potential $v_{\mathrm{xc}}(\mathbf{r})$. Unfortunately, we

do not have an explicit expression for this term. Before any solution of the Kohn-Sham equations can be attempted, it is therefore necessary to introduce some approximation for the exchange-correlation potential.

The simplest approximation is the local density approximation (LDA), already introduced in the paper of Hohenberg of Kohn [25]. In the LDA the exchange-correlation is written as

$$E_{\mathrm{XC}}^{\mathrm{LDA}}[n] = \int \mathrm{d}\mathbf{r}\, n(\mathbf{r}) \varepsilon_{\mathrm{xc}}^{\mathrm{hom}}(n(\mathbf{r}))\ , \tag{2.8}$$

where $\varepsilon_{\mathrm{xc}}^{\mathrm{hom}}(n(\mathbf{r}))$ is the exchange-correlation energy per electron for a *homogeneous* electron gas. Although one would expect the LDA to yield good results only for slowly varying densities, it has been remarkably successful [18] also for systems where the density is far from homogeneous, for example alumina oxide surfaces [29].

A natural extension of the LDA is to include gradients of the electron density. In the generalized gradient approximation (GGA) the exchange-correlation energy is generally expressed as

$$E_{\mathrm{XC}}^{\mathrm{GGA}}[n] = \int \mathrm{d}\mathbf{r}\, f(n(\mathbf{r}), |\nabla n(\mathbf{r})|)\ . \tag{2.9}$$

There are many different forms for GGAs available today, and we refer the reader to Refs. [30, 31] for a review and comparison of the performance of some of the more popular GGAs.

We have mainly employed the commonly used Perdew-Wang parametrisation (PW91) [32] in our work. In paper V, which deals with the adsorption of methoxy on NiAl(110), we have in addition used the RPBE functional to obtain adsorption energies as this functional has been shown to improve the chemisorption energies of molecules at transition-metal surfaces [31]. Rather recently a functional has been proposed which incorporates the long-range van der Waals interactions [33] into an implementation of density functional theory. In paper IV this functional is used to estimate the contribution from the van der Waals interaction to the adsorption energy for phenol on α-Al_2O_3(0001) and graphite.

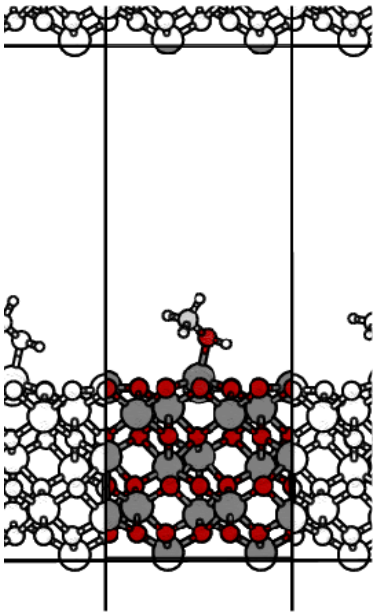

Figure 2.2: Schematic illustration of the supercell approach.

2.2.2 Plane wave expansion of the wave function

An important consideration in numerical schemes for solving the Kohn-Sham equations is which basis set the Kohn-Sham wave functions should be expanded in. In solid-state physics, where one deals with periodic structures, a natural choice is to expand the wave functions in a plane wave basis, as they are of the form required by Bloch's theorem [34]

$$\phi_{n\mathbf{k}}(\mathbf{r}) = \sum_{\mathbf{G}} c_{n\mathbf{G}} \exp \mathrm{i}(\mathbf{k}+\mathbf{G}) \ , \tag{2.10}$$

where $c_{n\mathbf{G}}$ are the expansion coefficients, and where $\mathbf{G}$ are the reciprocal lattice vectors defined by $\mathbf{G} \cdot \mathbf{T} = 2\pi m$ for an integer m and all lattice vector of the crystal $\mathbf{T}$. Even if the system is *not* periodic in all directions, such as for example

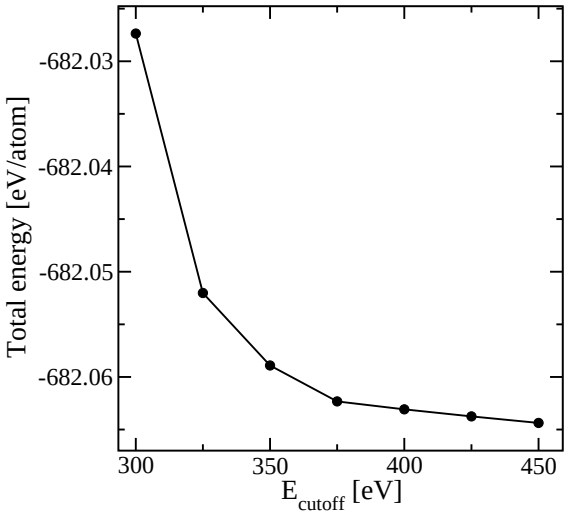

Figure 2.3: Convergence of the total energy for bulk NiAl with respect to the plane wave energy cutoff.

a surface or a defect, it is often possible to construct a unit cell, commonly referred to as a supercell [18], which *is* periodic, as illustrated in Fig. 2.2. We have exclusively used the supercell approach and a plane wave basis in this thesis.

In principle, an infinite plane wave basis is needed to expand the wave functions, however in practical implementations the basis-set must be truncated. Typically, the plane waves with small kinetic energies $\hbar^2(\mathbf{k}+\mathbf{G})^2/(2m)$ are more important than those with large kinetic energies. A good approximation to the total energy can therefore be achieved by only including plane waves that have kinetic energies less than some cutoff energy. This implies one of the great advantages of using a plane wave basis: the accuracy of the calculations can be systematically increased by adjusting the cutoff energy, as illustrated in Fig. 2.3.

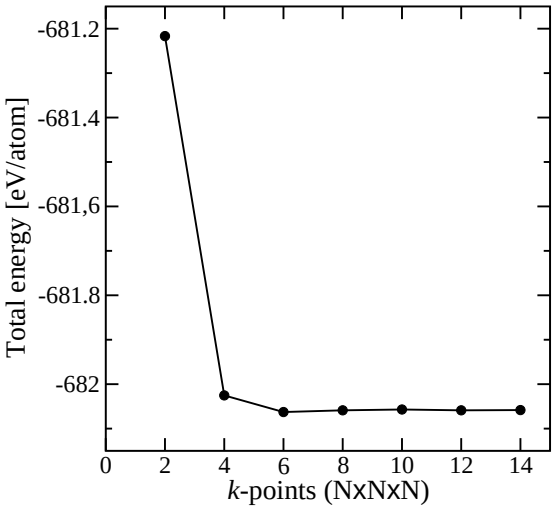

Figure 2.4: Convergence of the total energy for bulk NiAl with respect to the k-point sampling.

2.2.3 k-point sampling

Many calculations in periodic systems require integration over the Brillouin zone. For example, an essential step in the self-consistency loop, Fig. 2.1, is the evaluation of a new electron density once the Kohn-Sham wave functions have been obtained:

$$n(\mathbf{r}) = \sum_{n\mathbf{k}} |\phi_{n\mathbf{k}}|^2 \tag{2.11}$$

Evaluation of this sum is computationally very demanding, as it requires the knowledge of the value of the wave function at each k-point of the Brillouin zone. To circumvent this problem, several schemes have been proposed [34–36] where a set of 'special' points in the Brillouin zone is generated, with the property that a good approximation can be achieved by only summing over this reduced set of k-points. In our work we have used the method proposed by Monkhorst and Pack [37].

The error of using a finite number of k-point can be reduced systematically by increasing the number of k-points. Fig. 2.4 illustrates the convergence of the total energy for bulk NiAl as the grid size is increased from $2 \times 2 \times 2$ to $14 \times 14 \times 14$ using a Monkhorst-Pack grid.

2.2.4 Pseudopotentials

Figure 2.5 illustrates schematically the behaviour of a $3s$ wave function near a nucleus. The rapid oscillations in the core region arise from the requirement that the wave function must be orthogonal to the strongly localised core electrons. Such behaviour disqualifies the use of a plane wave basis in calculations because it would require a prohibitive large basis set and computational time for our applications.

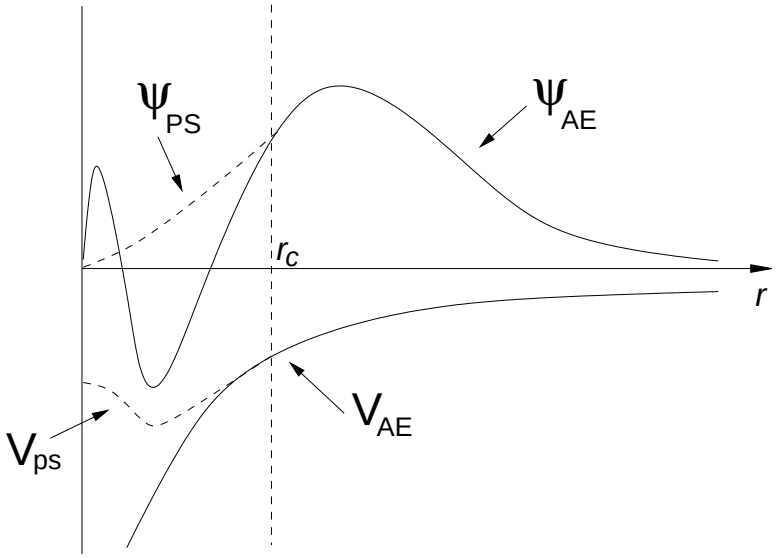

Figure 2.5: Schematic illustration of an all-electron (pseudo) $3s$ wave function and corresponding pseudo (full) potential drawn as solid (dashed) lines. The core radius r_c is indicated.

One solution to this problem is provided by the pseudopotential approximation. The basic assumption behind this approximation is that the physical and chemical properties of solids mostly depend on the valence electrons and not so much the core electrons. A good approximation should therefore be to replace the core electrons and the strong Coulomb potential by a weaker, effective pseudopotential. This has the added advantages that fewer electrons are treated explicitly in the calculations, and that relativistic effects, which are mainly due to the core electrons, can be incorporated into the pseudopotential. Ideally, the pseudopotential should be constructed so that outside some core radius r_c, the pseudo wave functions and the all-electron wave should coincide, while inside this radius the pseudo wave function is smooth and nodeless, thus reducing the required basis-set size, see Fig. 2.5.

Although the all-electron and pseudo wave function differ in shape inside the core radius, the integrated charge within this radius should agree. This is referred to as *norm-conservation* [38]. The O $2p$ wave function represents a problematic case for norm-conserving pseudo-potentials. It is nodeless and strongly localised, and it has been difficult to construct a pseudo wave function which is much smoother than the all-electron wave functions. Vanderbilt's ultrasoft pseudopotentials [39] overcome these difficulties by relaxing the norm-conservation and introducing so-called augmentation charges to ensure that the final charge is still equivalent to the all-electron charge. The ultrasoft pseudopotentials make it possible to describe the first row elements and $3d$-transition metals with a reasonably small energy cutoff, and therefore computational cost. We have exclusively used Vanderbilt's ultrasoft pseudopotentials [39] in this thesis.

2.3 Extracting information from DFT-calculations

In the included papers we have performed DFT-calculations to characterise the adsorption of selected organic molecules at the α-Al_2O_3(0001), α-Cr_2O_3(0001), and NiAl(110) surfaces. In particular we have determined the equilibrium atomic structure of the clean surfaces and free molecules as well as the geometry of the adsorbate systems, and we have analysed (difference) electron densities in order to discuss the nature of the bonds. This section we describe how this information

were obtained from DFT-calculations.

2.3.1 Atomic structure optimisation

We can use density functional theory to calculate the ground state energy for a given atomic structure, however we have usually no knowledge beforehand which particular configuration of the atoms corresponds to the most optimal structure. In the included papers we have used two different approaches to determine the equilibrium structures, one approach for the bulk structures and another for the surfaces, molecules and adsorbate systems.

Determination of the bulk atomic structures is relatively simple because of the high level of symmetry. The simplest example in this thesis is bulk NiAl (paper V). NiAl crystallises in a CsCl structure, a crystal structure which can be described by a single lattice parameter a, see Fig. 2.6. In this case the equilibrium lattice parameter a_0 is determined by calculating the total energy at various possible lattice constants. The resulting data points can be fitted to some equation of state, for example the Murnaghan equation [40]. We have rather followed the approach suggested in Ref. [41] and fitted the data to a fourth order polynomial (Fig. 2.6). The results can be found in paper V.

The method of Ref. [41] is independent of the number of parameters needed to describe the atomic structure, so the same approach was used to determine the bulk atomic structures of α-Al_2O_3 and α-Cr_2O_3 (paper I and II). These oxides are isostructural and have a rhombohedral primitive unit cell, each cell containing two formula units, see Fig. 2.7. The bulk structure can now be described by four parameters: two lattice parameters a and α, and two parameters describing the positions of the oxygen and metal atoms within the unit cell. To determine the bulk structures, the four parameters were varied independently, and resulting data points were fitted to a fourth order (hyper)surface. This procedure also allows a direct evaluation of elastic properties, such as the bulk modulus. The results of these structure determinations are presented in papers I and II.

For less symmetric structures, such as a surface, a direct approach as the one described above is rather cumbersome, and a minimisation scheme is preferable. The surface, molecular and adsorbate structures reported in papers I-V, have been obtained with the aid of the Hellmann-Feynman theorem [42, 43]. The basic pro-

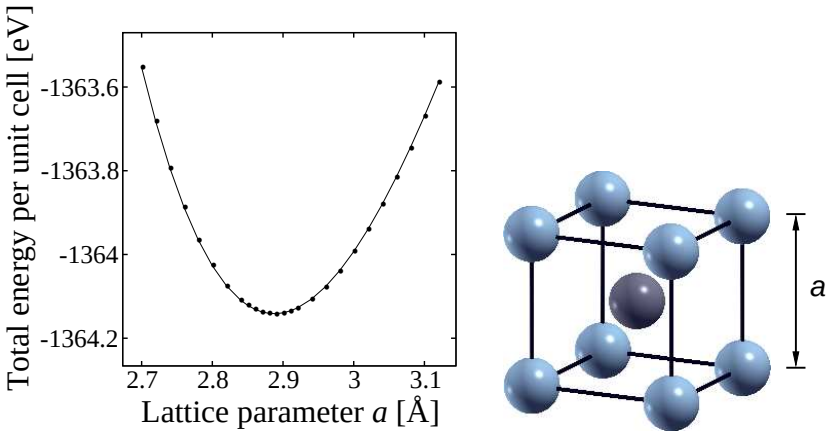

Figure 2.6: The total energy per unit cell as a function of the lattice parameter a for bulk NiAl. The data points obtained from a DFT calculation are indicated by circles. The solid line is a fourth-order polynomial fit to the data points. The NiAl unit cell is shown with Ni (Al) represented by blue (grey) spheres.

cedure is as follows: Starting from some initial guess for the position of the atoms, a total energy calculation is performed using density functional theory. Once the self-consistent electron density is available, the forces acting on the atoms are calculated utilising the Hellmann-Feynman theorem. An algorithm is used to minimise the forces. We have mainly used the Broyden-Fletcher-Goldfarb-Shanno (BFGS) algorithm [44] for this purpose.

2.3.2 Electron distribution and the chemical bond

From the DFT calculations the electron distribution can be determined as well as changes in the electron distribution upon, e.g., adsorption.

The electron density difference[1] is defined as the difference between the (total)

[1]This quantity is frequently referred to as the deformation density, especially in the crystallography community, see for example [21].

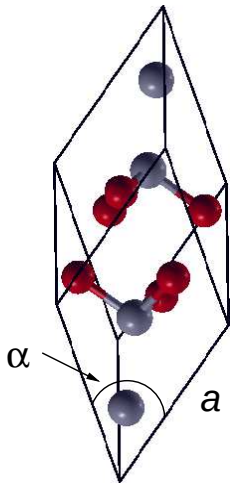

Figure 2.7: The rhombohedral unit cell of α-Al_2O_3 and α-Cr_2O_3. The lattice parameters a and α are indicated. The cation (anion) atoms are represented by grey (red) spheres.

electron density and the electron density of some reference state:

$$\Delta n(\mathbf{r}) = n_{\mathrm{tot}}(\mathbf{r}) - n_{\mathrm{ref}}(\mathbf{r}) \tag{2.12}$$

The electron density difference can give some insight into chemical bonding. Figure 2.8 shows contour plots of selected cross sections of the electron density difference for bulk α-Al_2O_3, α-Cr_2O_3, and NiAl respectively. In each case we have subtracted the electron density of the free atoms from the total densities. In these contour plots, red contours indicate a gain in electron density, while blue contours indicate a loss of density. The plots for α-Al_2O_3 and α-Cr_2O_3 are as expected for a ionic materials: a loss of electron density at the metal ion and a gain at the oxygen ion. Bulk NiAl exhibits both ionic and covalent contributions to the bonding [45]. There is a loss of electron density at the Al positions and gain at the Ni positions, expected for ionic bonding. But there are also lobes of electron density at Ni pointing towards Al, in support of a covalent contribution.

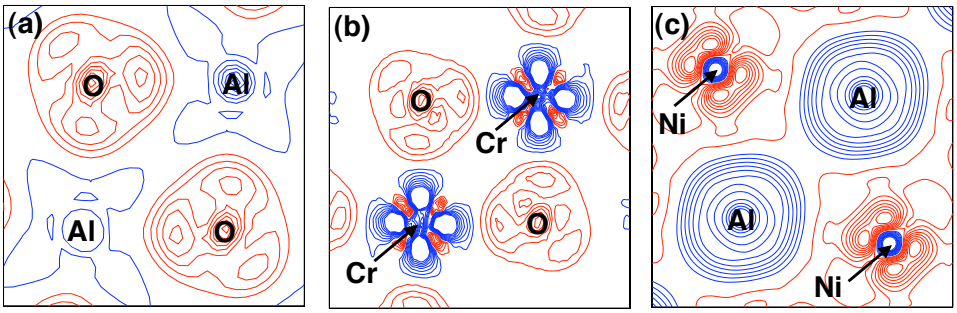

Figure 2.8: Contour plots of the electron density difference for (a) α-Al_2O_3 (b) α-Al_2O_3, and (c) NiAl. Red (blue) lines indicate gain (loss) of electron density, and the contour spacing is 0.01 e/Å^3, with the first contour at $\pm$ 0.01.

Frequently one is interested in the nature of the bonding between fragments of a molecular complex or between an adsorbate and a surface (see papers I-IV for examples). One can then define a fragment electron density difference. For example: to investigate the bonding between the CH_3 fragments of ethane C_2H_6 one subtracts the electron density of the isolated CH_3 fragments from the electron density of C_2H_6. The result of such a calculation is shown in Fig. 2.9. As expected of a covalent interaction, there is a gain in electron density in the bonding region between the carbon atoms.

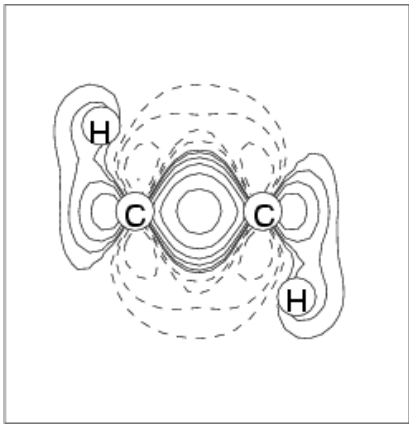

Figure 2.9: Contour plot of the electron density difference for C_2H_6. The cut plane contains the two C atoms and two H atoms. Contours at 0.01 e/Å^3. Gain (loss) of electron density is indicated by a solid (dashed) line.

Chapter 3

Summary of the included papers

The purpose of this chapter is to give a brief overview of the included papers.

Paper I:
First-principles study of the adsorption of methanol at the α-Al_2O_3(0001) surface
In this paper a study of the molecular adsorption of methanol (CH_3OH) at the α-Al_2O_3(0001) surface were performed. We find that methanol adsorbs via its oxygen atom to a surface layer aluminium atom, but also find indications that the hydrogen atom of the methanol hydroxyl group is involved in the stabilisation of methanol via an interaction with a surface layer O atom. Electron density difference plots indicate that the nature of the bond between Al and the methanol O atom is of a donor-acceptor type, where the methanol lone pair 'donates' electron density to form a bond with the 'acceptor' Al. Adsorption of methanol results in a significant relaxation of the surface structure. We estimate that 30% of the adsorption energy can be attributed to relaxation effects. Furthermore, the surface relaxations result in a repulsive adsorbate interaction, so that the adsorption energy decreases from 1.23 eV at $\Theta = 1/4$ ML to 1.03 at $\Theta = 1$ ML.

Paper II:
Adsorption of methanol and methoxy on the α-Cr_2O_3(0001) surface

On α-Cr_2O_3(0001) we find that methanol adsorbs with its oxygen atom situated in a three-fold O hollow site, in contrast to our result for methanol on α-Al_2O_3(0001), where the methanol O atom adsorbs nearly on top of a surface Al. The adsorption energy is somewhat smaller (0.82 eV at $\Theta = 1$ ML) than what we found for methanol on α-Al_2O_3(0001). Also in contrast to adsorption on α-Al_2O_3(0001), we find no indication of adsorbate interactions at the α-Cr_2O_3(0001).

Methoxy adsorbs with its O atom situated on top of a surface Cr atom, and with the CO-axis tilted away from the surface normal by $\sim$55°. Methoxy is strongly bound to the α-Cr_2O_3(0001) with an adsorption energy of 3.3 eV.

Paper III:
Adsorption of methylamine on α-Al_2O_3(0001) and α-Cr_2O_3(0001)
In this paper we studied the adsorption of methylamine (CH_3NH_2) at the α-Al_2O_3(0001) and α-Cr_2O_3(0001) surfaces. At the α-Al_2O_3(0001) surface methylamine adsorbs with its nitrogen atom slightly displaced ($\sim$0.36 Å) laterally from the precise aluminium ontop site, while at the α-Cr_2O_3(0001) it adsorbs with the nitrogen atom in a oxygen three-fold hollow site. These adsorption site preferences are similar to what we found for methanol on α-Al_2O_3(0001) and α-Cr_2O_3(0001).

At the α-Al_2O_3(0001) we find significant adsorbate-induced surface relaxations, similar to what we reported in paper I, and a decrease in adsorption energy from 1.65 eV at $\Theta = 1/4$ to 1.16 at $\Theta = 1$, i.e. an adsorbate-adsorbate repulsion. Extra calculations at two 'frozen' surfaces showed that the adsorbate interaction was caused by the surface relaxations.

Electron density difference plots and an analysis of the projected density of states suggest that methylamine binds to the surface via a lone-pair (donor-acceptor) interaction.

Paper IV:
Phenol adsorption on graphite and aluminum oxide In this paper we investigate the interaction of phenol with a graphite and an α-Al_2O_3(0001) surface using traditional DFT and a recently presented density functional (vdW-DF) that

in addition to the traditional version of DFT incorporates the dispersive van der Waals interactions [33]. The vdW-DF is of decisive importance for describing the interactions of phenol with graphite.

Phenol contains two functional groups (benzene and alcohol) that could conceivably interact with the α-Al_2O_3(0001) surface. We find a preferred orientation with the aromatic ring tilted away from the surface, while the phenol oxygen atom bind to a surface aluminium atom. The adsorption energy calculated using traditional DFT, $E_{\mathrm{ads}} = 1.00$ eV, is comparable to what we found for methanol adsorption, and the electron density difference plots are very similar indicating a similar nature of the binding mechanism. When the contribution from van der Waals interactions is accounted for, the adsorption energy increases to around 1.1-1.2 eV for the considered structures, and it is less clear which is the most favourable structure.

Paper V:
Density functional theory investigation of methoxy on NiAl(110) In this paper we report on density functional theory calculations to determine the preferred adsorption site and geometry of methoxy at the NiAl(110) surface. We find that methoxy adsorbs with its O situated in an Al bridge site ('Al-Al short-bridge'), and with the CO-axis oriented perpendicular to the surface plane. A charge transfer from the substrate to the adsorbate fills the 2e orbitals which are only partly in the free methoxy molecule, leading to a predominantly ionic bond.

Chapter 4

Conclusions and outlook

Density functional theory (DFT) is today, in combination with efficient algorithms and high-performance computers, a significant and frequent player on the field of materials science. The original aim of this thesis was to apply theoretical methods to the industrially interesting problem of polymer adhesion to oxide covered aluminium substrates. Facing the complexity of such systems, the investigation has focused on the interaction of small organic molecules with various surfaces, of metal oxides (α-Al_2O_3(0001) and α-Cr_2O_3(0001)), a bimetallic alloy (NiAl(110)), and graphite.

In the papers included in part II of the thesis there are several conclusions drawn on the systems under study. Although the substrates and adsorbates are chosen because of their relevance to industrial applications, the study is general enough to allow some general conclusions to be drawn.

Methanol, methylamine, and phenol are all closed-shell molecules with a lone-pair character. On α-Al_2O_3(0001) and α-Cr_2O_3(0001) we find that these molecules interact with the exposed surface cations. There is a build-up of electron density between the methanol/phenol O atom, methylamine N atom, and a surface cation, characteristic of a covalent bond formation. However, as only the adsorbates contribute electron density to the bond, we classify the adsorption mechanism as a donor-acceptor interaction [47]. Thus, our results confirms the expected adsorption mechanism for molecules with lone-pair character to oxide

surfaces [47]. The adsorption energies for these systems are in the range 0.80 eV to 1.65 eV (see Tab. 4.1), that is, not a very strong chemisorption.

The open-shell methoxy molecule forms a strong chemisorption bond to the α-Cr_2O_3(0001) and NiAl(110) surfaces, see Tab. 4.1. The valence orbital structure of gas-phase methoxy is characterised by a partially filled non-bonding π-orbital on oxygen, referred to as the 2e-orbital [48]. Adsorption involves a net electron transfer *from* the surface *to* methoxy of 0.41 $|e|$ and 0.90 $|e|$ for methoxy on α-Cr_2O_3(0001) and NiAl(110) respectively. The electron transfer is into the 2e orbital of methoxy. The relatively large charge transfers suggests that ionic bonding is an important component of the chemisorption bond for these systems. A similar adsorption behaviour has been reported for methoxy on other surfaces [49, 50].

In addition to the electron density rearrangements and bond formation, adsorption-induced surface relaxation effects play a significant role in determining the strength of the chemisorption. We find that adsorption induces a significant restructuring of the α-Al_2O_3(0001) surface, where the Al atoms are displaced in the direction normal to the surface. The surface deformations are coverage dependent, and result in an effective repulsive interaction between the adsorbates and thereby coverage dependent adsorption energy. We estimate that as much as 30% (at coverage $1/4$ ML) of the adsorption energy can be attributed to relaxation effects, demonstrating the importance of taking these effects into account. In contrast, on α-Cr_2O_3(0001) the surface deforms less upon adsorption, and we find no coverage dependence of adsorption energies, nor the surface relaxation. There have been published several papers pointing out the importance of surface relaxations for adsorption on α-Al_2O_3(0001), see e.g. Refs. [51, 52, 53], but, to my knowledge, non on α-Cr_2O_3(0001). It has been suggested that the large relaxations of the α-Al_2O_3(0001) surface is a result of the small size and large ionicity of the Al atoms [52]. Our results on α-Cr_2O_3 (paper II) suggests that it is has a higher degree of covalency than α-Al_2O_3. A stronger directionality of the bonding could be the reason why α-Cr_2O_3(0001) is 'stiffer' than α-Al_2O_3(0001).

The methods used in this thesis are mostly those of 'traditional' DFT, with electron exchange and correlation treated in various flavours of the generalized gradient approximation (GGA), and in standard pseudopotential-planewave implementations (DACAPO [46]). However, some applications are treated in a re-

cently presented extension of GGA that gives an account of the electron correlations that give van der Waals (vdW) forces, vdW-DF [33]. A self-evident such application is the adsorption of benzen-derived molecules (here exemplified by phenol) on graphite, which are predominantly governed by vdW interactions. However, the ubiquitous vdW forces are also studied for phenol on alumina, to compare their contribution to the adsorption bond to other forces.

It is noteworthy that although phenol in Paper IV is bound by what is considered a 'strong' bond to alumina, the nonlocal vdW-interactions increase the adsorption energy by approximately 20% compared to the value found from GGA alone.

A natural question that arises from that study — which chronologically was the last of the five studies presented in this thesis — is the following: Did we miss any vdW-interaction also in other covalently/ionic-bonded adsorption systems? Can we rely on our GGA values found for the adsorption energies of methanol, methoxy, methylamine on alumina, chromia and NiAl surfaces, or do we need to also correct these for the vdW-interaction?

As we did not do any explicit calculations of the vdW-interaction in the other systems yet the answer must be based on a qualified guess. Treatments within DFT of the vdW-interactions in strongly bonded systems is still in its infancy, and the study of phenol on alumina is one of a few first very recent studies (all initiated within the past 6 months) of dispersive interactions in systems that are

Table 4.1: Summary of calculated adsorption energies. Adsorption energies calculated at coverages $\Theta = 1$ ML and $\Theta = 1/4$ ML are given as a range of values. Unless specified, all adsorption energies are calculated using the PW91-GGA.

	Adsorption energy [eV]			
	α-Al_2O_3(0001)	α-Cr_2O_3(0001)	graphite(0001)	NiAl(110)
Methanol	1.03-1.23	0.82-0.80		
Methoxy		3.32-3.25		2.73
Methylamine	1.16-1.65	0.80		
Phenol	1.00,1.2[a]		0.56[a]	

[a]Calculated using the vdW-DF.

not clear-cut vdW-bonded systems.

Although we believe that within some error margin less than 20% (probably considerably smaller than 20%) our adsorption energy values can be trusted. What is special for the phenol system is the flat, benzene-like structure of the molecule, positioning itself on alumina so as to expose a large part of the molecule to the surface. This must be the optimal situation for the vdW-forces to act between the molecule and the surface. For the other small molecules considered in this thesis this is not so. Thus, we believe our GGA adsorption energies for the other molecules than phenol are reasonably well determined.

We end this chapter with some suggestions for future theoretical work. In spite of their industrial relevance relatively little research has been done on adsorption at oxide surfaces compared to metal surfaces. The possibilities for further work are therefore manifold. Of the many possible directions for future work we focus on two:

We have exclusively considered adsorption at clean and defect-free surfaces in this thesis. However, it is well known that even under UHV conditions most oxide surfaces contain defects [47], and the industrially interesting oxide surfaces are almost always covered by water. The presence of water and/or defects may influence the nature of binding at these surfaces. A natural extension of the work presented in this thesis would be to include such features. There have been published several theoretical studies of the hydroxylated α-Al_2O_3(0001) [51, 54], but to my knowledge no theoretical studies of adsorption of molecules at these surfaces has been carried out.

In this thesis we have considered relatively small molecules having at most two functional groups. A proper treatment of the interaction of a large molecule, such as a polymer, with a surface calls for a multiscale modelling approach due to the wildly disparate length and time scales that comes into play. One promising approach suggested by Delle Site *et al.* [7] is to use use information such as adsorption energies yielded by first-principles calculations of adsorption of fragments of a polymer as input in a 'coarse-grained' polymer model. Such studies have been conducted on metal surfaces [7] and should also be feasible on oxide surfaces.

References

[1] G. E. Totten and D. S. MacKenzie (Eds.), *Handbook of Aluminum. Volume 2: Alloy Production and Materials Manufacturing* (Marcel Dekker, New York, 2003).

[2] G. W. Critchlow and D. M. Brewis, Review of surface pretreatments for aluminium alloys, Int. J. Adhesion and Adhesives **16** (1996) 255.

[3] O. Lunder, J. C. Walmsley, P. Mack, and K. Nisancioglu, Formation and characterisation of a chromate conversion coating on AA6060 aluminium, Corrosion Science **47** (2005) 604.

[4] W. Zhang, B. Hurley, and R. G. Buchheit, Characterization of Chromate Conversion Coating Formation and Breakdown Using Electrode Arrays, J. Electrochem. Soc. **149** (2002) B357.

[5] Directive 2000/53/EC of the European Parliament and of the Council of 18 September 2000 on end-of-life vehicles, Off. J. Eur. Communities L**269** (2000) 3443.

[6] G. W. Critchlow, K. A. Yendall, D. Bahrani, A. Quinn, and F. Andrews, Int. J. Adhesion and Adhesives **26** (2006) 219.

[7] L. Delle Site, C. F. Adams, A. Alavi, and K. Kremer, Polymers near Metal Surfaces: Selective Adsorption and Global Conformations, Phys. Rev. Lett. **89** (2002) 156103.

[8] S. R. Cain, Quantum-mechanical approach to understanding acid-base interactions at metal-polymer interfaces, J. Adhesion Sci. Technol. **4** (1990) 333.

[9] J. W. Holubka, R. A. Dickie, and J. C. Cassatta, Molecular modeling of adhesion: the interaction of acrylate and methacrylate esters with aluminum oxide, J. Adhesion Sci. Technol. **6** (1992) 243.

[10] D. A. Drabold, J. B. Adams, D. C. Anderson, and J. Kieffer, First Principles Study of Polymer-Metal-Metal-Oxide Adhesion, J. Adhesion **42** (1993) 55.

[11] C. Noguera, Theoretical Investigation of Acid-Base Properties of Oxide Surfaces, J. Adhesion **57** (1996) 91.

[12] C. Noguera, *Physics and chemistry at oxide surfaces* (Cambridge University Press, Cambridge, 1996).

[13] A. I. Taube and R. L. Fleischer, Science **243** (1989) 616.

[14] R. M. Martin, *Electronic Structure. Basic Theory and Practical Methods* (Cambridge University Press, Cambridge, 2004).

[15] R. M. Dreizler and E. K. U. Gross, *Density Functional Theory: An Approach to the Quantum Many-Body Problem* (Springer-Verlag, Berlin, 1990).

[16] W. Holthausen and M. C. Holthausen, *A Chemist's Guide to Density Functional Theory*, 2nd Ed. (Wiley-VCH, Weinheim, 2001).

[17] R. O. Jones and O. Gunnarsson, The density functional formalism, its applications and prospects, Rev. Mod. Phys. **61** (1989) 689.

[18] M. C. Payne, M. P. Teter, D. C. Allan, T. A. Arias, and J. D. Joannopoulos, Iterative minimization techniques for *ab initio* total-energy calculations: molecular dynamics and conjugate gradients, Rev. Mod. Phys. **64** (1992) 1045.

[19] L. H. Thomas, The calculation of atomic fields, Proc. Cambridge Philos. Soc. **23** (1927) 542.

[20] E. Fermi, Un metodo statistice per la determinazione di alcune proprieta dell'atomo, Rend. Accad. Lincei **6** (1927) 602.

[21] P. Coppens, *X-Ray Charge Densities and Chemical Bonding* (Oxford University Press, Oxford, 1997).

[22] L. Spruch, Thomas-Fermi theory (atoms, stars,...), Rev. Mod. Phys. **63** (1991) 151.

[23] E. Teller, On the Stability of Molecules in the Thomas-Fermi Theory, Rev. Mod. Phys. **34** (1962) 627.

[24] E. H. Lieb and B. Simon, Thomas-Fermi Theory Revisited, Phys. Rev. Lett. **31** (1973) 681.

[25] P. Hohenberg and W. Kohn, Inhomogeneous Electron Gas, Phys. Rev. **136** (1964) B864.

[26] Y. A. Wang, N. Govind, and E. A. Carter, Orbital-free kinetic-energy functionals for the nearly free electron gas, Phys. Rev. B **58** (1998) 13465.

[27] W. Kohn and L. J. Sham, Self-Consistent Equations Including Exchange and Correlation Effects, Phys. Rev. **140** (1965) A1133.

[28] G. Kresse and J. Furthmüller, Efficiency of ab-initio total energy calculations for metals and semiconductors using a plane-wave basis set, Comp. Mat. Sci. **6** (1996) 15.

[29] C. Ruberto, Y. Yourdshahyan, and B. I. Lundqvist, Surface properties of metastable alumina: A comparative study of κ- and α-Al_2O_3 Phys. Rev. B **67** (2003) 195412.

[30] S. Kurth, J. P. Perdew, and P. Blaha, Molecular and Solid-State Tests of Density Functional Approximations: LSD, GGAs, and Meta-GGAs, Int. J. Quant. Chem. **75** (1999) 889.

[31] B. Hammer, L. B. Hansen, and J. K. Nørskov, Improved adsorption energetics within density-functional theory using revised Perdew-Burke-Ernzerhof functionals, Phys. Rev. B **59** (1999) 7413.

[32] J. P. Perdew, J. A. Chevary, S. H. Vosko, K. A. Jackson, M. R. Pederson, D. J. Singh, and C. Fiolhais, Atoms, molecules, solids, and surfaces: Applications of the generalized gradient approximation for exchange and correlation, Phys. Rev. B **46** (1992) 6671; **48** (1993) 4978(E).

[33] M. Dion, H. Rydberg, E. Schröder, D. C. Langreth, and B. I. Lundqvist, Van der Waals Density Functional for General Geometries, Phys. Rev. Lett. **92** (2004) 246401; **95** (2005) 109902(E).

[34] N. W. Aschcroft and D. Mermin, *Solid State Physics* (Holt, Rinehart and Winston, New York, 1976).

[35] A. Baldereschi, Mean-Value Point in the Brillouin Zone, Phys. Rev. B **7** (1973) 5212.

[36] D. J. Chadi and M. L. Cohen, Special Points in the Brillouin Zone, Phys. Rev. B **8** (1973) 5747.

[37] H. J. Monkhorst and J. D. Pack, Special points for Brillouin-zone integrations, Phys. Rev. B **13** (1976) 5188.

[38] D. R. Hamann, M. Schlüter, and C. Chiang, Norm-Conserving Pseudopotentials, Phys. Rev. Lett. **43** (1979) 1494.

[39] D. Vanderbilt, Soft self-consistent pseudopotentials in a generalized eigenvalue formalism, Phys. Rev. B **41** (1990) 7892.

[40] F. D. Murnaghan, The Compressibility of Media under Extreme Pressures, Proc. Natl. Acad. Sci. U.S.A. **30** (1944) 244.

[41] E. Ziambaras and E. Schröder, Theory for structure and bulk modulus determination, Phys. Rev. B **68** (2003) 064112.

[42] H. Hellmann, *Einführung in die Quantenchemie* (Franz Deuticke, Leipzig, 1937).

[43] R. P. Feynman, Forces in molecules, Phys. Rev. **56** (1939) 340.

[44] W. Press, B. Flannery, S. A. Teukolsky, and W. T. Vetterling, *Numerical Recipes in Fortran* 2nd ed (Cambridge University Press, Cambridge, 1992)

[45] Z. W. Lu, S.-H. Wei, and A. Zunger, Theory of bonding charge density in β' NiAl, Acta Metall. Mater. **40** (1992) 2155.

[46] `http://dcwww.fysik.dtu.dk/campos/Dacapo`

[47] V. E. Henrich and P. A. Cox, *The Surface Science of Metal Oxides* (Cambridge University Press, Cambridge, 1994).

[48] C. F. Jackels, Theoretical potential energy surface study of several states of the methoxy radical, J. Chem. Phys. **82** (1985) 311.

[49] G.-C. Wang, Y.-H. Zhou, and J. Nakamura, Characterization of methoxy adsorption on some transition metals: A first principles and density functional study, J. Chem Phys. **122** (2005) 044707.

[50] J. R. B. Gomes and J. A. N. F. Gomes, Comparative study of geometry and bonding character for methoxy radical adsorption on noble metals, J. Mol. Structure (Theochem) **503** (2000) 189.

[51] K. C. Hass, W. F. Scneider, A. Curioni, and W. Andreoni, The Chemistry of Water on Alumina Surfaces: Reaction Dynamics from First Principles, Science **282** (1998) 265.

[52] A. Bogicevic and D. R. Jennison, Varations in the Nature of Metal Adsorption on Ultrathin Al_2O_3 Films, Phys. Rev. Lett. **82** (1999) 4050.

[53] Z Łodziana and J. K. Nørskov, Interaction of Pd with steps on α-Al_2O_3(0001), Surface Science Letters **518** (2002) L577.

[54] Z. Łodziana, J. K. Nørskov, and P. Stoltze, The stablility of the hydroxylated (0001) surface of α-Al_2O_3, J. Chem. Phys. **118** (2003) 11179.

Part II

Papers

Paper I

First-principles study of the adsorption of methanol at the α-Al_2O_3(0001) surface

Ø. Borck and E. Schröder

J. Phys.: Condens. Matter **18** (2006) 1.

INSTITUTE OF PHYSICS PUBLISHING JOURNAL OF PHYSICS: CONDENSED MATTER

J. Phys.: Condens. Matter **18** (2006) 1–12 doi:10.1088/0953-8984/18/1/001

First-principles study of the adsorption of methanol at the α-Al_2O_3(0001) surface

Øyvind Borck[1,2] **and Elsebeth Schröder**[2]

[1] Department of Physics, Norwegian University of Science and Technology, NO-7034 Trondheim, Norway
[2] Department of Applied Physics, Chalmers University of Technology, SE-41296 Göteborg, Sweden

E-mail: oyvind.borck@phys.ntnu.no

Received 28 July 2005, in final form 6 November 2005
Published 9 December 2005
Online at stacks.iop.org/JPhysCM/18/1

Abstract

We present density functional theory calculations of methanol molecular adsorption at the (0001) surface of α-Al_2O_3, for methanol coverages of 1/4 to 1 monolayer (ML). Adsorption energies, adsorption-induced restructuring of the surface, and induced changes to the electronic structure are calculated. We find that methanol bonds with its O atom to Al atoms at the α-Al_2O_3(0001) surface with an adsorption energy of 1.23 eV at coverage 1/4 ML, decreasing with coverage to 1.03 eV at 1 ML coverage. From calculations of the relaxed adsorption geometry and the angular dependence of the total energy, we predict an orientation of the adsorbed methanol molecule that has the molecular COH plane tilted away from the surface normal. The adsorption of methanol significantly restructures α-Al_2O_3(0001), especially for the outermost Al layer. Upon adsorption a small charge transfer from the molecule to the substrate takes place.

1. Introduction

Understanding the surface properties of alumina (Al_2O_3) is of considerable importance for a wide variety of technological and industrial processes, ranging from catalysis to corrosion and adhesion [1, 2]. For this reason there have been a large number of experimental and theoretical studies on alumina addressing the properties of the clean α-Al_2O_3(0001) surface [3, 4], and the adsorption of various metal atoms [5] and molecules [6, 7], including water [8–10] and methanol [11–15].

Interest in the adsorption of methanol at alumina surfaces stems mainly from its relevance in heterogeneous catalysis [11–14]. Alumina in the γ-phase is catalytically active for the dehydration of alcohols [12, 16], and is used as a support for Cu- or Pd-based catalysts

employed in the decomposition of methanol [17, 18]. Methanol is also used as a probe molecule for investigating the surface chemistry of alumina and other metal oxides [19, 20].

In this paper we present density functional theory (DFT) calculations of the adsorption of methanol (CH_3OH) at the α-$Al_2O_3(0001)$ surface. Our work is motivated by the wider perspective of understanding how organic polymers interact with metal oxide surfaces. This is essential for a fundamental understanding of the adhesion of organic materials, such as adhesives and paints, to these surfaces. In this perspective, methanol is representative for the hydroxyl functionality of the polymer.

On the basis of experiments it has been suggested that the molecular (non-dissociative) adsorption dominates the adsorption mechanism [11, 13, 14] when methanol is adsorbed at the Al_2O_3 surface under ultra-high vacuum (UHV) conditions. It has been proposed that methanol chemisorbs through the interaction of the methanol oxygen lone pair with substrate aluminium atoms (cations) [11, 13]. Our investigation focuses on the energetics of and the changes to the atomic geometry and electronic structure that result from the adsorption of methanol at the α-$Al_2O_3(0001)$ surface. To determine the orientation of the methanol molecule on the α-$Al_2O_3(0001)$ surface we have, in addition to a geometry optimization, calculated the dependence of the total energy on the methanol angle with the surface.

2. Computational details

Experiments [11, 13, 14] indicate that the adsorption of methanol on α-$Al_2O_3(0001)$ is dominated by chemisorption. The distance from the most active part of the molecule to the surface (in our preliminary study found to be approximately 2 Å) is such that long-range interactions, e.g., the dispersion interaction [21], are expected to not give any significant contribution to the binding. Thus we can rely on a traditional semi-local implementation of DFT, using the generalized gradient approximation (GGA) for the exchange–correlation functional.

The calculations presented here are performed using the DACAPO DFT code [22], employing the Vanderbilt ultrasoft pseudopotentials [23], and the GGA Perdew–Wang 91 (PW91) parametrization [24] of the exchange–correlation energy. For comparison a number of energies have also been calculated in the two revised Perdew–Burke–Ernzerhof GGA parametrizations revPBE by Zhang and Yang [26] and RPBE by Hammer, Hansen, and Nørskov [25]. The Kohn–Sham wavefunctions are expanded in a plane wave basis, with a 400 eV energy cut-off.

The clean α-$Al_2O_3(0001)$ surface is modelled by a slab periodically repeated in all directions, with four layers of oxygen, keeping the bottom layer of oxygen and aluminium frozen in the bulk geometry. To reduce interactions between the periodically repeated images of the slab in the [0001] direction the slabs are separated by 15 Å of vacuum. In the (1×1) surface unit cell we use a $4 \times 4 \times 1$ mesh of Monkhorst–Pack [27] special k-points to describe the Brillouin zone. Tests with larger vacuum and slab thickness, higher cut-off energy and denser k-point sampling showed negligible changes to the energies and structural parameters. To investigate how the adsorption of methanol changes with coverage, (1×1), (2×1) and (2×2) unit cells of α-$Al_2O_3(0001)$ are employed, with k-point sampling and convergence criteria appropriately modified for the two larger surface unit cells.

In our calculations we place the molecules on one side of the slab only, and allow the atoms of both the adsorbate and of the corresponding slab surface to relax. We do not include symmetry constraints in the structural optimization. The artificial electric field created by the asymmetry of the system (also for the clean but structurally relaxed surface slab) is compensated by a self-consistently determined dipole correction applied in the vacuum region [28, 29].

This dipole correction, in combination with the 15 Å vacuum region, we find is sufficient to cancel the surface dipole. The atomic positions of the surface structure and of the CH_3OH molecules are found by locally minimizing the Hellmann–Feynman forces until the remaining total force on the unconstrained atoms is less than 0.05 eV $Å^{-1}$. For the relaxation of the atomic positions a preconditioned quasi-Newton method based on the Broyden–Fletcher–Goldfarb–Shanno algorithm [30] is used.

The adsorption energy per methanol molecule is calculated from

$$E_{\mathrm{ads}} = -(E_{\mathrm{SM}} - E_{\mathrm{S}} - E_{\mathrm{M}}), \tag{1}$$

where E_{SM} is the total energy of the α-Al_2O_3 slab with adsorbed methanol, E_{S} the energy of a clean slab of α-Al_2O_3, and E_{M} the energy of an isolated methanol molecule. With this definition, a positive adsorption energy indicates stabilization. All calculations are carried out at zero temperature, and the zero-point vibration is not taken into account. Thus the adsorption energy calculated from (1) does not include contributions from entropy.

3. Results and discussion

In this section we present our results for the adsorption of CH_3OH at the α-Al_2O_3(0001) surface, as well as the structure of the clean α-Al_2O_3(0001) surface and the gas-phase CH_3OH. We assume that the adsorption of methanol does not change the surface termination of α-Al_2O_3 (0001). We calculate and discuss how both the relaxation of the surface atom positions and the adsorbate relaxation contribute to the adsorption energy.

3.1. The clean α-Al_2O_3(0001) surface and gas phase CH_3OH

As a first step in our study, we investigate the properties of the clean α-Al_2O_3(0001) surface and the free (gas phase) methanol molecule. The bulk structure of α-Al_2O_3 is rhombohedral with a $D_{3d}^6(R\bar{3}c)$ symmetry and two Al_2O_3 formula units per primitive unit cell [31]. Following the approach described in [32] and section 2 we determine the calculated (compared to experimentally determined [33]) lattice parameters $a_0 = 5.173$ Å (5.128 Å) and $\alpha = 55.28°$ (55.28°) with internal Wyckoff positions [31] of Al, respectively O, within the unit cell $w = 0.3523$ (0.3520) and $u = 0.5561$ (0.555). These values are in good agreement with the experiments by Lee and Lagerlof [33] and previous DFT calculations [4, 34]. The calculated bulk modulus $B_0 = 228.4$ GPa is smaller than the experimental value 254 GPa by 10%.

The stacking sequence of α-Al_2O_3 along the [0001] direction is R–Al–Al–O_3–R, where R represents the continuing sequence. The (0001) surfaces can be obtained by cleaving the crystal between any of these layers, i.e., three chemically distinct (0001)-plane terminations may be produced. Previous theoretical and experimental studies have shown that under UHV conditions the Al-terminated surface obtained by cleaving between two Al sub-layers is the most stable one [10, 34–37].

Figure 1 shows a schematic side and top view of the Al-terminated α-Al_2O_3(0001) surface with the (1×1) surface unit cell indicated. The calculated surface relaxations for the first four layers are listed in table 1, and are in good agreement with previous calculations [4, 10, 37]. The surface Al atoms undergo large relaxations, leaving them almost coplanar with the surface O layer. The relaxations below the top layer are also significant, and show the necessity of using a relatively thick slab for a good description of the α-Al_2O_3(0001) surface. The discrepancies between the theoretical and the experimental values have been attributed to the presence of hydrogen on the experimentally observed surfaces [37].

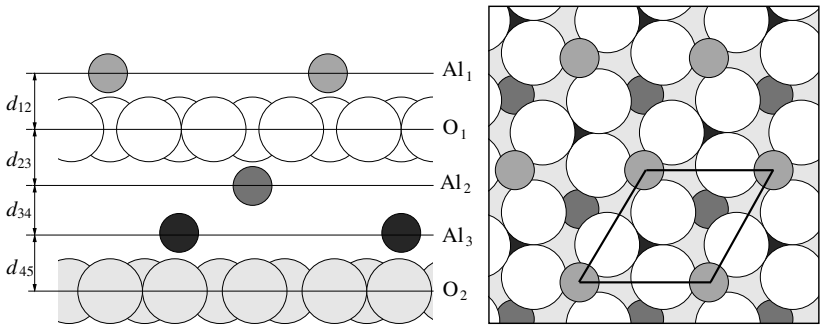

Figure 1. Schematic side and top view of the α-$Al_2O_3(0001)$ surface terminated by half a layer of aluminium. The large circles represent oxygen atoms. The (1×1) hexagonal surface unit cell is shown.

Table 1. Relaxations of the outermost atomic layers of the α-$Al_2O_3(0001)$ surface given in percentage deviation from the bulk structure. The PW91 parametrization of the exchange–correlation energy is used. Distances Δd_{ij} are defined in figure 1.

	Theory			Expt
	This work	[4]	[34]	[38]
$\Delta d_{12}(\%)$	−84.5	−85.5	−87.4	−51
$\Delta d_{23}(\%)$	+3.5	+3.2	+3.1	+16
$\Delta d_{34}(\%)$	−45.8	−45.4	−41.7	−29
$\Delta d_{45}(\%)$	+19.4	+19.8	+18.9	+20

In table 2 we list the geometry of the gas-phase methanol molecule as found in our calculations. We find the bond lengths and bond angles to be in excellent agreement with the experimental values of [39].

3.2. Adsorption geometries and energetics

A number of quantities may be used for describing methanol adsorption on α-$Al_2O_3(0001)$. The most immediate ones are the adsorption energy and the positional changes to the adsorbate and surface geometry upon adsorption. The adsorption energy is usually affected not only by electronic interactions in and between the adsorbate and the surface, as described for methanol on α-$Al_2O_3(0001)$ in section 3.3, but also by the energetic cost of changing the atomic geometry (deformation) of the surface and the adsorbate upon adsorption. These energy contributions to the adsorption energy are discussed below.

The adsorption of methanol was studied by initially placing the molecule with its O atom above a surface Al atom and performing a complete optimization of the adsorbate–surface geometry. We used several different initial orientations of the methanol molecule, to avoid any risk of the geometry getting stuck in a local energy minimum. The coverage dependence of methanol adsorption was studied by considering adsorption at coverages $\Theta = 1/4$ monolayers (ML), 1/2 ML, and 1 ML. Here the coverage Θ is defined with reference to the surface aluminium layer, so that $\Theta = 1$ ML corresponds to one adsorbed molecule per surface aluminium atom. At $\Theta = 1/4$ ML the closest distance between any two atoms of neighbouring methanol molecules is 7.4 Å, sufficiently far apart for the molecules to be considered 'isolated' if any indirect interaction through the surface is neglected.

We tested whether our 15 Å vacuum region and the dipole correction applied are sufficient to overcome the effect of the surface dipole at the bottom of the slab (the bulk-truncated frozen

Table 2. Adsorption energies and selected structural data for methanol adsorbed at the α-Al_2O_3(0001) surface at three different coverages. Some of the structural parameters are depicted in figure 2. The parameter $r_{Al-O_{ads}}$ is the bond length between the methanol O and the nearest surface Al, h is the height of Al bounded to a methanol molecule above the average position of the layer of top O atoms, and r_{H-O_s} is the shortest distance between the H of the molecule OH group and an O atom at the surface. ϕ_{CO} is the tilt angle of the C–O axis away from the surface normal, and ϕ_{COH} is the tilt angle of the COH plane with respect to the surface plane. All calculations were carried out in the PW91 parametrization of the exchange–correlation functional unless explicitly noted.

	Expt [39]	Theory			
Θ (ML)	Free	Free	1/4	1/2	1
Internal geometry of the methanol molecule					
r_{C-O} (Å)	1.429	1.43	1.45	1.45	1.44
r_{O-H} (Å)	0.975	0.98	1.00	1.00	1.02
r_{C-H} (Å)	1.098	1.10	1.10	1.09	1.10
∠COH (deg)	107.6	109	110	110	111
∠OCH (deg)	—	112	110	109	110
	—	112	109	109	109
	—	107	107	107	108
Geometry of the adsorption bonds					
h (Å)	—	0.13	0.43	0.42	0.32
$r_{Al-Oads}$ (Å)	—	—	1.93	1.95	2.00
r_{H-Os} (Å)	—	—	2.03	1.91	1.77
ϕ_{CO} (deg)	—	—	57	57	57
ϕ_{COH} (deg)	—	—	34	36	39
Adsorption energy contributions					
E_{ads} (eV)	—	—	1.23	1.16	1.03
Methanol deform. (eV)	—	—	0.04	0.03	0.03
Surface deform. (eV)	—	—	0.29	0.29	0.15
E_{ads} surf. undeform. (eV)	—	—	0.85	0.86	0.87
E_{ads} (RPBE) (eV)	—	—	0.97	0.88	0.71
E_{ads} (revPBE) (eV)	—	—	0.97	0.88	0.70

surface). We found that with methanol adsorbed on the top of the slab, the adsorption energy only changes by 0.009 eV when instead using a slab with the bottom of the slab in the relaxed geometry. Having both sides of the slab in the relaxed structure requires a thicker slab for convergence in number of atomic layers. We thus for all further calculations keep the bottom of the slab in the bulk-truncated structure.

Figure 2 shows a schematic top and side view of the optimum adsorption geometry found in our calculations, and in table 2 the calculated adsorption energies and selected bond lengths and angles are listed.

We find that methanol adsorbs with its O atom (denoted O_{ads}) approximately on top of a surface Al atom, with the methyl group pointing away from the surface and the OH group pointing toward one of the three equivalent surface O atoms (denoted O_s) around the Al adsorption site. The methanol C–O axis is tilted away from the surface normal by $\phi_{CO} = 57°$ at the coverages considered here. Experiments indicate that the C–O axis is indeed tilted away from the surface normal on Al_2O_3 [11, 14]; however, to the best of our knowledge, no detailed experimental structural data are yet available for this system.

The methanol molecule is laterally displaced from the precise Al atop site by ∼0.6 Å towards the surface O_s atom; see figure 2. The OH group is oriented towards O_s, and the

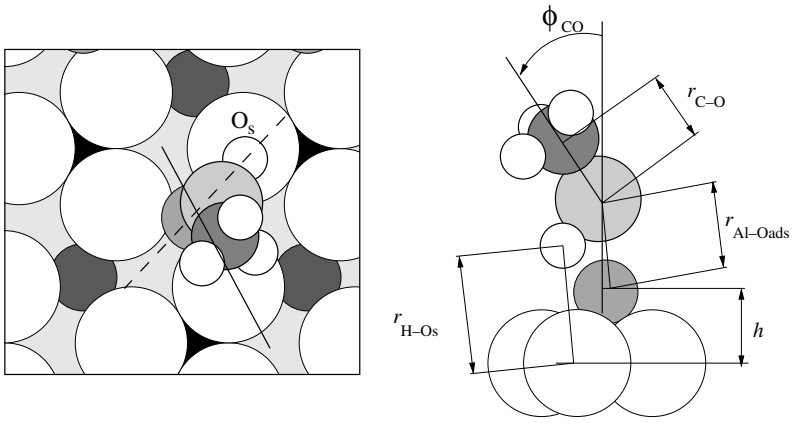

Figure 2. Schematic top (left panel) and side view (right panel) of the stable configuration of the CH_3OH molecule on the α-$Al_2O_3(0001)$ surface. In the left panel, the full and dashed lines indicate the positions of the planes used for the cross sections of the electron density difference displayed in figure 4. In the right panel some of the structural parameters of table 2 are defined.

O_{ads}–H bond length is elongated by 0.02–0.04 Å compared to the gas phase value (table 2). This suggests that the H–O_s interaction is significant. Further evidence of this interaction is that the H–O_s distances, 1.77–2.03 Å, are significantly shorter than the sum of the respective van der Waals radii (2.72 Å, [40]).

Apart from the above-mentioned elongation of the molecular O_{ads}–H bond, the geometry of the molecule is only moderately affected by the adsorption. The COH angle opens up compared to the gas phase value by 1°–2°, and the C–O_{ads} bond lengths are increased, but by no more than 0.02 Å. There are no changes to the C–H bond lengths, but the HCH angles open up by $\sim$2°.

As the coverage is increased from $\Theta = 1/4$ ML to 1 ML we find a slight change in the geometry of the adsorbed methanol atom. The tilt angle ϕ_{COH} between the molecular dipole plane (the COH plane) and the surface plane changes from 34° to 39°, and the Al–O_{ads} distance is elongated from 1.93 to 2.00 Å. These bond lengths are comparable to the two Al–O bonds in the α-Al_2O_3 bulk crystal, in our calculations 1.87 and 1.99 Å, and to Al–O_{ads} distances reported in DFT studies of adsorption of water molecules onto the α-$Al_2O_3(0001)$ surface [8, 10].

Whereas the geometrical changes to the methanol molecule are small, adsorption of methanol results in significant surface relaxations in α-$Al_2O_3(0001)$. The most prominent change is the displacement of the Al atoms along the surface normal. The Al atoms directly beneath CH_3OH relax outwards by 0.19–0.30 Å. At $\Theta < 1$ ML, the surface Al atoms *without* methanol bounded to them descend into the outermost O layer, so that at $\Theta = 1/4$ ML they are coplanar with the O layer (less than 0.05 Å above the O layer) and at $\Theta = 1/2$ ML they are positioned slightly below the O layer (-0.14 Å). Similar relaxation effects have been reported in theoretical studies of the adsorption of water [10, 8] and HCl [7] at the α-$Al_2O_3(0001)$ surface.

To study the sensitivity of the adsorption geometry to positional perturbations (e.g., at finite temperatures) additional static calculations were carried out, changing the orientation of the molecule with the O_{ads} position kept fixed. In the left panel of figure 3 we plot the variation of the adsorption energy as a function of the C–O axis tilt angle, ϕ_{CO}. A tilt angle of 0° corresponds to the C–O axis being parallel to the surface normal. The plot has a minimum at $\phi_{CO} \approx 60°$, confirming the result of our geometry optimization.

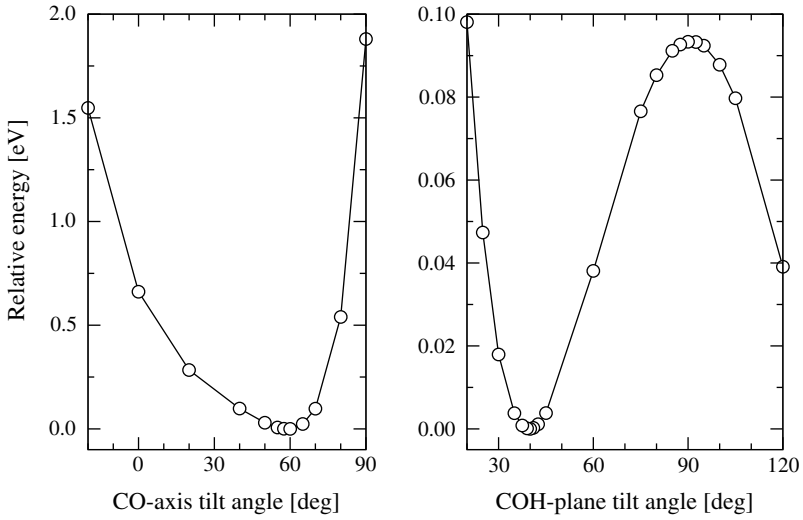

Figure 3. The variation of the total energy for CH_3OH on α-Al_2O_3(0001) as a function of the tilt angle of the C–O axis (left panel) and the COH plane (right panel). In the left panel a tilt angle of 0° corresponds to the C–O axis parallel to the surface normal. In the right panel a tilt angle of 90° corresponds to upright CH_3OH with the O end down. The calculations were carried out at $\Theta = 1$ ML.

We found that changing the direction of the C–O axis even slightly causes a huge energetic cost. Exploring the variation of the adsorption energy as the COH-plane tilt angle (ϕ_{COH}) is changed, we therefore kept $\phi_{CO} = 60°$ fixed. In this case $\phi_{COH} = 0°$ corresponds to the COH plane parallel to the surface, while at $\phi_{COH} = 90°$ the COH plane is in the plane of the surface normal. The results, displayed in the right panel of figure 3, show an energy minimum at about $\phi_{COH} \approx 40°$, consistent with our optimized adsorption geometry. However, the energy variation with ϕ_{COH} is much smaller than the dependence on ϕ_{CO}. This agrees with our finding (in table 2) that ϕ_{COH} does change, although only by a few degrees, as the methanol coverage is increased. We note that at $\phi_{COH} = 90°$ the energy is at its maximum, reflecting the fact that upright methanol molecules are not only energetically unfavourable, compared to the 40° tilt, but also unstable.

The energetic gain of adsorbing one methanol molecule, relative to the clean α-Al_2O_3(0001) and the gas-phase methanol molecule, is approximately 1 eV per molecule (table 2). Methanol is thus rather strongly bound to the surface. As noted above, methanol adsorption induces significant surface deformations (whereas the deformation of the methanol molecule is small). The net adsorption energy is thus composed of both an energetic cost of deforming the surface (and a small cost of deforming the molecule), as well as a gain from the interaction in the electronic charge density, resulting in a net energy gain.

We calculated the energetic cost of the surface and molecule deformation (table 2) and found the cost of surface deformations to be 0.29 eV per molecule at $\Theta < 1$. This is about one-quarter of the net adsorption energy, thus the surface deformation is a very important part of the adsorption energetics. For denser coverage ($\Theta = 1$) the surface deformation is less, and the energetic cost at 0.15 eV per molecule is not quite as important, although still not negligible. The deformation of methanol has a smaller energy cost of only 0.03–0.04 eV per molecule and is at $\Theta < 1$ negligible compared to the surface deformation cost.

A different way of estimating the importance of surface relaxations is to calculate the adsorption energy of methanol adsorbed at a frozen surface, i.e., with all surface atoms frozen

in the clean-slab positions. At $\Theta = 1/4$ ML we calculated a (frozen surface) adsorption energy of 0.85 eV/molecule, which is a reduction of 0.38 eV/molecule compared to the situation when surface relaxations are included. On the *frozen* surface the adsorption energies at $\Theta = 1$ ML and 1/4 ML are almost equivalent, differing by only 0.02 eV/molecule.

The adsorption energy (on the deformed surface) decreases with coverage from 1.23 eV/molecule at $\Theta = 1/4$ ML to 1.03 eV/molecule at $\Theta = 1$ ML, indicating repulsive adsorbate–adsorbate interactions on the surface. Since methanol adsorption induces significant surface deformations the repulsion may be caused by indirect adsorbate interactions mediated by the local deformation of the surface [41]. This is strongly supported by the fact that the frozen-surface adsorption energies do not change with coverage.

The molecules adsorbed on the surface may interact with neighbouring adsorbed molecules indirectly, through the deformation of the surface as discussed above, but also more directly, e.g., by mutually imposed static changes to the electron structure or by dispersive interactions. Below we discuss contributions from these short- and long-range direct interactions.

In the 2×2 structure the adsorbates are too far apart (>7 Å) for the direct interactions to have any significant influence on the adsorbate repulsion, compared to the size of the indirect interactions (0.29 eV cost per adsorbed molecule, table 2). This includes the long-range, dispersive interactions. In the 2×2 structure direct interactions can thus be ignored.

In the denser 1×1 and 1×2 structures the shortest distance between atoms in two neighbouring molecules is 2.7 Å. Thus direct interaction could possibly influence the adsorbate repulsion. The *short-ranged* part of the direct interaction between these molecules (as calculated within the GGA approximation) shows an attraction of 0.03 eV per pair interaction. In the 1×1 structure with six nearest neighbours per adsorbate the short-range part of the direct interaction thus provides a gain in adsorption energy of approximately 0.09 eV per adsorbate, compared to that of the 2×2 structure or even less dense structures. In the 1×2 structure, with only two nearest neighbours per adsorbate, this gain is merely 0.03 eV per adsorbate. Although in general the *long-range* interactions may also become important at the 2.7 Å distance, already the surface relaxations contribute an energy repulsion much larger than any realistic value of the (direct) long-range interaction between the methanol molecules. We therefore neglect any dispersive direct interaction between the molecules also in the 1×1 and 1×2 structures.

The deformation of the surface at adsorption carries a significant energy cost, at any coverage. For adsorption to still be favourable over no adsorption the energy gain due to changes in the electron structure must more than overcome this deformation cost. From the net adsorption energy E_{ads} and the costs of deforming the surface and the methanol molecule (table 2) the gross interface electron-density-related energy gain E_{gross} is calculated to be 1.56, 1.48, and 1.21 eV per molecule for coverages 1/4, 1/2, and 1 ML. Although the dense 1×1 structure is the structure most favoured both by the direct adsorbate–adsorbate interaction (largest gain in adsorption energy), and by the indirect interaction through the deformation of the surface (smallest cost of deformation), this is not sufficient to overcome the E_{gross} advantage of the 2×2 structure.

All adsorption energy and geometry calculations mentioned above were found by using the PW91 approximation for the exchange–correlation energy. To test our results we also carried out some of the calculations in the revPBE and RPBE approximation (table 2). Although all values of E_{ads} are found to be smaller using revPBE and RPBE the changes in magnitude with coverage are very close to those of the PW91 calculations. Thus the calculations using the revPBE or RPBE approximation support our finding that on α-Al_2O_3(0001) methanol adsorbs in a 2×2 structure rather than in the denser 1×2 or 1×1 structures. A similar decrease in adsorption energy going from the PW91 to the revPBE and RPBE approximations is also seen for O, CO, and NO adsorption on late transition metal surfaces [25].

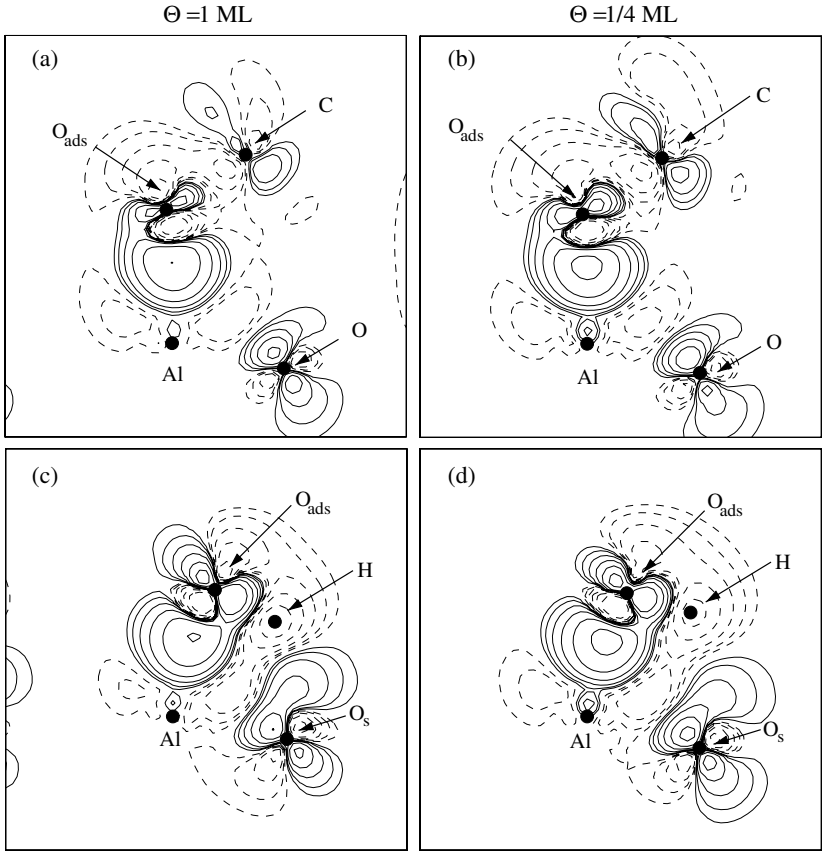

Figure 4. Contour plots of the electron density difference $\Delta n(\mathbf{r})$. Panels (a) and (b) show a cut through a plane containing one surface Al and O atom, and the methanol O and C atoms. Panels (c) and (d) show a cut through the plane containing one surface Al and the O_s atom, and the methanol O and H atoms, where the H atom is the one belonging to the methanol OH-group. Solid (dashed) lines indicate gain (loss) of electron density. The contours are drawn at densities $\Delta n = \pm 0.005 \times 2^k$ e Å^{-3} for $k = 0, 1, 2, 3, 4, 5$.

3.3. Adsorbate-induced changes to the electronic structure

Insight into the nature of the bonding of methanol at the α-Al_2O_3 is gained from the change in the electron density distribution as a result of the adsorbate bonding. To this end, we have calculated the electron density difference, $\Delta n(\mathbf{r})$, defined by

$$\Delta n(\mathbf{r}) = n^{\mathrm{SM}}(\mathbf{r}) - n^{\mathrm{S}}(\mathbf{r}) - n^{\mathrm{M}}(\mathbf{r}). \tag{2}$$

Here, n^{SM} is the electron density of the adsorption system, and n^{S} and n^{M} the electron density of the clean slab and a free methanol layer, respectively. The atomic geometry of the relaxed adsorption system is kept in the calculation of n^{S} and n^{M}. The quantity Δn gives a measure of the charge rearrangements induced by the adsorption, with a positive (negative) value in regions with a gain (loss) in electron density.

In figure 4 we display contour plots of cross sections of Δn. We chose two different planes for these cross sections. Left panels show Δn at $\Theta = 1$ ML, right panels $\Theta = 1/4$ ML. Figures 4(a) and (b) show a cut through the plane containing the O_{ads} and C atoms of the molecule, the Al bound to O_{ads}, and one of the surface O atoms. In figures 4(c) and (d) the

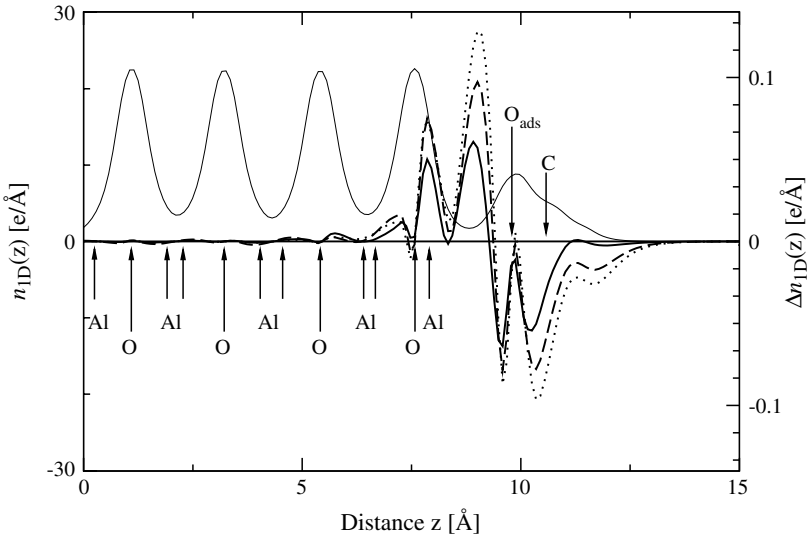

Figure 5. Profiles of the total electron density, n_{1D}, (at $\Theta = 1$ ML, thin solid line) and electron density difference, Δn_{1D}, across the slab. The thick dotted, dashed and solid lines represent Δn_{1D} at coverage $\Theta = 1/4$, $1/2$, and 1 ML, respectively. The zero-point of the z-axis is arbitrarily set to the bottom of the slab used. The positions of the Al and O layers of the slab and the O_{ads} and C atoms of the methanol molecule are indicated.

cut is through the plane defined by the methanol O_{ads} and H atoms, the Al bound to O_{ads}, and one of the surface O atoms. We first of all note the similarity in the shape of the difference densities for coverages $\Theta = 1$ ML and $1/4$ ML. This suggests that the nature of the bonding is similar.

Adsorption of methanol mainly perturbs the part of the electron density related to the topmost layer of the slab. This can most easily be seen from the electron density difference profile, $\Delta n_{1D}(z)$, displayed in figure 5 for $\Theta = 1$ ML. The figure shows that there is a net gain in electron density in the surface and interface region, and a loss of electron density in the region associated with the molecule. Thus, a small charge transfer from the molecule to the surface takes place at the adsorption (for $\Theta = 1$ ML the transfer is $\sim 0.04|e|$ as estimated by integrating $\Delta n_{1D}(z)$ in figure 5 up to its minimum above the top Al atom). The plots of $\Delta n_{1D}(z)$ for $\Theta = 1/4$, $1/2$, and 1 ML are similar in shape. Each curve represents the electron density change on one methanol molecule. We see that at low coverage ($\Theta = 1/4$ ML) the redistribution of charge over the molecule is more pronounced than at higher coverages. This is consistent with the findings in figure 4.

Returning to the cross section plots of Δn in figures 4(a)–(d) we see that the electron density gain in the interface region, seen in figure 5, is the result of a pronounced accumulation of electron density in the region between the O_{ads} and Al atoms. The accumulated electron density mainly comes from the region close to the O_{ads} atom of the methanol molecule. This redistribution of electrons is suggestive of the formation of a donor–acceptor bond, where the methanol O lone pair donates electron density to the acceptor Al [1].

In the surface region, the most prominent change in the electron density is a redistribution of electron density around the surface O atoms. This is clearly a repolarization in response to the adsorption. There is a depletion of electron density in the region between the surface O atoms and the O_{ads} atom, indicating an O–O_{ads} repulsive interaction. The decreased electron

density at the H atom, as seen in figures 4(c) and (d), is consistent with the elongation of the O_{ads}–H bond, and gives further evidence that the H–O_s bond contributes to the bonding of methanol at the α-$Al_2O_3(0001)$ surface.

The redistribution of the electron density may be quantified by assigning charge to the individual atoms according to the Bader space-partitioning scheme [42]. The analysis shows that upon adsorption the surface O atom closest to the hydroxyl H atom loses 0.04–0.06 electrons compared to the same atom in the clean α-$Al_2O_3(0001)$, with the largest loss at occurring at $\Theta = 1$ ML. The analysis also shows that there is no such loss when simply deforming the surface to its adsorption geometry without adding the molecule; the actual adsorption of methanol is essential for the change in assigned charge to this surface O atom. In contrast, the change in charge is insignificant at the Al atom directly beneath the molecule, both after obtaining the adsorption geometry and after adsorbing the methanol molecule.

As mentioned in the previous section, the gross interface electron-density-related energy gain E_{gross} is higher for $\Theta = 1/4$ ML than for $\Theta = 1$ ML. This is consistent with the somewhat larger magnitude of the induced density for $\Theta = 1/4$ ML compared to $\Theta = 1$ ML, seen in figure 4.

4. Summary and conclusions

We have applied first-principles density-functional theory calculations to study the adsorption of methanol on α-$Al_2O_3(0001)$ at coverages $\Theta = 1/4$ ML, $\Theta = 1/2$ ML and 1 ML.

We find that methanol bonds to the surface Al atoms via the methanol O atom. Plots of the electron density difference, figure 4, indicate that the adsorption mechanism is a donor–acceptor interaction, where the methanol lone pair orbital donates electron density to the surface Al cations. This is the expected adsorption mechanism for alcohols at wide bandgap insulator surfaces, such as α-$Al_2O_3(0001)$ [1].

In addition to this mechanism, we find evidence that the interaction of the hydroxyl hydrogen with a surface oxygen atom also contributes to the bonding. The methanol molecule is preferentially oriented with the C–O axis tilted away from the surface normal, and the OH group oriented toward one of the surface O atoms. The elongated O_{ads}–H bonds, the short H–O_s nearest-nearest-neighbour distance, table 2, and the depletion of electron density around the H atom, figure 4, is evidence of a significant H–O_s interaction. A similar adsorption mechanism has been proposed for adsorption of methanol on NiO_x/Ni{110} [43].

The adsorption of methanol results in a significant relaxation of the surface structure. In particular, the surface Al atoms are displaced along the surface normal so that the Al bounded to methanol molecules increase their distance to the oxygen layer, and the Al not bounded to methanol descend into the topmost O layer. Our calculations show the importance of taking surface relaxation into account: At $\Theta = 1/4$ ML about 30% of the adsorption energy can be attributed to the relaxation effects. The surface deformation results in repulsive adsorbate interactions at the coverages considered here, so that the adsorption energy decreases from $E_{ads} = 1.23$ eV/molecule at $\Theta = 1/4$ ML to $E_{ads} = 1.03$ eV/molecule at $\Theta = 1$ ML.

Acknowledgments

This work was partly carried out within ‘Light metal surface science’, a joint project between SINTEF and NTNU, financed by The Norwegian Research Council (NFR), Hydro Aluminium, Profillakkering AS, Norsk Industrilakkering AS, Fundamus AS, Jotun Powder Coatings AS, and DuPont Powder Coating. NFR and NTNU are acknowledged for support

through computing time at the Norwegian High Performance Computing Centre (NOTUR). ØB acknowledges financial support from NordForsk through a mobility scholarship. The work of ES was supported by the Swedish Research Council (VR) and the Swedish Foundation for Strategic Research (SSF) through the consortium ATOMICS.

References

[1] Henrich V E and Cox P A 1994 *The Surface Science of Metal Oxides* (Cambridge: Cambridge University Press)
[2] Chorkendorff I and Niemantsverdriet J W 2003 *Concepts of Modern Catalysis and Kinetics* (Weinheim: Wiley–VCH)
[3] Lodziana Z and Nørskov J K 2003 *J. Chem. Phys.* **118** 11179
[4] Ruberto C, Yourdshahyan Y and Lundqvist B I 2003 *Phys. Rev.* B **67** 195412
[5] Lodziana Z and Nørskov J K 2001 *J. Chem. Phys.* **115** 11261
[6] Nelson C E, Elam J W, Tolbert M A and George S M 2001 *Appl. Surf. Sci.* **21** 171
[7] Alavi S and Thompson D L 2003 *J. Phys. Chem.* B **107** 186
[8] Moskaleva L V, Nasluzov V A, Chen Z-X and Rösch N 2004 *J. Phys. Chem. Chem. Phys.* **6** 4505
[9] Elam J W, Nelson C E and Cameron M A 1998 *J. Phys. Chem.* B **102** 7008
[10] Hass K C, Schneider W F, Curioni A and Andreoni W 2000 *J. Phys. Chem.* B **104** 5527
[11] Frederick B G, Apai G and Rhodin T N 1992 *Surf. Sci.* **277** 337
[12] Xu M, Lunsford J H, Goodman D W and Bhattacharyya A 1997 *Appl. Catal.* A **149** 289
[13] Nishimura S Y, Gibbons R F and Tro N J 1998 *J. Phys. Chem.* B **102** 6831
[14] Schauermann S, Hoffman J, Johánek V and Libuda J 2002 *J. Phys. Chem. Chem. Phys.* **4** 3909
[15] Borck Ø and Schröder E 2003 *ATB Metallurgie* **43** 342
[16] Shi B C and Davis B H 1995 *J. Catal.* **157** 359
[17] Waugh K C 1992 *Catal. Today* **15** 51
[18] Shen W-J, Ichihashi Y and Matsumura Y 2002 *Catal. Lett.* **79** 125
[19] Tatibouët J M 1997 *Appl. Catal.* A **148** 213
[20] Badlani M and Wachs I E 2001 *Catal. Lett.* **75** 137
[21] Langreth D C, Dion M, Rydberg H, Schröder E, Hyldgaard P and Lundqvist B I 2005 *Int. J. Quantum Chem.* **101** 599
[22] http://dcwww.fysik.dtu.dk/campos/Dacapo/
[23] Vanderbilt D 1990 *Phys. Rev.* B **41** 7892
[24] Perdew J P, Chevary J A, Vosko S H, Jackson K A, Pederson M R, Singh D J and Fiolhais C 1992 *Phys. Rev.* B **46** 6671
[25] Hammer B, Hansen L B and Nørskov J K 1999 *Phys. Rev.* B **59** 7413
[26] Zhang Y and Yang W 1998 *Phys. Rev. Lett.* **80** 890
[27] Monkhorst H J and Pack J D 1976 *Phys. Rev.* B **13** 5188
[28] Neugebauer J and Scheffler M 1992 *Phys. Rev.* B **46** 16067
[29] Bengtsson L 1999 *Phys. Rev.* B **59** 12301
[30] Press W, Flannery B, Teukolsky S A and Vetterling W T 1992 *Numerical Recipes in Fortran* 2nd edn (Cambridge: Cambridge University Press)
[31] Wyckoff R W G 1964 *Crystal Structures* 2nd edn (New York: Interscience)
[32] Ziambaras E and Schröder E 2003 *Phys. Rev.* B **68** 064112
[33] Lee W E and Lagerlof K P 1985 *J. Electron Microsc. Tech.* **2** 247
[34] Verdozzi C, Jennison D R, Schultz P A and Sears M P 1999 *Phys. Rev. Lett.* **82** 799
[35] Ahn J and Rabalais J W 1997 *Surf. Sci.* **388** 121
[36] Toofan J and Wilson P R 1998 *Surf. Sci.* **401** 162
[37] Wang X-G, Chaka A and Scheffler M 2000 *Phys. Rev. Lett.* **84** 3650
[38] Guenard P 1997 *Surf. Rev. Lett.* **5** 321
[39] Iijima T 1989 *J. Mol. Struct.* **212** 137
[40] Values taken from WebElements (http://www.webelements.com)
[41] Einstein T L 1996 *Handbook in Surface Science* vol 1, ed W N Unertl (Amsterdam: Elsevier) chapter 11
[42] Bader R F W 1990 *Atoms in Molecules. A Quantum Theory* (Oxford: Clarendon)
[43] Sanders H E, Gardner P and King D A 1995 *Surf. Sci.* **331** 1496

Paper II

Adsorption of methanol and methoxy on the α-Cr_2O_3(0001) surface

Ø. Borck and E. Schröder

Preprint 2006

Adsorption of methanol and methoxy on the α-Cr_2O_3(0001) surface

Øyvind Borck[1,2] and Elsebeth Schröder[2]

[1] *Department of Physics, Norwegian University of Science and Technology, NO–7034 Trondheim, Norway*
[2] *Department of Applied Physics, Chalmers University of Technology, SE–41296 Göteborg, Sweden*

(Dated: March 7, 2006)

We present density functional theory calculations of the molecular adsorption of methanol and methoxy at the Cr-terminated α-Cr_2O_3(0001) surface. We report on the equilibrium geometries of methanol and methoxy upon adsorption, and discuss the bonding of these molecules to the surface. We find that methanol adsorbs with its O atom situated above a three-fold coordinated hollow site in the surface O layer at a distance of 2.12 Å from the nearest-neighbour Cr atom, and with a calculated adsorption energy of 0.82 eV. For the methoxy molecule we find the optimum adsorption geometry to be with the methoxy O on top of a Cr atom and with the C-O axis tilted away from the surface normal by $\sim 55^\circ$. Methoxy is strongly bound at the surface with an estimated adsorption energy of 3.3 eV.

PACS numbers:

I. INTRODUCTION

The chromium oxides find a wide variety of uses in technological applications, as catalysts (polymerization of ethylene,[1,2] hydrogenation, NO_x reduction, etc.), gas sensors, protective layer (corrosion/resistance promotion, wear resistance, coating/anti-wear protection, stainless/steel passivation layer), adhesion promoter, and magnetic recording media. Aluminium in construction materials are aluminum alloys, whose surfaces are often treated by a chromate conversion coating (CCC) process.[3] The CCC improves the corrosive resistance and adhesive properties of the metal surface.[3,4] The coating can be applied by spraying, or by dipping the aluminium product in an aqueous acidic solution containing chromium salts.[3] The precise composition of the coating that results from this treatment depends on several factors, including the preceding surface preparation, the composition of the bath, and the presence of intermetallic particles in the substrate, though it is known that Cr_2O_3 is a major constituent of the outermost part of the coating. Unfortunately, the hexavalent chromium found in the solution presents severe health and environmental concerns. In either case, the interaction with organic molecules is of interest.

Searching for alternatives to CCC a detailed knowledge of how CCC improves adhesion would be helpful. At a basic fundamental level, adhesion results from the interaction of organic polymers, e.g. epoxy resins, of the paint or adhesive with the substrate surface. The complexity of polymer-surface interactions is such that the full polymer interaction cannot be fully described on an atomic length scale. One strategy is thus to focus on how fragments of the polymer — single functional groups — interact with the surface, focusing on those fragments known or expected to have the largest influence on the adhesion of the full polymer. In this study methanol and methoxy are chosen as representative molecules.

Theoretical studies of such molecules on ionic crystals are largely lacking in the literature. We have previously[5,6] studied adsorption of methanol on α-Al_2O_3(0001), a surface which is isostructural to α-Cr_2O_3(0001), and found that the adsorption bond there is relatively strong with a pronounced ionic character in the sense that one of the atoms (methanol O) contributes electron charge to create the binding of methanol O in the stable site on top of a surface Al ion. In the present work we report on density functional theory (DFT) calculations of molecular adsorption of methanol (CH_3OH) at the α-Cr_2O_3(0001) surface. Methanol is the smallest member of the alcohols and adsorption of methanol on α-Cr_2O_3(0001) represents a prototype for understanding the interaction of hydroxyl (OH) groups in alcohols and some biological molecules with flexible oxide surfaces. Targets for our study are adsorption site and strength, nature of adsorption bond, and other characteristica of the adsorbate. It is not uncommon for the hydroxyl group to loose its hydrogen atom in a reaction with the surface, we therefore also report on the adsorption of methoxy (CH_3O) on this surface. Furthermore, it is of interest to contrast the interaction of the closed-shell methanol molecule and open-shell methoxy molecule with the α-Cr_2O_3(0001) surface.

The paper is organized as follows: A brief account of our computational method is given in Section II. In Section III we present results for bulk α-Cr_2O_3 and the clean (0001) surface. Section IV contains our results for the adsorption geometries and energies for methanol and methoxy at 1 ML and 1/4 ML and we discuss the nature of bonding between the adsorbates and the substrate. The paper is concluded with a short discussion and concluding remarks in Section V.

II. COMPUTATIONAL METHOD

The density functional theory calculations presented here are conducted using the plane-wave pseudopotential code DACAPO.[7] We employed ultrasoft pseudopotentials[8] and the generalized gradient approximation in the PW91-

parametrization.[9] In all calculations, spin-polarization is allowed for. The energy cut-off for the plane-wave expansion is 400 eV, and the irreducible Brillouin zone is sampled using the Monkhorst-Pack scheme.[10]

The α-$Cr_2O_3(0001)$ surface is represented by a slab periodically repeated in all directions, consisting of a finite number of layers of Cr-O_3-Cr that are separated by a vacuum gap. For most of the calculations on the methanol and methoxy adsorption, a slab of four layers separated by a vacuum gap of width 15 Å is used, with a (1×1) superstructure containing one molecule per surface unit cell. Defining coverage with respect to the surface Cr layer we will refer to this coverage as $\Theta = 1$ ML. Molecules are placed on one side of the slab only, and the artificial electric field created by the asymmetry of the system is compensated by a self-consistently determined dipole correction applied in the vacuum region.[11,12]

The equilibrium structures are found by locally minimizing the Hellmann-Feynman forces until the remaining total force on the unconstrained atoms is less than 0.05 eV/Å. A preconditioned quasi-Newton method based on the Broyden-Fletcher-Goldfarb-Shanno algorithm[13] is used for the structure optimization. During structure optimizations, the atoms of the bottom Cr-O_3-Cr layer of the slab are kept fixed in the bulk geometry. All other atoms are allowed to relax freely, no symmetry constraints are applied. For the (1×1) surface unit cell we employ a $4 \times 4 \times 1$ k-point mesh. The geometries of isolated (gas-phase) methanol and methoxy are optimized in fcc-cells of side length 14 Å where only the Γ-point of the Brillouin zone is sampled.

To investigate the coverage dependence of the methanol and methoxy adsorption additional calculations are carried out using a (2×2) surface unit cell corresponding to $\Theta = 1/4$ ML. Tests with larger vacuum and slab thickness, higher cutoff energy and denser k-point sampling show negligible changes in the energies and structural parameters, as described and discussed in Section IV.

The heat of formation per formula unit for the α-Cr_2O_3 bulk, ΔH_f^0, is calculated using

$$\Delta H_f^0 = -\left(E_{Cr_2O_3}^{bulk} - 2E_{Cr}^{bulk} - 3/2E_{O_2}\right) \qquad (1)$$

where $E_{Cr_2O_3}^{bulk}$, E_{Cr}^{bulk}, and E_{O_2} are the total energies of bulk α-Cr_2O_3, of bulk Cr, and of the gas phase oxygen molecule. The adsorption energy per molecule is calculated from

$$E_{ads} = -(E_{SM} - E_S - E_M)\ , \qquad (2)$$

where E_{SM} is the total energy of the α-Cr_2O_3 slab with adsorbed methanol (or methoxy), E_S is the energy of a clean slab of α-Cr_2O_3, and E_M is the energy of an isolated methanol (or methoxy) molecule. With this definition, a positive energy indicates that the adsorption is exothermic (stable).

To calculate local properties like atomic charge (ionicity) and the magnetic moment of the individual atoms

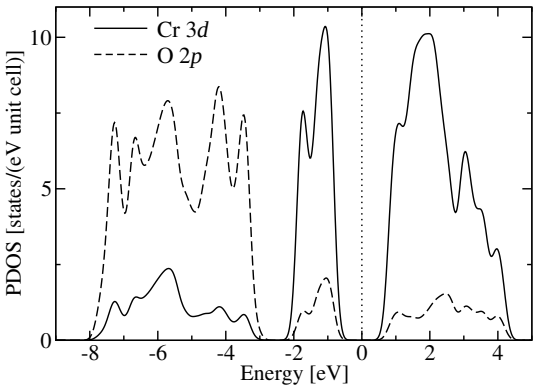

FIG. 1: Projected density of states (PDOS) for bulk Cr_2O_3. The density of states has been projected onto the $3d$ state of Cr and $2p$ state of O. The Fermi energy as calculated by DACAPO is used as the reference energy.

and to quantify charge transfer we use Bader's 'Atoms-in-Molecules' (AIM) method.[14] Here the electron density is divided into atomic regions Ω, or basins, enclosed by surfaces defined by:

$$\nabla n(\mathbf{r}) \cdot \mathbf{l} = 0\ , \qquad (3)$$

where $\mathbf{l}$ is the unit vector normal to the surface. Atomic properties are obtained by integrating over the individual basins, e.g. the charge of an atom A enclosed within basin Ω_A is obtained by integrating the electron density over Ω_A and subtracting the obtained value from the charge of the isolated atom:

$$Q_A = Z_A - \int_{\Omega_A} d\mathbf{r}\, n(\mathbf{r}) \qquad (4)$$

Similarily, the magnetic moment is calculated by integrating the difference between the spin-up and spin-down electron density over the atomic basin,

$$m_A = \int_{\Omega_A} d\mathbf{r}\ [n_\uparrow(\mathbf{r}) - n_\downarrow(\mathbf{r})] \qquad (5)$$

We use the algorithm described in Ref. 15 to decompose the electron density into Bader's atomic basins. In this scheme the accuracy of the results can be systematically improved by decreasing the grid-point separation of the FFT-grid used to represent the electron density. We used a gridpoint-separation of 0.08 Å. Test calculations indicate that this choice will result in errors in the order of 0.01 $|e|$.

III. BULK α-CR_2O_3 AND CLEAN α-$CR_2O_3(0001)$

Bulk α-Cr_2O_3, like α-Al_2O_3, crystallizes in a rhombohedral structure with the space group $D_{3d}^6(R\bar{3}c)$, and the primitive unit cell contains two formula units.[16] The crystal structure can alternatively be described as a hexagonal close-packed array of oxygens, where the Cr atoms occupy 2/3 of the interstitial octahedral sites. The Cr layer

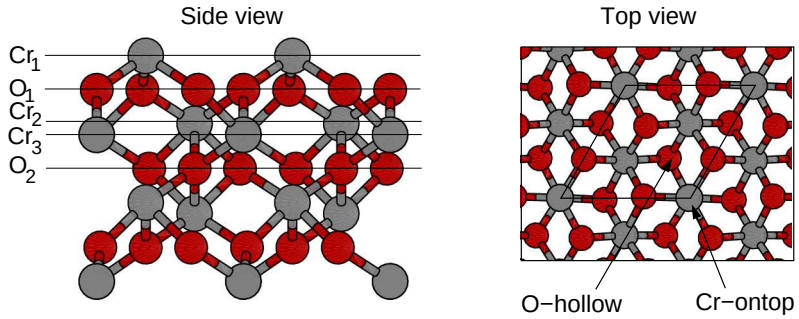

FIG. 2: Schematic side and top view of the α-Cr_2O_3(0001) surface terminated by chromium. O (Cr) atoms are shown as dark (light) circles. The sites indicated are discussed in the text.

is slightly rumpled, resulting in two distinct interatomic Cr-O distances. Below the Néel temperature $T_N \sim 310$ K,[17] α-Cr_2O_3 is an antiferromagnetic insulator with the spin sequence $+-+-$ along the threefold axis.

Table I lists calculated and experimental bulk structural properties for α-Cr_2O_3. The optimized geometry and bulk modulus have been obtained following the procedure proposed in Ref. 21. The calculated bulk properties listed in table I compare well with the experimental values, and with other GGA calculations.[22,23] The slight overestimation of the structural parameters and underestimation of the bulk modulus is a well known feature of GGA. We find that the antiferromagnetic spin-ordering yields a ground-state energy that is lower than the ferromagnetic and paramagnetic phase equilibrium energies by 0.2 eV and 1.6 eV per formula unit, respectively. In the antiferromagnetic spin-ordering we calculate the magnetic moment per Cr atom $m_{\mathrm{Cr}} = 2.66\,\mu_{\mathrm{B}}$, a result that should be compared to the experimental values 2.76 μ_{B} (Ref. 17) and 2.48 μ_{B} (Ref. 24). We find no net magnetic moment on the O atoms.

The atomic charge can be calculated by integrating the charge density over the Bader atomic basins. Doing this we find charges $Q_{\mathrm{Cr}} = +1.73\,|e|$ and $Q_{\mathrm{O}} = -1.15\,|e|$ respectively. The deviation from the formal ionicity (+3 and −2) may be interpreted as due to a covalent contribution to the bonding in α-Cr_2O_3. In comparison, in α-Al_2O_3 the charges $Q_{\mathrm{Al}} = +2.50\,|e|$ and $Q_{\mathrm{O}} = -1.67\,|e|$ are closer to the formal ionicity, the bonds in α-Al_2O_3 having more of an ionic character than in α-Cr_2O_3.

Figure 1 shows the density of states projected (PDOS) onto the Cr-3d and O-2p states. The O and Cr s-states and Cr 3p states have no significant weight in the energy range shown. The valence band structure compares well to spectroscopic data.[25] The upper part of the valence band consist mainly of Cr-3d derived states separated from a broad band of mainly O-2p character. Note however that there is a significant hybridization of Cr-3d and O-2p states over the whole valence band region. The calculated band gap is $\mathrm{E}_g = 1.7$ eV which is 47% smaller than the experimental value $\mathrm{E}_g = 3.2$ eV determined from combined PE/BIS spectra.[25]

Along the trigonal [0001]-axis of α-Cr_2O_3, layers of oxygen alternate with two metal layers in the stacking sequence $\cdots$Cr-Cr-O_3-Cr-Cr-$O_3\cdots$. The (0001) surface can be obtained by cleaving the crystal in between any of these layers, hence there are three different chemical terminations. LEED[26] and STM[27] experiments indicate that under UHV conditions the α-Cr_2O_3(0001) surface is terminated by a single layer of Cr. Theoretical work has shown that depending on temperature and oxygen partial pressure, the surface may be oxygen or chromyl (Cr=O) terminated.[23,28] In the present work we consider the chromium terminated surface, which corresponds to the surface observed under UHV conditions (Figure 2).

Similar to other corundum type oxides (α-Al_2O_3 and α-Fe_2O_3), α-Cr_2O_3(0001) shows a significant relaxation of the surface layers compared to the ideal bulk termination. Table II gives an overview of our relaxation data compared to previous theoretical works and a LEED experiment by Rohr *et al.*, Ref. 26. The theoretical results are in qualitative agreement with each other and are — with the exception of the the second atomic layer where we predict an expansion rather than a contraction — in good agreement the experimental data, showing a strong relaxation of the surface compared to the bulk-truncated surface.

TABLE I: Bulk properties of α-Cr_2O_3: The lattice constants a and c of the hexagonal unit cell, the short and long Cr-O distances d_{CrO1} and d_{CrO2}, the bulk modulus B_0, and the heat of formation ΔH_f^0.

	a [Å]	c [Å]	d_{CrO1} [Å]	d_{CrO2} [Å]	B_0 [GPa]	ΔH_f^0 [eV/Cr_2O_3]
Calc.	4.96	13.81	1.98	2.02	209	10.41
Expt.	4.951[a]	13.566[a]	1.962[a]	2.009[a]	238[a], 231[b]	11.76[c]

[a]Reference 18
[b]Reference 19
[c]Reference 20

TABLE II: Relaxations of the outermost atomic layers of the α-$Cr_2O_3(0001)$ surface given in percentage of bulk interlayer separations.

	This work	Previous theoretical works					Experiment
	GGA	HF[a]	MD simul.[b]	FP-LAPW[c]	GGA[d]	GGA+U[d]	LEED[b]
Cr_1-O_1	−60.9	−49.8	−58	−59	−62	−60	−60
O_1-Cr_2	+4.4	+3.3	0	+1	+10	+12	−3
Cr_2-Cr_3	−36.5	-	−36	−38	−41	−44	−21
Cr_3-O_2	+5.6	-	+17	+10	+6.5	+9.2	+6

[a]Reference 29; only the two topmost -CrO_3Cr- layers were allowed to relax.
[b]Reference 26
[c]Reference 30
[d]Reference 23

IV. ADSORPTION OF METHANOL AND METHOXY

The key properties of the adsorption are the preferred adsorption site, the orientation of the adsorbed molecule with respect to the surface, the adsorption energy, and the change in electronic structure upon adsorption.

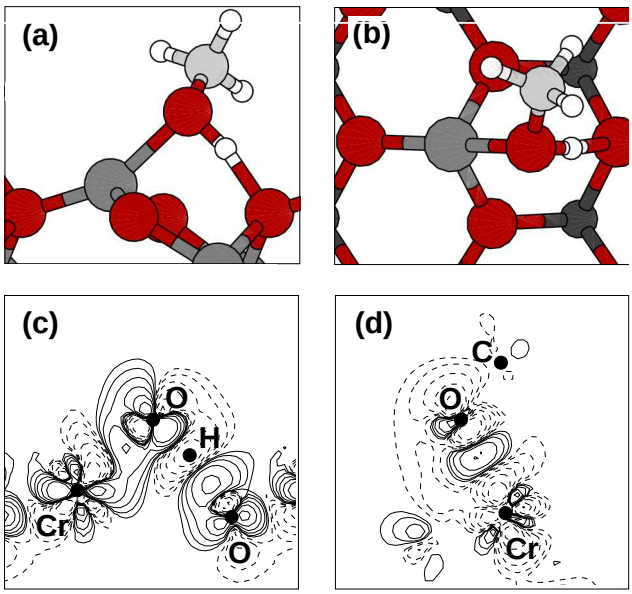

FIG. 3: Schematic side view, (a), and top view, (b), of the optimum adsorption geometry for methanol on $Cr_2O_3(0001)$ found in our calculation. Panels (c) and (d) show contour plots of the valence electron density difference, Δn(r). Panel (c) displays a cross section containing one surface Cr and O atom, and the methanol O and H atoms, where the H atom is the one belonging to the methanol OH-group. In panel (d), the cross section passes through the C and O atoms of methanol and the surface layer Cr atom. Solid (dashed) lines indicate gain (loss) of electron density. The contours are drawn at densities $\Delta n = \pm 0.005 \times 2^k$ e/Å^3 for $k = 0, 1, 2, 3, 4, 5$.

A. Adsorption geometry and energetics

To determine the optimum adsorption structure for methanol and methoxy on α-$Cr_2O_3(0001)$ we perform a series of structure optimizations with the adsorbate initially placed with its O-atom on top of one of the five different high-symmetry sites on exposed atoms of the surface. We also consider various starting orientations of the molecules with respect to the surface. During the optimizations, no motional constraints are placed on the atoms of the adsorbates or the slab, with the exception of the bottom Cr–O_3–Cr layer which is kept fixed in the bulk-truncated geometry. The molecules are therefore allowed to move freely on the surface and to change their orientation to locate the minimum energy structure. From this set of calculations, we find that all candidate structures optimize to only one adsorption structure for methanol (site "O-hollow" in Figure 2) and one for methoxy (site "Cr-ontop" in Figure 2), independent of the starting site and initial orientation. These adsorption optimum structures are shown schematically in figures 3 and 4, and table III summarizes the adsorption energies and geometric data.

Convergence tests. We explore the influence of the number of slab layers on the results by using slabs of three, four and five Cr-O_3-Cr layers, where in each case the bottom layer is kept fixed in the bulk-truncated geometry. The results for the three- and four-layer slab, summarized in table III, show only small differences in the adsorption geometry from a three to a four-layer slab, and the difference in adsorption energy is 0.02–0.04 eV. The adsorption energy using a five-layer slab differs by less than 0.01 eV compared to the four-layer slab, and the changes in adsorption geometry are negligible. The four-layer slab is therefore sufficient to describe the adsorption of methanol and methoxy, and even the three-layer slab gives adequate results.

To investigate the influence of coverage we do additional calculations with one adsorbate per (2×2) surface unit cell, i.e., at coverage $\Theta = 1/4$ ML. For these calculations we used a three-layer slab and a $2 \times 2 \times 1$ Monkhorst-Pack mesh. As can be seen from table III,

there are only small or no changes in the adsorption energies and geometries at coverage $\Theta = 1/4$ ML compared to coverage $\Theta = 1$ ML.

To test whether the use of a fixed bottom layer influences the adsorption energies and geometries we also carry out a test where all atoms of the slab and adsorbate are allowed to relax. We find no significant changes to the adsorption geometry, and a change in adsorption energy of less than 0.01 eV, thus validating our use of a slab with fixed bottom layer.

We investigate the influence of k-point sampling and plane-wave cut-off energy, and find the $4 \times 4 \times 1$ Monkhorst-Pack mesh and plane-wave cut-off of 400 eV sufficient: Using a $6 \times 6 \times 1$ Monkhorst-Pack mesh or 450 eV cut-off yields essentially the same adsorption energies (differing by less than 0.01 eV) and geometries.

Finally, a test of the vacuum gap size gives converged adsorption energies for a gap equivalent to three slab layers, or 6.9 Å; however, for the structure optimizations a more cautious size of ∼15 Å is used.

Here below we give a more detailed description of the calculated optimum adsorption structures for methanol and methoxy.

Methanol. We find that methanol adsorbs with the O atom situated in the site termed "O-hollow" in figure 2, independently of our initial positioning of the molecule before structural relaxations. This adsorption site is in contrast to our previous results[5,6] for methanol adsorption on α-Al_2O_3(0001), where the methanol O atom adsorbed nearly on top of an Al-atom. In fact, we find that a methanol molecule placed on top of a Cr atom in chromia is strongly repelled by the surface. Comparing also the adsorption energies $E_{\rm ads}$ (Table III) we find that the 0.80–0.82 eV adsorption energy on α-Cr_2O_3(0001), almost unchanged with coverage, is smaller by 0.2–0.4 eV than what we find for adsorption on alumina, on which there is a stronger coverage-dependence.

The methanol molecule on chromia is oriented with the methyl (CH_3) group pointing out from the surface, while the hydroxyl group (OH) points towards a surface layer O (Fig. 3). The C-O axis is tilted away (by the angle $\phi_{\rm CO}$) from the surface normal, slightly less than on alumina, and the molecular dipole plane (the COH plane) is tilted by $\phi_{\rm COH} = 54°$ with respect to the surface plane. In contrast to adsorption on alumina with larger changes to the surface upon adsorption, the only significant change to the substrate geometry for chromia is that the surface Cr atom is pulled outward by 0.2 Å. In alumina this change in position is coverage-dependent, from 0.2 Å at 1 ML to 0.3 Å at 1/4 ML. As argued in Ref. 6 the coverage dependence in alumina originates mostly from deformations in the surface and less on the direct methanol-methanol interaction, and since the surface deforms less in chromia it is to be expected that having relatively close methanol molecules, as in coverage 1 ML, does not change the adsorption energetics or structure in chromia relative to a more sparse coverage (1/4 ML).

¿From an atomic structure point of view the methanol adsorbs passively on α-Cr_2O_3: Like on alumina, the geometry of the molecule is almost unchanged from the gas phase molecule, with the exception of an elongation of the O-H bond length $r_{\rm O-H}$ by 0.05–0.07 Å. The nearest-neighbor distance of Cr to methanol-O is $r_{\rm Cr-O_{ads}} = 2.12$ Å, significantly larger than the longest Cr-to-O distance in bulk α-Cr_2O_3 of $d_{\rm CrO2} = 2.02$ Å (Table I). *Methoxy.* While methanol is repelled from the position with methanol-O on top of Cr, the same site is energetically preferred for methoxy (Fig. 2). Methoxy has its CO-axis tilted away from the surface normal by $\phi_{\rm CO} = 55°$. ¿From a separate calculation where the CO-axis is constrained to be parallel with the surface normal, we estimate the gain in adsorption energy for the tilted compared to the non-tilted geometry to be 0.31 eV. The azimuthal direction of the tilt, on the other hand, is less important energetically: The energy difference in tilting the CO-axis towards the surface O atom compared to a tilt towards an O-bridge site is only 0.02 eV, an indication that there is no clear azimuthal preference.

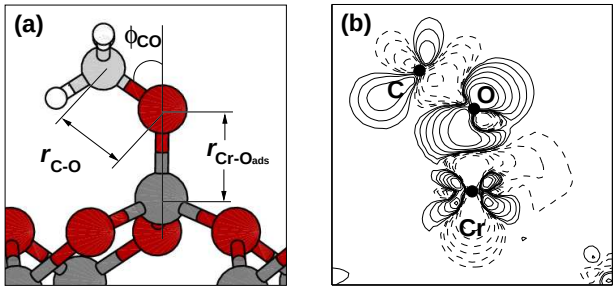

FIG. 4: (a) Schematic side view of the optimum adsorption structure for methoxy on Cr_2O_3(0001). (b) Contour plot of the electron density difference in a cross section containing one Cr and the methoxy O and C atoms. Solid (dashed) lines indicate gain (loss) of electron density. The contours are drawn at densities $\Delta n = \pm 0.005 \times 2^k$ e/Å^3 for $k = 0, 1, 2, 3, 4, 5$.

The adsorption energies are considerably larger than what we find for methanol adsorption and gives evidence of a rather strong substrate-adsorbate interaction. The calculated Cr-$O_{\rm ads}$ bond length is $r_{\rm Cr-O_{ads}} = 1.77$ Å, considerably shorter than the bulk Cr-O bond lengths, and also slightly less than the nearest-neighbour distance of 1.79 Å between surface layer Cr and O at the clean surface. The C-O bond of methoxy is elongated from the calculated gas-phase value $r_{\rm C-O} = 1.36$ Å to 1.42–1.43 Å, indicating a weakening of the internal C-O bond due to an electron redistribution to strengthen the surface-molecule bond.

B. Electronic structure and bonding

To gain insight into the electronic nature of the bonding of methanol and methoxy to the α-Cr_2O_3(0001) sur-

TABLE III: Calculated adsorption energy and selected geometrical data for adsorption of methanol and methoxy on α-$Cr_2O_3(0001)$. The distance $r_{Cr-O_{ads}}$ is the distance between the O of the adsorbate and the nearest Cr atom (nearest Al atom), r_{H-O_s} is the shortest distance between H of the molecule hydroxyl group and an O atom at the surface, and h is the vertical spacing between the Cr top layer and the underlying O plane.

	Θ [ML]	Layers	E_{ads} [eV]	h [Å]	$r_{Cr-O_{ads}}$ [Å]	r_{H-O_s} [Å]	r_{O-H}[Å]	r_{C-O} [Å]	$\angle$COH [deg]	ϕ_{CO} [deg]
CH_3OH	Free			0.40			0.98	1.43	109	
	1/4	3	0.80	0.60	2.12	1.59	1.03	1.44	108	53
	1	3	0.80	0.59	2.12	1.52	1.05	1.43	109	52
	1	4	0.82	0.61	2.12	1.54	1.05	1.44	109	52
CH_3O	Free			0.40				1.36		
	1/4	3	3.25	0.62	1.77			1.42		55
	1	3	3.28	0.64	1.77			1.43		55
	1	4	3.32	0.66	1.77			1.43		55
CH_3OH on	Free			0.13			0.98	1.43	109	
α-Al_2O_3,	1/4	4	1.23	0.43	1.93	2.03	1.00	1.45	110	57
Ref. 6	1	4	1.03	0.32	2.00	1.77	1.02	1.44	111	57

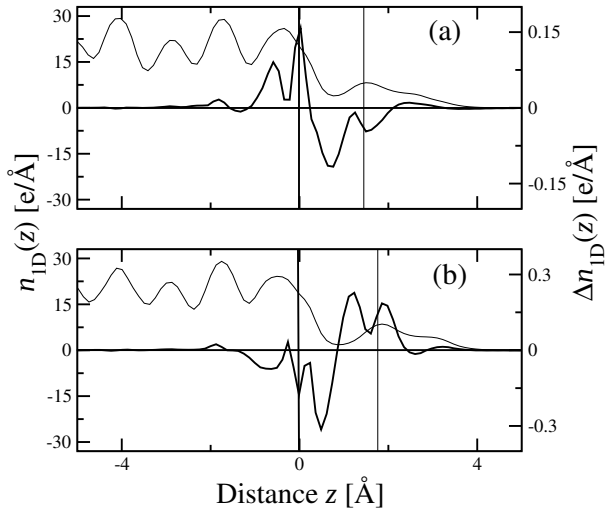

FIG. 5: Profile of the total electron density, $n_{1D}(z)$, (thin curve) and electron density difference, $\Delta n_{1D}(z)$, (thick curve) at $\Theta = 1$ ML for (a) adsorbed methanol and (b) adsorbed methoxy. The zero-point of the z-axis is set to the position of the topmost Cr layer. The positions of the molecule O atoms are indicated by thin vertical lines.

face, we perform separate calculations of the clean surface and isolated molecule in their adsorption geometries, and from these results calculate the valence electron density difference $\Delta n(\mathbf{r})$ defined as

$$\Delta n(\mathbf{r}) = n_{SM}(\mathbf{r}) - n_S(\mathbf{r}) - n_M(\mathbf{r}) \qquad (6)$$

with the densities of the total system (SM), and the clean surface (S) and isolated molecule (M), the latter two constrained to stay in the atomic geometry of the adsorbed system. The density difference shows how the electrons rearrange upon the adsorption. The results are presented in figures 3 and 4. The full lines indicate an increase in electron density, and the dashed line a decrease in electron density. The plots show a small build-up of electrons in the region between the Cr and molecule O atoms, and for methanol also between the hydroxyl group H atom and the nearest surface O atom. To estimate the charge transfer between the adsorbates and the surface we summed over the Bader-charges corresponding to the atoms of the molecule. For *methanol* this calculation yields a loss of electron density, corresponding to an increase of positive charge of 0.02 $|e|$ compared to the gas phase molecule, for *methoxy* a similar calculation shows gain of electron density corresponding to a reduction of positive charge of 0.41 $|e|$.

In Figure 5 we have plotted the difference charge density $\Delta n(\mathbf{r})$ integrated in the plane parallel to the [0001] direction, which we denote the z-direction,

$$\Delta n_{1D}(z) = \int d\sigma \, \Delta n(\mathbf{r}) \, . \qquad (7)$$

This plot reveals that in both cases only the top layer of the oxide is affected by the adsorption, whereas the lower lying layers are unaffected. For *methanol* the top panel of Figure 5 shows that there is gain of electrons in the slab region, whereas for *methoxy* the bottom panel shows a loss of electrons.

V. DISCUSSION AND CONCLUSIONS

We finally note that our DFT results for the structure of the methanol adsorption, Fig. 3, is consistent with expectations of a a simple, electrostatic model analysis. There one expects the electron-rich O atom to sit close to an exposed surface cation while the hydrogen atom of the OH-group points towards a surface anion. This is also expected from simple chemical (lone pair) bonding arguments. Whereas methanol adsorption on the clean, free-of-H-atom α-$Al_2O_3(0001)$ is not dissociative our results for methanol adsorption on α-$Cr_2O_3(0001)$ indicates that dissociation may take place in order to instead obtain the energetically preferred methoxy adsorption.

The adsorption energy and structure on α-$Cr_2O_3(0001)$ does not change with coverage, in contrast

to our previous results for adsorption on α-$Al_2O_3(0001)$. Further, the adsorption sites for methanol on the two surfaces differ. Thus, although both materials are similar in atomic structure, the electronic (and magnetic) structure of the materials differs sufficiently to lead to different adsorption situations.

In conclusion, we have by first-principles calculations characterized the α-$Cr_2O_3(0001)$ surface and its adsorption of methanol and methoxy molecules at different coverages. We find strong (3.3 eV) binding of methoxy to the surface, while the methanol binding is weaker (0.8 eV). We describe the geometrical structure of the molecules and surface upon adsorption, and analyse the changes on the electron density due to adsorption.

Acknowledgments

This work was partly carried out within *Light Metal Surface Science*, a joint project between SINTEF and NTNU, financed by The Norwegian Research Council (NFR), Hydro Aluminium, Profillakkering AS, Norsk Industrilakkering AS, Fundamus AS, Jotun Powder Coatings AS, and DuPont Powder Coating. NFR and NTNU are acknowledged for support through computing time at the Norwegian High Performance Computing Center (NOTUR). The work of E.S. was supported by the Swedish Research Council (VR) and the Swedish Foundation for Strategic Research (SSF) through the consortium ATOMICS.

[1] M. P. McDaniel, Adv. Catal. **33** (1985) 47.
[2] D. Scarano, S. Spoto, S. Bordigia, L. Carnelli, G. Ricchiardi, and A. Zecchina, Langmuir **10** (1994) 3094.
[3] W. Huppatz, M. Paul, and S. Friedrich, Surface Treatment of Aluminium, in: G. Drossel *et al* (Ed.), Aluminium Handbook, vol. 2 (Aluminium-Verlag, Düsseldorf, 2003).
[4] P. Marcus and V. Maurice, Passivity of Metals and Alloys, in: M. Schütze (Ed.), Corrosion and Environmental Degredation (Wiley-VCH, Wennheim, 1999).
[5] Ø. Borck and E. Schröder, ATB-Metallurgie **43** (2003) 342.
[6] Ø. Borck and E. Schröder, J. Phys.: Condens. Matter **18** (2006) 1.
[7] The plane-wave DFT code DACAPO can be downloaded from `http://dcwww.fysik.dtu.dk/campos/Dacapo`
[8] D. Vanderbilt, Phys. Rev. B **41** (1990) 7892.
[9] J. P. Perdew, J. A. Chevary, S. H. Vosko, K. A. Jackson, M. R. Pederson, D. J. Singh, and C. Fiolhais, Phys. Rev. B **46** (1992) 6671; **48** (1993) 4978(E).
[10] H. J. Monkhorst and J. D. Pack, Phys. Rev. B **13** (1976) 5188.
[11] J. Neugebauer and M. Scheffler, Phys. Rev. B **46** (1992) 16067.
[12] L. Bengtsson, Phys. Rev. B **59** 12301 (1999) 12301.
[13] W. Press, B. Flannery, S. A. Teukolsky, and W. T. Vetterling, *Numerical Recipes* (Cambridge University Press, Cambridge, 1986).
[14] R. F. W. Bader, *Atoms in Molecules - A Quantum Theory* (Oxford University Press, Oxford, 1990).
[15] G. Henkelman, A. Arnaldsson, and H. Jónsson, Comput. Mater. Sci. (in press, 2005).
[16] R. W. G. Wyckoff, *Crystal Structures*, 2nd ed. (Interscience, New York, 1964).
[17] L. M. Corliss, J. M. Hastings, R. Nathans, and G. Shirane, J. Appl. Phys. **36** (1965) 1099.
[18] L. W. Finger and R. M. Hazen, J. Appl. Phys. **51** (1980) 5362.
[19] Y. Sato and A. Akimoto, J. Appl. Phys. **50** (1979) 5285.
[20] *NIST-JANAF Thermochemical Tables* 4th ed., edited by M. W. Chase, Jr. (AIP and ACS, New York, 1998).
[21] E. Ziambaras and E. Schröder, Phys. Rev. B **68** (2003) 064112.
[22] J. E. Jaffe, M. Dupuis, and M. Gutowski, Phys. Rev. B **69** (2004) 205106.
[23] A. Rohrbach, J. Hafner, and G. Kresse, Phys. Rev. B **70** (2004) 125426.
[24] P. J. Brown, J. B. Forsyth, E. Lelièvre-Berna, and F. Tasset, J. Phys.: Condens. Matter **14** (2002) 1957.
[25] R. Zimmermann, P. Steiner, R. Claessen, F. Reinert, S. Hüfner, P. Blaha, and P. Dufek, J. Phys.: Condens. Matter **11** (1999) 1657.
[26] F. Rohr, M. Bäumer, H.-J. Freund, J. A. Mejias, V. Staemmler, S. Müller, L. Hammer, and K. Heinz, Surf. Sci. **372** (1997) L291; **389** (1997) 391 (E).
[27] V. Maurice, S. Cadot, and P. Marcus, Surf. Sci. **458** (2000) 195.
[28] X.-G. Wang and J. R. Smith, Phys. Rev. B **68** (2003) 201402.
[29] C. Rehbein, N. M. Harrison, and A. Wander, Phys. Rev. B **54** (1996) 14066.
[30] K. Wolter, D. Scarano, J. Fritsch, H. Kuhlenbeck, A. Zecchina, and H.-J. Freund, Chem. Phys. Lett. **320** (2000) 206.

Paper III

Adsorption of methylamine on α-Al_2O_3(0001) and α-Cr_2O_3(0001)

Ø. Borck, P. Hyldgaard, and E. Schröder

Preprint 2006

Adsorption of methylamine on α-Al_2O_3(0001) and α-Cr_2O_3(0001)

Øyvind Borck,[1] Per Hyldgaard,[2] and Elsebeth Schröder[2]

[1]*Department of Physics, Norwegian University of Science and Technology, NO–7034 Trondheim, Norway*
[2]*Department of Applied Physics, Chalmers University of Technology and Göteborg University, SE–41296 Göteborg, Sweden*

(Dated: March 9, 2006)

Molecular adsorption of methylamine (CH_3NH_2) at the α-Al_2O_3 and α-Cr_2O_3 (0001) surface is investigated and compared by means of first-principles density functional theory calculations. We report ab initio results for both the adsorption structure and bonding as documented by analysis of the adsorption induced changes in the electron density and in the projected density of states. We find that methylamine bond to exposed surface cations via the N lone-pair.

PACS numbers:

I. INTRODUCTION

Organic compounds containing amino groups have important applications in adhesives, surface coatings, corrosion inhibitors, and catalysis.[1] Understanding the adsorption of these organic compounds on oxide surfaces represents an important problem for such technological applications.

Aluminium alloy surfaces are often subject to a surface pre-treatment prior to structural bonding or painting, with the aim of improving the adhesive properties and corrosion resistance of the substrate.[2] Common pretreatments are anodizing and chromium chromate conversion coating (CCC). Essentially, anodizing is an electrochemical process which produces a thick aluminium oxide film with greatly improved adhesive properties and corrosion protection compared to the naturally occurring thin aluminium oxide film. Anodizing is extensively used by the aerospace industry to prepare the aluminium surface for painting and structural bonding.[2] The result of the CCC is the capping of the aluminium oxide by a chromium oxide surface layer (film). These coatings provide excellent corrosion protection and adhesive properties, however the presence of hexavalent chromium in the coating solution is a major health and environmental concern, and has led to an active search for chromium-free alternatives.

A key property that a surface pre-treatment should provide is good adhesion to organic coatings and adhesives. However, the nature of the interfacial bonds involved in such systems are not well known. Amine cured epoxy polymers are widely used as adhesives and coatings. The complexity of these systems are such that a detailed, molecular level understanding of the interactions taking place between the polymer and the substrate is difficult to obtain. One strategy is to focus directly on the functional groups of the polymer, and use small analogue molecules containing one of these chemically interesting groups to directly investigate the interaction of the functional group with the surface.

Methylamine (CH_3NH_2) represents a prototype of organics containing an amino group, and is a natural test case for the study of amino adsorption on metal oxide surfaces.

Here we compare the adsorption of methylamine on α-Al_2O_3 (0001) and α-Cr_2O_3 (0001) as investigated using density functional theory (DFT) calculations. We determine the structural relaxation and resulting geometries and report the adsorption energies as well as adsorption-induced differences in the electron density for the alumina and chromium surfaces. By further calculating and comparing the projected density of states we characterize the differences in the nature of the methylamine bonding on the two surfaces.

II. COMPUTATIONAL DETAILS

The calculations presented here are performed within the DFT approach using ultrasoft pseudopotentials[7] and a plane-wave basis set.[6] The exchange and correlation contributions to the total energy are approximated within the generalised gradient approximation (GGA), using the PW91 parametrisation.[8]

For the isolated methylamine we use a fcc unit cell with lattice constant of 12 Å, sampling the Brillouin zone only at the Γ-point.

To investigate the methylamine adsorption we use slab models with periodic boundary conditions to describe the (0001) surfaces of α-Al_2O_3 and α-Cr_2O_3 corundum structures. Each slab consists of four M-O_2-M layers (M=Al,Cr), the periodic repetition of slabs are separated by $\sim$ 15 Å of vacuum. We investigate the adsorption by placing molecules on one side of the slab only and we apply a dipole layer the unit cell to exclude electrostatic effects. In both corundum studies we use the Hellmann-Feynman forces to follow the atomic relaxation from a large number of initial molecular arrangement and thus determine the optimal adsorption configuration.

Our investigations of the adsorption on the α-Cr_2O_3 (α-Al_2O_3) surface are performed using spin-polarized (spin-balanced) calculations. In both cases, the Brillouin zone is sampled using a $4 \times 4 \times 1$ Monkhorst-Pack mesh, and we use a 400 eV energy cut-off for the plane-wave expansion. We have in a pair of previous investigations[4,5] documented that these choice produce an accurate description of the both the bulk structure and pronounced

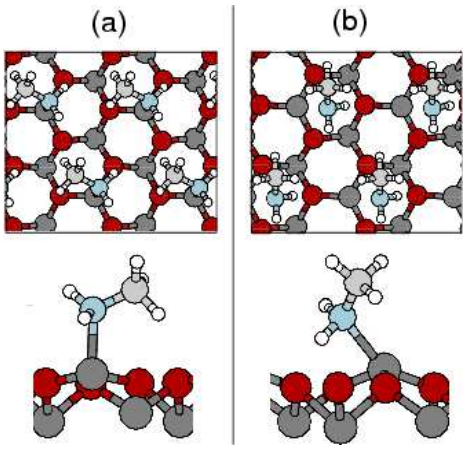

FIG. 1: Schematic side and top view of methylamine adsorbed at the (a) α-Al_2O_3(0001) surface and (b) α-Cr_2O_3(0001) surface. The surface metal (O) atoms are represented by medium (dark) grey balls.

atomic relaxations on the clean α-Al_2O_3(0001) and α-Cr_2O_3(0001) surfaces.[4,5] We also stress that the description accurately reproduces the antiferromagnetic distribution of atomic moments in bulk α-Cr_2O_3.[5] We argue that the description therefore allows a detailed investigation and comparison of the nature of molecular bonding on the two corundum surfaces.

Adsorption of methylamine on α-Al_2O_3 is considered both at coverage $\Theta = 1/4$ monolayer (ML) and at coverage $\Theta = 1$ ML in geometrical arrangements indicated in Fig. 1(a). In this definition of coverage, $\Theta = 1$ ML corresponds to one adsorbed molecule per surface layer metal atom (that is, ~ 5 Å separation between the adsorbed methylamine molecules). Adsorption of methylamine on α-Cr_2O_3 is considered at coverage $\Theta = 1$ ML. The spin-polarized nature make investigations of the $\Theta = 1/4$ ML α-Cr_2O_3 adsorption intractable.

III. RESULTS AND DISCUSSION

A. The methylamine molecule

Table I summarizes our DFT result for the isolated methylamine molecule. This equilibrium structure agrees well with the experimental data. The DFT results accurately reproduces the internal bond lengths and characteristic angles.

Figure 2 reports our corresponding DFT result for the highest-occupied molecular orbital (HOMO) of the methylamine molecule. The plot illustrates the molecular structure, identifying the relaxed positions of the H atoms by the set of small balls, and those of N/C atoms by the topmost/lowest of the large balls. The plot also reports an isosurface plot of the HOMO wavefunction that identifies the likely adsorption mechanism and possible adsorption geometries. We find that the HOMO

TABLE I: Comparison of the calculated and experimental geometry for the isolated methylamine molecule. Methylamine has a C_s point group symmetry, possessing a mirror plane along the C-N bond that bisects the H-N-H plane. In the equilibrium, staggered, conformation one methyl group hydrogen atom lie in the mirror plane at a distance d_{CHip} from the C atom, while the other two hydrogen atoms are out-of-plane at a distance of d_{CHp} from the C. All distances are in Å and angles in degrees.

	This work	Expt.[a]
d_{NH}	1.02	1.031
d_{CN}	1.46	1.472
d_{CHip}	1.11	1.112
d_{CHop}	1.10	1.112
$\angle$(CNH)	112	111.5
$\angle$(HNH)	107	106.0
$\angle$(HCH)	107	108.4

[a]Reference 13

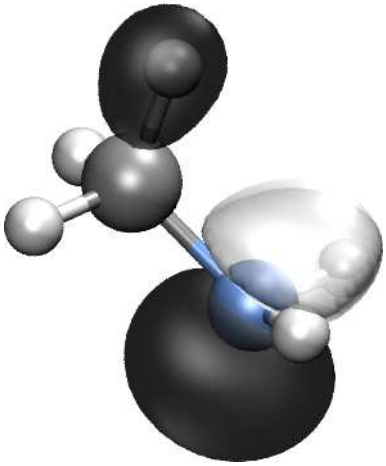

FIG. 2: The highest occupied molecular orbital of methylamine. The orbital is nonbonding with a predominant 2p character located at the N atom.

of the methylamine molecule is a nonbonding lone-pair orbital dominated by the $2p$ character of the nitrogen atom. The common view in chemical bonding theory is that the bonding at oxide surfaces results from a donation of methylamine lone-pair electron density to a partially empty cation orbital. This observation is used to limit our search for possible adsorption geometries below: we focus our search to cases where the initial molecular arrangement has the nitrogen atom and its potentially reactive lone-pair orbital closest to the pair of corundum surfaces.

B. Adsorption geometries and energetics

Table II and Fig. 1 summarize the main structural and energetic results of the present study. We comment on each of the adsorbate systems separately.

TABLE II: Calculated adsorption energy and selected geometrical data for adsorption of methylamine on the (0001) surfaces of α-Al_2O_3 and α-Cr_2O_3 surface. The distance d_{MN} is the nearest-neighbour separation between the N of CH_3NH_2 and a surface metal atom, d_{HO} is the shortest distance between a H atom of the amine group and a surface layer O atom. h_{MO} is the layer spacing between the metal atom to which the methylamine is bonded and the underlying O plane, with numbers in parenthesis giving the differences compared to the clean surface. Φ is the tilt angle of the C-O bond with respect to the surface normal.

	Θ [ML]	E_{ads} [eV]	h_{MO} [Å]	d_{MN} [Å]	d_{CN}[Å]	d_{HO}[Å]	d_{NH1}[Å]	d_{NH2}[Å]	$\angle$ CNH1 [°]	$\angle$ CNH2 [°]	Φ [°]
α-Al_2O_3(0001)											
	1/4	1.65	0.43(+0.32)	1.98	1.48	2.99	1.03	1.03	111	111	60
	1	1.16	0.32(+0.21)	2.05	1.46	2.11	1.02	1.05	113	112	49
α-Cr_2O_3(0001)											
	1	0.80	0.56(+0.17)	2.17	1.46	1.79	1.03	1.05	112	112	52

1. *Methylamine adsorption on α-Al_2O_3(0001)*

Fig. 1(a) shows the geometrical structure in the calculated optimal configuration for methylamine adsorption on α-Al_2O_3(0001) at 1 ML coverage. The medium (dark) grey balls identify final, relaxed positions of Al (O) atoms. This optimal adsorption structure is determined by following the atomic relaxation from a number of possible initial configurations of the molecule approaching the surface. In addition to using a variety of initial molecular configurations, we consider adsorption at different high-symmetry sites at the α-Al_2O_3(0001) surface. During the structure optimization we place no constraints on the motion of the molecule, so it is free to move laterally on (as well as perpendicularly to) the surface, and to reorient itself to locate the minimum energy adsorption structure.

Table II summarizes the optimal adsorption geometries that we calculate for both 1ML and 1/4 ML coverage. We find that methylamine adsorbs with its N atom slightly displaced laterally from the Al on-top site by 0.36 Å in the case of 1 ML coverage and 0.15 Å in the case of 1/4 ML. The Al atom coordinated to methylamine experiences a very strong outwards relaxation, as it is originally located below the outermost oxide layer.

We also determine the barrier for azimuthal rotation as less than 0.05 eV in the case of 1 ML coverage of methylamine adsorption on α-Al_2O_3. The smallness of this barrier is in contrast to the large adsorption energies that we find for the adsorption produced by the formation of a direct N-Al bond.

We note the adsorption of methylamine (Table II) shows no qualitative dependence on the coverage. Elastic deformations[14,15] and deformation energies play a significant but indirect role in determining the adsorption energy. However, it is clear that the coverage has almost no impact on the intra-molecular arrangement. Instead the differences in the adsorption energies result from the elastic coupling mediated through the oxide surface, lowering of the adsorption energy with coverage (from 1.65 to 1.16 eV). The mechanism is similar to what we have previously discussed in a study of methanol adsorption.[4]

To test the observation directly, we also calculate the dependence of the adsorption energies with coverage on a pair of frozen surfaces. This study allows us, in part, to separate out the effects of electronic coupling which we find has a much smaller coverage dependence. Specifically, we find for the frozen-surface calculations that the adsorption energies only reduce from 1.11 eV at 1/4 ML to 0.94 eV at 1 ML coverage. The observation that the nature of bonding exhibits no dependence on coverage is confirmed by the analysis, below, in terms of the adsorption-induced changes to the electron density.

2. *Methylamine adsorption on α-Cr_2O_3(0001)*

Fig. 1(b) shows the final relaxed adsorption structure for the chromia surface. Again, the medium (dark) grey balls represent the metal (oxygen) atoms. We find that the methylamine on α-Cr_2O_3(0001) binds to a chromium atom but now with a different preferred lateral positions for the N atom. Rather than adsorbing on top of Cr, the molecule adsorbs with the N atom in a three-fold hollow oxygen site (Fig.(b)). A corresponding adsorption geometry on chromia has been documented for CO,[16] H_2O,[17] and methanol.[4]

Table II summarizes this optimal adsorption structure for methylamine on α-Cr_2O_3 and allows a comparison with the above-presented results for α-Al_2O_3. Similar to what we found for the α-Al_2O_3(0001) surface, the adsorption induces an outward relaxation of the Cr atom bound to the methylamine N. However, the relaxation is smaller as the Cr atom here originates from a position outside the oxygen atoms. We find that the adsorption energy is weaker than in the aluminium oxide case, and is of the same size as the adsorption energy found in an earlier investigation[5] for methanol adsorbed at this surface.

C. General discussion and nature of the methylamine bonding

To gain insight into the nature of the surface-molecular bond we compare the adsorption mechanisms at the α-Al_2O_3(0001) and α-Cr_2O_3(0001) surfaces. In this study we exploit the power of DFT to not only characterize

the spatial variation of the bonding orbitals (Fig. 2) but also calculate the adsorption-induced differences in the electron density and in the orbital-projected density of states.

1. *Methylamine adsorption on α-Al_2O_3(0001)*

Fig. 3 reports our DFT results for the adsorption-induced differences in the electron density in the case of methylamine bonding on the α-Al_2O_3(0001) surface. We simply subtract the electron densities for the isolated molecule and surface from the electron density that we calculate for the adsorbed system. The left panel reports the isosurface variation in the electron-density difference with areas of light (dark) shading indicating an electron gain (loss). The prominent feature of this figure is the increased density in the bonding region between N and Al. The loss of electron density appears to be largely from the N atom.

The middle and right panels of Fig. 3 show contour plots of the electron density difference in a plane containing the methylamine C and N atoms and a surface Al at coverages 1 ML and 1/4 ML respectively. The shape of the electron density difference is very similar for these two coverages, suggesting that the bonding nature is similar. By comparing the contour plots in the middle and leftmost panels we conclude that the adsorption mechanism is only weakly dependent on the methylamine coverage. Some minor quantitative differences appears in the C-O bond region, however, it is evident in our comparison that the nature of bonding remains unchanged.

Important insight into the chemical bond formation can be extracted from such maps of the adsorption-induced differences in the electron density.[18] An electron build-up between two atoms, as seen between the N and Al atom (Fig. 3), is a strong indication of a bond formation with a covalent character.

As mentioned above, the HOMO of methylamine is a nonbonding (lone-pair) orbital of predominantly N $2p$ character (Fig. 2). The expectations from simple chemical bonding arguments is that bonding of the methylamine to an oxide surface is of a donor-acceptor character where the methylamine N lone-pair electron density 'donates' electron density to a (partially) empty cation orbital.[19,20] This leads to a stabilization where, within a simplified one-electron picture, the (filled) lone-pair orbital moves down in energy, while the empty cation orbital acquires some anti-bonding character and is raised in energy.[20] A donor-acceptor interaction does not necessarily involve a charge transfer.

A comparison of Fig. 2 and Fig. 3 suggests that the lone-pair orbital of methylamine is involved in the methylamine-surface bonding. The density of states shown in Fig. 4, confirms this expectation. The upper panel displays the density of states projected onto the N $2p$ state. A comparison of the peaks corresponding to the free (dashed line) and adsorbed molecule shows a general downshift in energy of the N $2p$ states due to the adsorption. There is an additional downshift (stabilization) of the N $2p$ state corresponding to the HOMO relative to the lower energy orbitals by ~ 2 eV, and also some broadening, indicating that mainly the the lone-pair orbital is involved in the bonding of methylamine to the α-Al_2O_3(0001) surface.

The middle and bottom panels of Fig. 4 display the DOS projected onto the $3p_z$ and $3p_{xy}$ of the Al atom bound to the methylamine N. The z-axis is chosen to be parallel with the surface normal. As is evident from these plots, the Al $3p_{xy}$ state is affected very little by the adsorption, however the Al $3p_z$ state shows some small but important changes: The empty Al $3p_z$ band move up in energy, and a peak appears in the valence band at the same energy as the HOMO N $2p$ state. As mentioned above, the up-shift in energy of the empty cation states is expected from a donor-acceptor interaction. Furthermore, the changes to the valence band indicates some mixing of N $2p$ and Al $3p_z$ states.

Summarizing, our DFT calculations confirm the expectations from chemical bonding theory of a a donor-acceptor interaction between the methylamine N lone-pair and an exposed surface (Al) cation.

2. *Methylamine adsorption on α-Cr_2O_3(0001)*

Fig. 5 shows our DFT results for the adsorption-induced changes in the electron density for the chromia surface. The most striking difference compared to adsorption on alumina is the more pronounced involvement of the cation (d-)states in the methylamine-chromia interactions.

The middle panel of Fig. 5 displays a contour plot of a cut in the electron density difference passing through the methylamine N and C atoms, and a surface Cr atom. The contour reveals an accumulation of electron density between the N and Cr atom as would also be expected for a covalent bonding of methylamine to the nearest-neighbour Cr atom via the N lone-pair. In the rightmost panel, the methylamine N and one of the amine-group H atoms, and surface Cr and O atoms are intersected by the cut. A prominent feature in this contour plot is the loss of electron density around the H atom, and an increased electron density between the H atom and a surface O atom, indicating some H-O interaction in addition to the N-Cr interaction.

Fig. 6 displays the DOS projected onto the N $2p$ (upper panel), and Cr $3d$ states (middle and lower panel), where we in the middle panel show DOS projected onto the 'e_g' orbitals (we have summed over the d_{xy},d_{xz}, and d_{yz}) and in the lower panel the 't_{2g}' orbitals (sum over d_{z^2} and $d_{x^2-y^2}$) where the z-axis is chosen to be parallel with the surface normal. The adsorption-induced changes to the N $2p$ state is somewhat similar to that of the alumina case. Specifically, a similar stabilization of the HOMO level arises with the adsorption but here, in the chromia

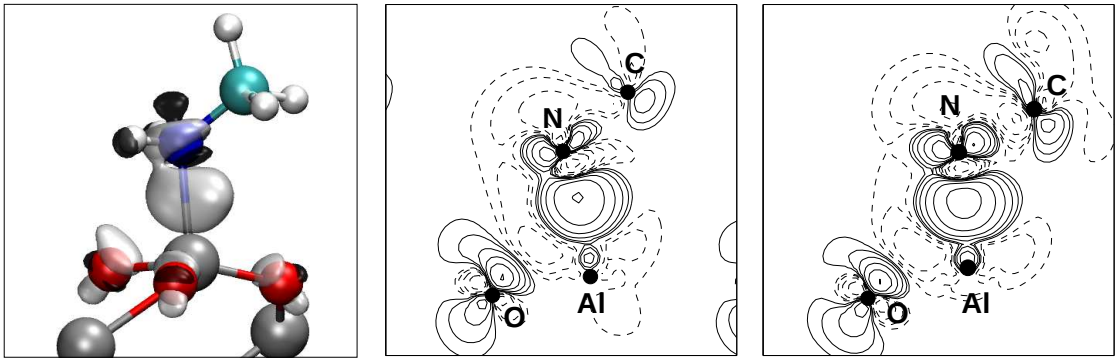

FIG. 3: Isosurface and contour variation in the adsorption-induced electron-density change for methylamine bonding on α-$Al_2O_3(0001)$. Leftmost panel shows the isosurface variation with light (dark) regions identifying a gain (loss) of electron density. The middle and rightmost panels shows contour plots of the electron density difference at 1 ML and 1/4 ML coverage, respectively. The contour plots are obtained in a plane through the C and N atom of methylamine and a surface layer Al atom. Solid (dashed) lines indicate gain (loss) of electron density. The contours are drawn at densities $\Delta n = \pm 0.005 \times 2^k$ e/Å^3 for $k = 0, 1, 2, 3, 4, 5$.

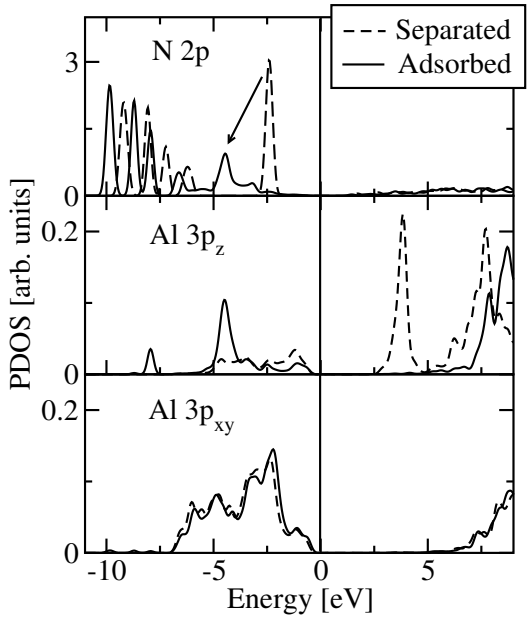

FIG. 4: Density of states projected onto the p orbitals of N and surface layer Al for separated (noninteracting, ~ 4 Å above the surface) methylamine and α-$Al_2O_3(0001)$ compared to the adsorbate

case, the effect is somewhat more pronounced ($\sim$2.4 eV as opposed to 2 eV on alumina). The broadening is also larger here, reflecting the larger ability (Fig. 5) to hybridize with the states in the chromia surface layer. The 't_{2g}'-like states (Fig. 6, bottom panel) only show a small perturbation as result of the adsorption. The 'e_g'-like orbitals, however, show some shift towards higher energy, that can be interpreted as due to a donor-acceptor interaction with the methylamine N 'lone-pair.'

Comparing the adsorption-induced changes in electron density for the chromia and alumina adsorption systems we identify some differences which directly reflect the more pronounced covalent character of the bonding on chromia. Unlike in the alumina case, the charge build up at the N-metal bond is compensated with finite intra-surface charge transfers also in the chromia surface layer. This difference emphasize that the methylamine adsorption on chromia cannot be viewed strictly within a simple electrostatic bonding model involving a coupling of the N atom to an exposed cation.

IV. CONCLUSIONS

We find that the methylamine adsorbs strongly to both the α-$Al_2O_3(0001)$ and the α-$Cr_2O_3(0001)$ by the amino group and onto an exposed surface layer cation atom. We also find that adsorption induce strong relaxation of the surface structure and is associated by large elastic deformations and deformations energies. We have analysed and compared the nature of bonding by studying the adsorption-induced changes in both the electron density and in the projected density of states. Our analysis confirms expectations from chemical bonding theory of a donor-acceptor interaction involving a lone-pair on the methylamine N atom and an exposed surface cation.

Acknowledgments

This work was partly carried out within *Light Metal Surface Science*, a joint project between SINTEF and NTNU, financed by The Norwegian Research Council (NFR), Hydro Aluminium, Profillakkering AS, Norsk Industrilakkering AS, Fundamus AS, Jotun Powder Coatings AS, and DuPont Powder Coating. NFR and NTNU are acknowledged for support through computing time at the Norwegian High Performance Computing Center

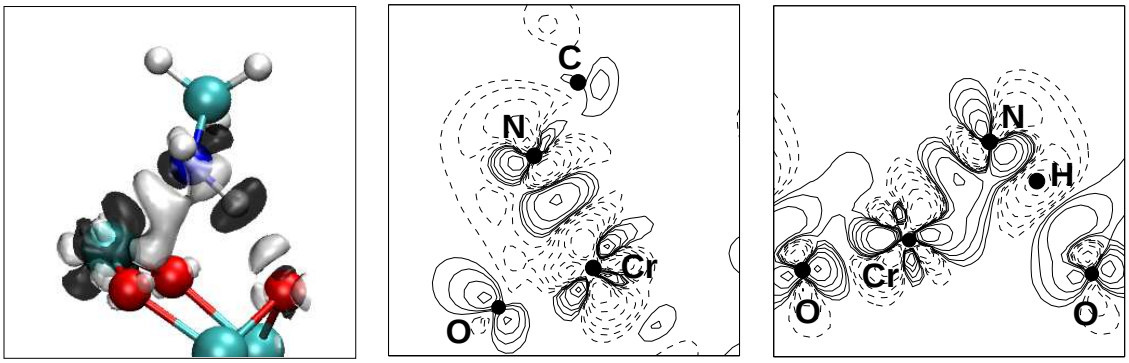

FIG. 5: Isosurface and contour variation in the adsorption-induced electron-density change for methylamine adsorption on α-Cr_2O_3(0001). The leftmost panel shows the isosurface variation while the middle (rightmost) panel shows contour plots in the plane containing the bonding chromium atom and the molecule C and N (molecule N and the amine-group H) atoms. Solid (dashed) lines indicate gain (loss) of electron density. The contours are drawn at densities $\Delta n = \pm 0.005 \times 2^k$ e/Å^3 for $k = 0, 1, 2, 3, 4, 5$.

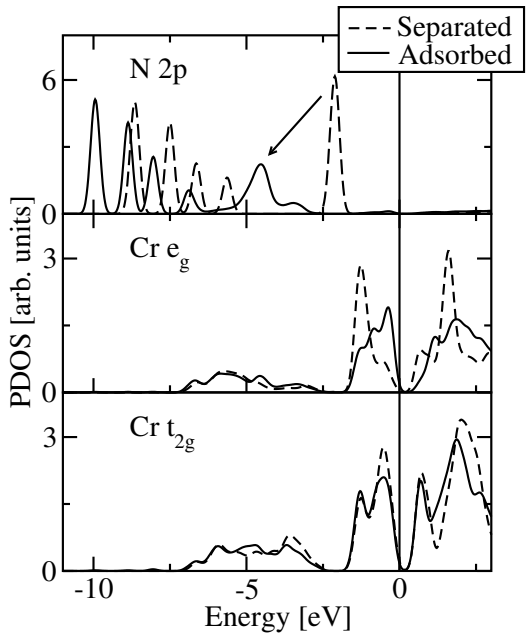

FIG. 6: Density of states projected onto the p orbitals of N and onto the d orbitals of the surface layer Cr for separated (noninteracting, ~ 4 Å above the surface) methylamine and α-Cr_2O_3(0001) compared to the adsorbate system.

(NOTUR). The work of E.S. and P.H. was supported by the Swedish Research Council (VR) and the Swedish Foundation for Strategic Research (SSF) through the consortium ATOMICS.

[1] S. A. Lawrence, *Amines: Synthesis, Properties and Applications* (Cambridge University Press, Cambridge, 2004).
[2] M. M. Hyland, Surface Chemistry of Adhesion to Aluminum, in G. E. Totten and D. S. MacKenzie (Eds.): *Handbook of Aluminum. Volume 2: Alloy Production and Materials Manufacturing* (Marcel Dekker, New York, 2003).
[3] Ø. Borck and E. Schröder, ATB-Metallurgie **43** (2003) 342.
[4] Ø. Borck and E. Schröder, J. Phys.: Condens. Matter **18** (2006) 1.
[5] Ø. Borck and E. Schröder, Adsorption of methanol and methoxy at the α-Cr_2O_3(0001) surface, unpublished.
[6] The DACAPO code can be downloaded at `http://www.fysik.dtu.dk/campos`.
[7] D. Vanderbilt, Phys. Rev. B **41** (1990) 7892.
[8] J. P. Perdew, J. A. Chevary, S. H. Vosko, K. A. Jackson,

M. R. Pederson, D. J. Singh, and C. Fiolhais, Phys. Rev. B **46** (1992) 6671.
[9] H. J. Monkhorst and J. D. Pack, Phys. Rev. B **13** (1976) 5188.
[10] J. Neugebauer and M. Scheffler, Phys. Rev. B **46** (1992) 16067.
[11] L. Bengtsson, Phys. Rev. B **59** 12301 (1999) 12301.
[12] W. Press, B. Flannery, S. A. Teukolsky, and W. T. Vetterling, *Numerical Recipes* (Cambridge University Press, Cambridge, 1986).
[13] T. Iijima, H. Jimbo, and M. Taguchi, J. Mol. Structure **144** (1986) 381.
[14] K. H. Lau and W. Kohn, Surf. Sci. **65** (1977) 607.
[15] K. H. Lau and W. Kohn, Surf. Sci. **75** (1978) 69.
[16] M. Pykavy, V. Staemmler, O. Seiferth, and H.-J. freund, Surf. Sci. **479** (2001) 11.
[17] T. Bredow, Surf. Sci. **401** (1998) 82.
[18] V. G. Tsirelson and R. P. Ozerov, *Electron Density and Bonding in Crystals* (Institute of Physics Publishing, Bristol, 1996).
[19] R. Hoffmann, Rev. Mod. Phys. **60** (1988) 601.
[20] V. Henrich and P. Cox, *The Surface Science of Metal Oxides* (Cambridge University Press, Oxford, 1994).

Paper IV

Phenol adsorption on graphite and aluminum oxide

S. D. Chakarova-Käck, Ø. Borck, E. Schröder, and B. I. Lundqvist

Preprint 2006

Phenol adsorption on graphite and aluminum oxide

Svetla D. Chakarova-Käck[1], Øyvind Borck[1,2], Elsebeth Schröder[1], and Bengt I. Lundqvist[1]
[1] *Department of Applied Physics, Chalmers University of Technology, SE–412 96 Göteborg, Sweden*
[2] *Department of Physics, Norwegian University of Science and Technology, NO–7034 Trondheim, Norway*
(Dated: April 18, 2006)

First-principles calculations of phenol adsorbed on two different surfaces, alumina, α-Al_2O_3(0001), and graphite(0001), modeled by a single graphene sheet, are performed with traditional density functional theory (DFT) and with a recently presented density functional (vdW-DF) that in addition to the traditional version of DFT incorporates the dispersive van der Waals (vdW) interactions [Phys. Rev. Lett. **92**, 246401 (2004)]. The vdW-DF is of decisive importance for describing the vdW bond of the phenol–graphite system and gives a secondary but not negligible vdW contribution on the alumina surface. We find a predominantly covalent bond at the alumina surface where adsorption within traditional DFT results in a binding separation (distance between surface Al and the O of the inclining phenol molecule) of 1.95 Å and a binding energy of 1.00 eV, evaluated within the generalized gradient approximation (GGA) of DFT, *i.e.* from covalency, with the energy increasing to around 1.2 eV when the contribution from vdW interactions is also accounted for. On graphite, with its pure vdW bond, the adsorption distance (separation between parallel surface and phenol molecule) is found to be 3.47 Å and the adsorption strength 0.56 eV. Comparison of the results for alumina and graphite mutually and with published results for nickel reveals significant differences in the adsorption of this model biomolecule.

I. INTRODUCTION

Phenol (C_6H_5OH), a small but important organic molecule, consists of a benzene ring, where one hydrogen atom is substituted by an OH group. In the amino acid *tyrosine* phenol is a side group, which makes it relevant for protein folding and protein adsorption [1]. It also appears as end or side groups in a number of polymers and therefore likewise plays an active role in the polymer adhesion processes, for instance, for paint adhesion on surfaces. Further, phenol is a frequent and toxic by-product in industrial processes and thus interesting from an environmental perspective.

Atomic-scale studies of phenol adsorption are rare, in particular modern first-principles theory studies on different kinds of substrates. Earlier studies include mainly phenol adsorption on nickel in connection with polymer adhesion studies [2]. We here present first-principles density functional theory (DFT) calculations of phenol adsorption on alumina (α-Al_2O_3(0001)) and graphite, representatives of both important classes of materials, ionic and dielectric, and surfaces, hydrophilic and hydrophobic, respectively. They are anticipated to have different adsorption mechanisms with significantly different strengths, as confirmed by our calculated results, adsorption energies found being roughly 1.2 and 0.56 eV on alumina and graphite, respectively, as compared to the value 0.9 eV found in the recent study of phenol on the metallic Ni(111) surface [2]. Behind these three numbers, there are three quite different adsorption mechanisms, whose natures are revealed below by in-depth studies of the adsorbate-induced electronic structures.

For calculations of electronic structure, bonding, structure, and elasticity, DFT has proved to be a powerful tool. However, the traditional implementations lack the ability to describe dispersive interactions, which are important for, *e.g.*, vdW complexes and phenol-graphite binding. Hence, the standard DFT in the generalized gradient approximation (GGA) is here supplemented by a new density functional (vdW-DF) that incorporates the dispersive vdW interactions into DFT [3].

Phenol adsorption on graphite has earlier been studied by Monte Carlo computer simulations [4]. Interactions between adsorbate and adsorbent and mutually between adsorbates are there described by parameter-dependent effective potentials, aimed at accounting for dispersive and electrostatic forces [4]. Thus a configuration with the molecule lying flat a distance 3.44 Å from the surface and with a binding energy of around 0.5 eV is found. The three phenol orientations considered in Ref. 4 differ in adsorption-energy values by less than the error caused by the use of empirical atomic effective parameters, as estimated by us. In our study we find values for the adsorption energy and the binding distance similar to those in Ref. 4, however, by using a first-principles method, with only the atomic numbers as input.

The application of the vdW-DF method to the phenol system is very much encouraged by the recently found excellent agreement between theory and experiment for benzene on graphite (calculated adsorption energy being 0.5 eV) [5]. The mere substitution of an H atom in the benzene molecule by an OH group gives phenol an electronic structure similar to that of benzene. Successful applications of vdW-DF to interaction energies of monosubstituted dimers, including phenol [6], are also encouraging in this respect.

The rest of the paper is organized as follows: First we describe the details of the density functional calculations for the alumina and graphite adsorption studies. The description of how we include the vdW interaction is deferred to a later section. Then comes a short description of the phenol molecule in the gas phase, a section on

adsorption on alumina, and then on graphite, the later including a short description of the the actual implementation of the vdW-DF. Finally, a discussion of our results is provided.

II. METHOD

All calculations presented here are based on the plane-wave-based implementation DACAPO [7] of DFT. To account for exchange and correlation, three different functionals are used: (i) the standard GGA in the PW91 flavor [7, 8], (ii) the GGA in the revPBE flavor [7, 9], and (iii) the vdW-DF [3]. GGA has well proved its abilities to describe short-range interactions in strongly bonded systems, where vdW forces usually can be ignored (such as the isolated gas-phase phenol molecule, the alumina surface, and the graphene sheet) it is used for the determination of the atomic structure and energy of each of these objects isolated, the differences between PW91 and revPBE here being negligible. For adsorption on graphite the GGA's have, indeed, to be extended by explicit calculation of the vdW interactions, here done in vdW-DF [3]. The ubiquitous vdW forces should contribute also to the adsorption of phenol on alumina, and we perform also a vdW-DF calculations on this system to assess its magnitude, in particular in relation to other contributions.

The structure, lattice parameters, and energetics for the clean alumina and graphite surfaces have previously been determined with the same code and choice of pseudopotentials, with results consistent with other modern theoretical and experimental results [10–12].

Alumina is here represented by the Al-terminated α-$Al_2O_3(0001)$ surface. α-alumina is the stable phase, and α-$Al_2O_3(0001)$ the most stable surface, so most other alumina surfaces are more reactive. The bulk unit cell is rhombohedral with lattice parameters $a_0 = 5.173$ Å and $\alpha = 55.28°$ and with internal Wyckoff positions [13] of Al respectively O within the unit cell $w = 0.3523$ and $u = 0.5561$. For the surface we use a periodic unit cell consisting of (2×2) hexagonal surface unit cells, with one phenol molecule adsorbed per (2×2) surface unit cell, thus corresponding to a coverage of a quarter of a monolayer.

This leads to a nearest-neighbor separation of 9.60 Å for the adsorbed molecule with its periodic images. The slab modeling the surface consists of 4 layers of Al-O_3-Al, with the atomic positions of the bottom O_3 and Al layer kept fixed in the bulk structure and the remaining layers relaxed using the PW91 [8] GGA and the Broyden-Fletcher-Goldfarb-Shanno (BFGS) algorithm [14]. We use 15 Å of vacuum perpendicular to the slab surface between the periodically repeated images of the slab. To describe the Brillouin zone in the (2×2) surface cell used in the adsorption studies we use a $2 \times 2 \times 1$ mesh of Monkhorst-Pack [15] special k-points and the planewave cutoff energy 450 eV. Other computational details are similar to our previous methanol-on-alumina study and are described in Ref. 11.

The graphite surface is modeled by one sheet of graphene. When calculating the interaction of phenol with graphite, we should add also the interaction energy of the second and lower graphene sheets, below the top layer. However, already the change in the interaction when including the second layer is found small ($\approx 4\%$), so these extra contributions will be ignored here. In order to accommodate the long-range vdW interactions in a post-processing of the nonlocal-correlation energy [3], we use a rather long (in the direction perpendicular to the sheet) unit cell of size 26 Å. The unit cell used for the calculations for phenol on graphene is hexagonal with a 5×5 surface cell, corresponding to a cell side length of 12.32 Å, which equals the nearest-neighbor separation for the adsorbed molecule with its periodic images. For the graphite calculation we also use a $2 \times 2 \times 1$ mesh of Monkhorst-Pack [15] special k-points, and the planewave cutoff energy 450 eV.

III. GAS PHASE PHENOL

According to our calculations, the isolated phenol molecule (in the "gas phase") is flat, with values for the intramolecular bond lengths given in Table I. This is consistent with earlier experimental and theoretical reports, although some experiments [17] report a small deviation (2–3°) of the OH-bond direction from the plane of the carbon ring.

The two GGA versions revPBE and PW91 give rather similar geometrical structures, as shown in Table I. All C–C bond lengths in phenol are slightly smaller than those of graphene (1.4226 Å, when calculated in revPBE), and similar to those of benzene.

IV. PHENOL ON ALUMINA

In this section we report on the adsorption of phenol on alumina within the GGA formalism. In Section VI we discuss how this adsorption is affected by the presence also of vdW interactions between the phenol molecule and the surface.

The Al-terminated α-$Al_2O_3(0001)$ surface has the layered structure Al–O_3–Al–Al–O_3–Al–... and the unit cell exposes one layer of O-atoms and three layers of Al-atoms, of which one is the Al-termination, as shown in the top panel of Fig. 1.

Adsorption of phenol raises several geometric issues. For a molecule oriented with its plane flat on the surface, symmetry considerations lead to approximately 30 different possible positions and directions of phenol on the surface, counting structures with the phenol ring on top of a surface ring (like structure (iv) in Fig. 1) and structures with the phenol ring on top of one of the exposed surface atoms (like structures (i) and (iii)). However,

TABLE I: Geometric structure of phenol (C_6H_5OH), expressed in bond lengths and C-O-H angle. The bond length $d_{CC}^{nearest}$ (d_{CC}^{far}) is the average values of the two (four) C-C bonds nearest to (away from) the OH-group, and d_{CC} averages all six C-C-bonds. For comparison, we also include the gas phase benzene bond lengths, calculated using the same settings as in the present (revPBE) phenol gas phase study. The bond lengths for phenol adsorbed on alumina are listed below, while for phenol on graphite we assume the gas-phase bond lengths are retained upon adsorption.

	$d_{CC}^{nearest}$ [Å]	d_{CC}^{far} [Å]	d_{CC} [Å]	d_{CH} [Å]	d_{CO} [Å]	d_{OH} [Å]	∠COH [°]
Gas phase phenol							
This study, revPBE	1.399	1.395	1.396	1.091	1.374	0.980	109.3
This study, PW91	1.397	1.393	1.394	1.091	1.372	0.980	109.3
Gaussian, AM1 Ref. 4	1.404	1.394	1.397	1.099	1.377	0.968	107.9
B3LYP/6-311+G(3df,2p) Ref. 16	1.3926	1.3898	1.3907	1.0822	1.3664	0.9618	109.895
CCD/6-31G* Ref. 16	1.3959	1.3949	1.3952	1.0886	1.3746	0.9705	108.760
Exp. Ref. 17	1.3912	1.3944	1.3933	1.0828	1.3745	0.9574	108.7
Phenol on Al_2O_3							
This study, "tilted" (ii) PW91	1.387	1.393	1.392	1.091	1.405	0.988	112.9
This study, (i) PW91	1.386	1.398	1.392	1.090	1.424	0.986	109.4
This study, (iii) PW91	1.387	1.390	1.391	1.090	1.409	0.987	110.0
This study, (iv) PW91	1.386	1.390	1.392	1.090	1.416	0.989	110.9
Gas phase benzene							
This study, revPBE	-	-	1.396	1.091	-	-	-

TABLE II: Adsorption energies and separations for phenol on graphite (a single graphene sheet) and α-Al_2O_3(0001). Results of different methods are shown. The naming of the structures is given in the caption of Fig. 1.

	d_{ads} [Å]	ads. angle [°]	E_{ads} [eV]
Phenol on graphite			
AB2 (vi) (vdW-DF)	3.47	0	0.56
AB1 (v) (vdW-DF)	3.47	0	0.55
AB1 (v) (revPBE)	4.77	-	0.01
AB1 (v) (PW91)	4.19	-	0.06
Phenol on α-Al_2O_3(0001)			
(i) (PW91)	2.00	10.3	0.88
(ii) (PW91)	1.95	44.7	1.00
(iii) (PW91)	1.97	21.3	0.91
(iv) (PW91)	1.98	21.5	0.91

our previous study of methanol adsorption on the Al-terminated α-Al_2O_3(0001) surface [10, 11] tells us that it is reasonable to assume that the O atom of phenol is not positioned on top of the lower-lying Al-atoms or the alumina O-atom, but rather adsorbs close to the top Al-atom. Further, if the direction of the OH-group H-atom is ignored, three relevant possible adsorption structures parallel to the surface, shown as (i), (iii), and (iv) in Fig. 1. For non-parallel (tilted) orientations, only one adsorption structure, (ii) in Fig. 1, is relevant, given that the barriers for rotation around the phenol-O-surface-Al bond are low and possible to overcome in the structural BFGS-relaxations.

For each of these four initial structures ((i) – (iv) in Fig. 1) the local energy minimum regarding the atomic positions is found by optimizing the atomic positions according to the Hellmann-Feynman forces from the electronic charge density. Upon adsorption each of the initially parallel structures [(i), (iii), and (iv)] are found to to tilt its aromatic ring slightly, when all atoms are allowed to relax. The final adsorption energies for these are found to be very similar and around 0.9 eV. Also the phenol-O to alumina-Al adsorption distances d_{ads} found (1.97–2.00 Å), and the geometrical structures upon adsorption, listed in Table I, are very similar for the three "parallel" structures. As expected, the largest change from the gas phase molecule is associated with the OH group (which binds to the surface), although the changes are small.

A larger PW91 binding energy is found for the initially tilted structure (ii). Upon relaxation, the optimum tilt angle found is 44.5°. In this case the angle ∠COH of the adsorbed phenol opens up slightly compared to the gas phase molecule, but otherwise the (small) changes are similar to those in the parallel structures. The PW91 adsorption energies and separations of the structures (i)–(iv) are given in Table II. The optimal adsorption structure is the "tilted" structure (ii) with adsorption energy 1.00 eV, occurring for $d_{ads} = 1.95$ Å, followed in energy by the "parallel" structures. This may be compared with the adsorption energy 1.23 eV for methanol on the same surface [11]. An analysis of the bonding reveals that, similarly to methanol on alumina [11], the electron density increases in the region of space between the phenol O atom and the alumina Al atom compared to the situation without a bond. However, only the phenol O atom contributes electrons to the bond, see Fig. 3. Methanol

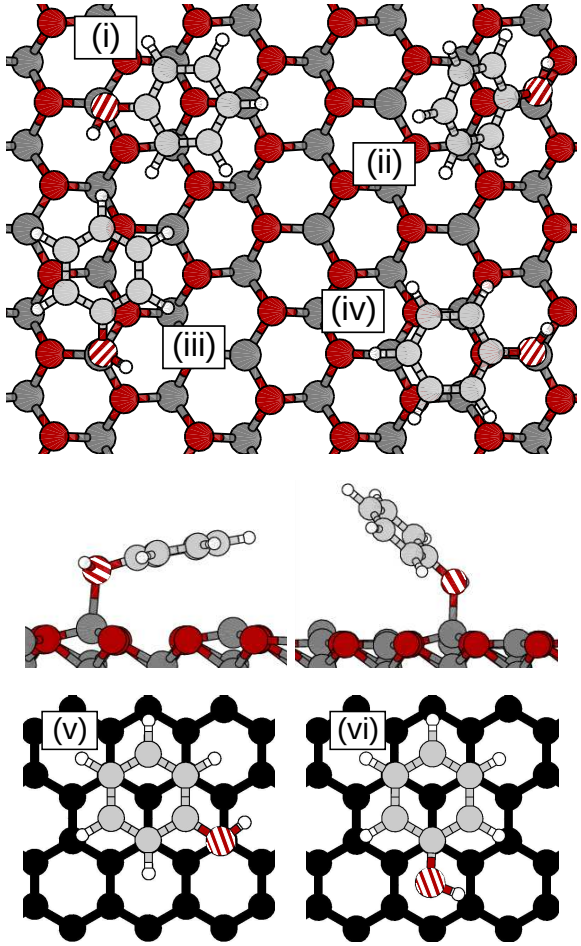

FIG. 1: *Top and middle panels:* Phenol on the Al-terminated α-$Al_2O_3(0001)$ surface, showing only exposed surface atoms. *Bottom panels:* Phenol on a graphene sheet, in AB stacking. The carbon atoms of graphite are colored black to distinguish them from the phenol carbon atoms (light gray). The two structures in the bottom panels differ in the orientation of the OH group relative to the carbon atoms of the underlying graphene sheet. The molecule is assumed to remain flat after adsorption.

and phenol have lone pair electrons with highest weight on the O atom (cf. H_2O) that interact with the Al atom in the top layer, thus forming a bond of covalent character. The result can be seen in the density plots as an increased electron density between the phenol O atom and the nearest Al atom (Fig. 3).

Although phenol is thus bound to the alumina surface by covalent forces, we have also estimated the contribution to the binding from the vdW interaction. Our vdW-DF calculation of phenol on alumina, similar to the one described below for phenol on graphite, indicates a small but not negligible increase in the adsorption energies of the structures studied This is discussed in more detail in section VI.

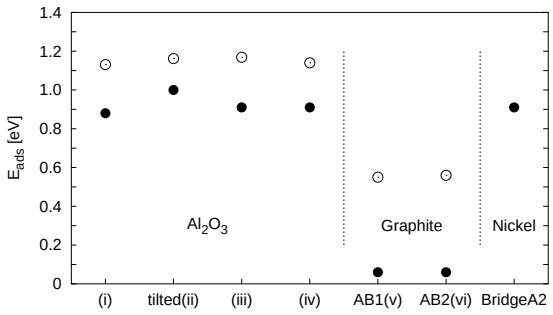

FIG. 2: Adsorption energies of phenol on various surfaces: Alumina (this study), graphite (this study), and Ni(111) (Ref. 18). For alumina and graphite the numbers reflect the different adsorption sites and orientations, as named in Fig. 1. For Ni only the energy for the most favorable adsorption site (BridgeA2, with the naming used in Ref. 18) is shown. Solid circles are PW91 calculations (except for Ni where the functional used is the Perdew-Burke-Ernzerhof GGA functional [19]) and open circles are calculations using vdW-DF.

V. PHENOL ON GRAPHITE

Phenol adsorption on graphite is calculated as that of an inert phenol molecule on a single graphene layer. The molecule is placed parallel to the surface, so that the center of its aromatic ring lies above a carbon atom in the graphite sheet (resembling the AB stacking found in graphite). This choice is analogous to what applies to benzene dimers and the related polycyclic aromatic hydrocarbon (PAH) dimers, where the slipped-parallel, *i.e.* AB, stacking is energetically favored [20]. The assumption that the molecules experience negligible changes in the intramolecular structure upon adsorption, relative to the gas phase structure, is based on the weakness of the dispersive adsorbate-substrate interaction compared to the intramolecular bonds, and was shown to be true for benzene in Ref. 21. The potential-energy or binding curve is found by varying the separation $d_{\rm ads}$ between the graphene sheet and the phenol molecule with phenol kept as a rigid molecule. The phenol bond to a graphene layer positioned as the second layer of graphite is also calculated and found small (adding 4% to the binding energy), and that to further graphite layers is estimated to be negligible. In this way the adsorption energy for phenol on graphite can be obtained.

As shown in Fig. 1, there are two different AB positions for phenol: AB1 (Fig.1 (v)), when the OH group is oriented toward a carbon atom in the graphene sheet; and AB2 (Fig. 1 (vi)), when it is oriented toward the center of a ring in the sheet. We find almost identical results for the two structures (Table II).

As shown in Table II, the GGA's produce very little binding for phenol on graphite. From earlier studies [5] we know that this is the case also for benzene on graphite, where the small binding predicted by PW91 is in large

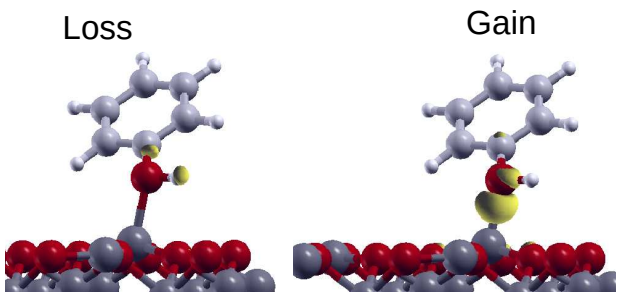

FIG. 3: Change in electron charge density after adsorption of phenol on α-Al_2O_3(0001). The left (right) panel shows the isosurface for loss (gain) of 0.05 e/Å^3. Atom color coding as in Fig. 1.

contrast to the experimental data. Similar problems with standard GGA implementations arise whenever the vdW dispersive forces dominate the actual bond, as inherent to graphitic systems. These problems have long been known [22, 23]. Any apparent attraction in GGA at these separations is a result of inadequate representation of exchange [21] and correlation in the tails of the electron distribution. In order to provide a proper description of the system, we here benefit from the virtues of the vdW-DF density functional [3] with vdW interactions in addition to the traditional GGA-DFT. In the vdW-DF, the nonlocal correlation part of the energy is included by calculating the total energy in the following manner:

$$E_{\text{vdW-DF}} = E_{\text{GGA}} - E_{\text{GGA,c}} + E_{\text{LDA,c}} + E_{\text{c}}^{\text{nl}}, \quad (1)$$

where the correlation $E_{\text{GGA,c}}$ is substituted by a local one, $E_{\text{LDA,c}}$, and a nonlocal correlation part E_{c}^{nl}. The latter contains the correlation effects with a nonlocal dependence on the density and is approximated in the fashion described in Ref. 3, *i.e.*, via the general-geometry density functional. For reasons described in more detail elsewhere [3, 24], we use the exchange of the revPBE flavor, and not that of PW91, as revPBE is the GGA exchange closest to exact exchange calculations at these separations.

The nonlocal correlation E_{c}^{nl} used in Eq. (1) takes the form of a six-dimensional integral over the density and is calculated for the phenol molecule interacting with a large piece of the graphene sheet extending over a range of radius 14 Å (see Ref. 5 for details). Thus, the binding energy calculated here for phenol on graphite is calculated in the same fashion as done for benzene and naphthalene on graphite in Ref. 5. There a direct comparison to experimental data is made — thermal desorption measurements give an adsorption-energy value for benzene on graphite of 500 meV [25], which is very well reproduced by the vdW-DF result (495 meV). The general geometry vdW-DF [3] has also been used to treat phenol dimers successfully [6].

With vdW-DF we find the binding-energy, E_{ads}, and equilibrium-separation, d_{ads}, values shown in Table II. These are the energies for adsorption on a graphene sheet; by evaluating also the binding from the second layer of graphene in a graphite surface, namely the interaction at d_{ads} plus the layer separation in graphite, we find the energy of adsorption on a graphite surface to be approximately 4% larger than the E_{ads} given in Table II.

The earlier study of phenol on graphene by means of Monte Carlo simulations and empirical potentials using atomic effective interaction parameters [4] gave an optimum configuration with a molecule lying flat a distance 3.44 Å from the surface and with binding energy of around 6000K (0.5 eV). The configurations treated there are of three types: (a) when the center of phenol lies above a center of a graphene aromatic ring, (b) when the center of phenol lies above a saddle point between two graphene carbon atoms, and (c) when the center of phenol lies above a graphene carbon atom. While the third case corresponds to our two structures, Ref. 4 finds the second one to be energetically most favorable. However, the difference between the adsorption energies of the worst and the best configuration in Ref. 4 is negligible (less than 4 meV).

VI. DISCUSSION AND CONCLUSIONS

While the adsorption of phenol on graphite is clearly of vdW nature, this is not the case for the adsorption on alumina. However, it is of interest to establish the size of the energetic contribution when including the vdW interactions also in the latter case. Here the vdW evaluation is more difficult for a number of reasons, besides increased system size. Firstly, we have large electron-density overlap between adsorbate and surface. Secondly, the relaxation of the surface makes it more difficult to increase the unit cell size for the vdW calculation by supplementing with the charge density of a clean surface, as is done here for phenol on graphite, and for benzene and naphthalene on graphite in Ref. [5]. Our calculation of the adsorption energy on alumina including the vdW interactions is therefore not quite as rigorous as for phenol on graphite although we used almost the same method. The vdW contribution on alumina is evaluated for the original unit cell (contrary to the case for graphite where the cell is enlarged), and is performed in two steps. In the first step we use vdW-DF to evaluate the energy difference between the adsorption structure and the corresponding "far-apart" system where the atoms have been fixed in their adsorption positions, but where the phenol molecule is translated a large distance (5.8 Å) away from the surface. In the next step we evaluate within standard PW91 the energy gained by relaxing the atom positions in the "far-apart" system to phenol in its gas phase geometry plus a clean surface.

The sum of the total energy changes after the two steps result in adsorption energies of around 1.1–1.2 eV for all the structures (i) to (iv), making it less clear which is the most favorable structure. While the tendency of struc-

ture (i) being the least favorable and (iv) being the next-to-least favorable is preserved, we find that including the vdW contribution makes structure (iii) slightly more favorable than (ii). For the latter structure we find as expected the smallest vdW contribution, as this structure has the largest adsorption angle of the four, see Table II. Comparing structures (iii) and (iv), which have very similar adsorption angles and distances, we find a larger vdW contribution for (iii). This may be explained by the placement of the aromatic ring in phenol, which for (iii) resembles the more favorable AB stacking. The use of the "far-apart" system described above was argued for in Ref. 26 to avoid small spurious energy contributions. In the present system substituting the "far-apart" system directly with systems of isolated phenol and alumina in their respective adsorption geometries yields similar results.

Together with the Ni(111) results of Refs. 2 and 18 three types of substrates have been studied, with different bonds to the phenol molecule. On graphite, phenol adsorbs in a clean vdW bond. On α-$Al_2O_3(0001)$, the bond is primarily covalent in nature, that is, similar to the one between methanol and alumina [10, 11]. On Ni(111), the bond seems to be metallic, maybe of a donation-backdonation type [27]. No estimate of the vdW interaction between phenol and Ni(111) has been made yet. The adsorption-energy values for the three surfaces end up in a narrow range, 0.6–1.2 eV (Fig. 2), yet the bonds are characteristically different. As a matter of fact, the covalent bond on alumina and the covalent-metallic bond on Ni are each weak for their classes, whereas on graphite the physisorption bond is a strong one. The differences between these hydrophobic and hydrophilic surfaces are thus illustrated by their different phenol adsorption-energy values and adsorption distances. Phenol molecules interacting with surfaces constitute interesting prototype systems for such varied phenomena as proteins, polymers (*e.g.*, relation of chain-termination to multiscale behavior near surfaces), paint, catalysis, toxicity, and widespread occurrence as a by-product. This calls for an understanding of the interaction and the possibility of bridging the atomic and macroscopic scales starts to open up. However, understanding of the adsorption step has to be established first by careful comparisons between experiment and theory.

Part of the information from the calculations is geometric. Even if energy differences between different sites and orientations sometimes are small, the calculations give results for atomic positions that should challenge the experimentalists. The scanning-tunneling microscope (STM) here offers outstanding possibilities. STM provides results for adsorbates on several types of substrates, see e.g. Ref. 28. In fact, STM work is presently performed even on several systems that are probably physisorbed or for which at least vdW interactions must be important (*e.g.*, organic molecules with benzene rings). On the latter systems, traditional DFT fails to describe the experimental structure that is seen in the STM. Hopefully the phenol-on-graphene results above (and similar ones coming successively) will stimulate measurements on such systems.

Another part of the information obtained is the energetics. The adsorption energy of phenol (Fig. 2) is about 0.9–1.2 eV on alumina and the dense Ni-metal surface and about 0.6 eV on graphite. These rather similar values should be looked upon as weak covalent and metallic chemisorption bonds on alumina and Ni(111), respectively, and strong physisorption bond on graphite. The numbers must be compared to other relevant energy values in order to describe the more complex phenomena. To confirm the theoretical adsorption picture, the energy values could be compared with thermal-desorption data, as has been done for, *e.g.*, the PAH's on graphite [25].

Further, there is information on the nature of the adsorption. While phenol is physisorbed on graphite, its adsorption is covalent on alumina and metallic (largely covalent) on Ni(111). Also here STM offers great possibilities, as the tunneling-current characteristics should be quite different for the three types of adsorption.

In summary, the results for phenol adsorption on the three types of surfaces, with three types of bonds, are thus very instructive for the understanding of the interaction of organic molecules with surfaces and interfaces relevant in biology.

VII. ACKNOWLEDGMENTS

Partial support from the Swedish Foundation for Strategic Research (SSF) via the ATOMICS consortium, the Swedish Research Council (VR), and NordForsk through a mobility scholarship for ØB is gratefully acknowledged, as well as allocation of computer time at UNICC (Chalmers) and SNIC (Swedish National Infrastructure for Computing).

[1] S.D. Chakarova and A.E. Carlsson, Phys. Rev. E **69**, 021907 (2004).
[2] L. Delle Site, C.F. Abrams, A. Alavi, and K. Kremer, Phys. Rev. Lett. **89**, 156103 (2002).
[3] M. Dion, H. Rydberg, E. Schröder, D.C. Langreth, and B.I. Lundqvist, Phys. Rev. Lett. **92**, 246401 (2004); **95**, 109902(E) (2005).
[4] C. Bertocini, H. Odetti, and E.J. Bottani, Langmuir **16**, 7457 (2000).
[5] S.D. Chakarova-Käck, E. Schröder, Bengt I. Lundqvist, and D.C. Langreth, Phys. Rev. Lett. **96** 146107 (2006).
[6] T. Thonhauser, A. Puzder, and D.C. Langreth, J. Chem. Phys. **124** (2006) *in press.*
[7] Open-source plane-wave DFT computer code DACAPO,

http://www.fysik.dtu.dk/CAMPOS/
[8] J.P. Perdew, J.A. Chevary, S.H. Vosko, K.A. Jackson, M.R. Pederson, D.J. Singh, and C. Fiolhais, Phys. Rev. B **46**, 6671 (1992); **48**, 4978(E) (1993).
[9] Y. Zhang and W. Yang, Phys. Rev. Lett. **80**, 890 (1998).
[10] Ø. Borck and E. Schröder, ATB-Metallurgie **43**, 342 (2003).
[11] Ø. Borck and E. Schröder, Journ. Physics: Cond. Matter **18**, 1 (2006).
[12] H. Rydberg, M. Dion, N. Jacobson, E. Schröder, P. Hyldgaard, S.I. Simak, B.I. Lundqvist, and D.C. Langreth, Phys. Rev. Lett. **91**, 126402 (2003).
[13] R.W.G. Wyckoff, *Crystal Structures* 2nd edition (New York, Interscience, 1964).
[14] C. G. Broyden, J. Inst. Maths. Applics. **6**, 76 (1970); R. Fletcher, Computer Journ. **8**, 317 (1970); D. Goldfarb, Math. Computation **24**, 23 (1970); D.F. Shanno, Math. Computation **24**, 647 (1970).
[15] H.J. Monkhorst and J.D. Pack, Phys. Rev. B **13**, 5188 (1976).
[16] NIST Computational Chemistry Comparison and Benchmark Database, NIST Standard Reference Database Number 101, Release 12, Aug 2005, Editor: Russell D. Johnson III, http://srdata.nist.gov/cccbdb.
[17] N.W. Larsen, J. Mol. Struct. **51** (1979) 175.
[18] L. Delle Site, A. Alavi, and C.F. Abrams, Phys. Rev. B **67**, 193406 (2003).
[19] J. P. Perdew, K. Burke, and M. Ernzerhof, Phys. Rev. Lett. **77**, 3865 (1996).
[20] S. D. Chakarova Käck, J. Kleis, and E. Schröder, *Dimers of polycyclic aromatic hydrocarbons in density functional theory*, to be published.
[21] A. Puzder, M. Dion, and D. C. Langreth, J. Chem. Phys. **124** (2006) *in press*.
[22] H. Rydberg, N. Jacobson, P. Hyldgaard, S. I. Simak, B. I. Lundqvist, and D. C. Langreth, Surf. Sci. **532**, 606 (2003).
[23] H. Rydberg, M. Dion, N. Jacobson, E. Schröder, P. Hyldgaard, S. I. Simak, D. C. Langreth, and B. I. Lundqvist, Phys. Rev. Lett. **91**, 126402 (2003).
[24] D.C. Langreth, M. Dion, H. Rydberg, E. Schröder, P. Hyldgaard, and B.I. Lundqvist, Int. J. Quantum Chem. **101**, 599 (2005).
[25] R. Zacharia, H. Ulbricht, and T. Hertel, Phys. Rev. B **69**, 155406 (2004).
[26] S.D. Chakarova and E. Schröder, Mat. Sc. Eng. C **25**, 787 (2005).
[27] This interpretation is ours, not from the published articles Refs. 2, 18.
[28] M.-L. Bocquet, H. Lesnard and N. Lorente, Phys. Rev. Lett. **96**, 096101 (2006).

Paper V

Density functional theory investigation of methoxy on NiAl(110)

Ø. Borck, H. Dalaker, and K. Mo

Preprint 2006

Density functional theory investigation of methoxy on NiAl(110)

Ø. Borck,* H. Dalaker, and K. Mo

Department of Physics, Norwegian University of Science and Technology, NO–7034 Trondheim, Norway

(Dated: April 24, 2006)

Abstract

The adsorption of methoxy (CH_3O) on NiAl(110) has been studied using density functional theory within the generalized gradient approximation, and applying a slab geometry. We have performed structure optimizations for a large number of initial orientations of methoxy at the high-symmetry sites of NiAl(110) in an effort to determine the energetically preferred adsorption site and local adsorption geometry. We found that methoxy adsorbs with the oxygen atom situated in the Al bridge site, with a nearest-neighbour Al–O distance is of 1.94 Å, and is oriented with the CO-axis perpendicular to the surface plane. We discuss the binding mechanism.

*Electronic address: oyvind.borck@ntnu.no

I. INTRODUCTION

The surface methoxy species (CH_3O) is formed as a stable species on a wide range of metal surfaces by a scission of the methanol O–H bond, making it an ideal model system for surface science studies of polyatomic adsorbates. Furthermore, methoxy is postulated to be a key intermediate in catalytic processes involving methanol as a product or a reactant. Much effort has therefore been devoted to studying the surface chemistry of methoxy, see e.g. Refs. [1–3] and references therein.

The NiAl(110) surface has been studied extensively, its physical properties are well known, and it represents a prototypical bimetallic alloy surface [4]. The clean (110) surface exhibits no major reconstructions, but maintains the bulk stoichiometry with 50% Al and 50% Ni. The two components show very different chemical properties [5]. NiAl(110) therefore provides an ideal substrate to test whether the interaction of adsorbates with the surface are determined by the properties of the individual components, or the global properties of the system.

Svenum *et al.* have investigated the adsorption and decomposition of methanol on NiAl(110) [6] using photoelectron spectroscopy (PES). They found that both methanol and methoxy are formed on NiAl(110) upon methanol adsorption at 120 K. Upon heating to 200 K, methanol decomposed into methoxy and other decompositional products. The PES results showed a contribution due to methoxy bonded to Al in the Al $2p$ spectra. No chemical shift was found in the Ni 2p spectra, indicating that methoxy only binds to Al. Low energy electron diffraction (LEED) showed no ordered methanol induced structures [6], thus an experimental determination of the adsorption site through, e.g., qualitative LEED is difficult to obtain.

To determine the adsorption site of methoxy for this system we have performed density functional theory (DFT) calculations where adsorption at the seven high-symmetry sites of NiAl(110) was considered. The results for different adsorption sites suggests that methoxy binds most strongly in the Al bridge site (indicated in Fig. 1), with the CO-axis perpendicular to the surface. Upon adsorption there is a charge transfer from the substrate into the incomplete 2e orbital of methoxy of 0.90 $|e|$, revealing a significant ionic contribution to the surface-adsorbate bond.

No such prior calculations on NiAl(110) have been reported, however the literature on

theoretical calculations on methoxy adsorption at metal surfaces is quite extensive, see Refs. [1, 3] and references therein.

II. COMPUTATIONAL DETAILS

The calculations presented here were performed within density functional theory (DFT), using the DACAPO [7] plane-wave psudopotential code. Vanderbilt's ultrasoft pseudopotentials [8] were used to describe the ionic cores, and the Kohn-Sham wavefunctions were expanded in a plane-wave basis with an energy cutoff of 350 eV. The exchange-correlation contribution to the total energy was approximated within the generalized gradient approximation (GGA). We employed the Perdew-Wang parametrization [9] (PW91) of the GGA exchange-correlation functional for the structural optimizations, but also report on adsorption energies calculated using the RPBE parametrization [10], as this parametrization has been reported to give improved chemisorption energies for molecular adsorption on transition metal surfaces. Although we found a small difference in the optimized lattice constant for bulk NiAl using RPBE ($a_0 = 2.90$ Å) compared to PW91 ($a_0 = 2.89$ Å), all the reported RPBE energies have been calculated using geometries optimized employing the PW91-functional.

The NiAl(110) surface was modeled by a slab consisting of five layers separated by a vacuum region equivalent to seven bulk layers (≈ 14 Å). We used a $c(2 \times 2)$ surface unit cell (Fig. 1) for all the calculations, each containing one molecule (corresponding to a coverage of $\Theta = 0.5$ ML). This choice was a compromise between low computational effort and minimizing the interaction between the methoxy radical and its periodic images. With this surface unit cell the distance between the adsorbed molecules is ~ 5 Å.

We placed the molecules at one side of the slab only, and allowed the atoms of the adsorbate and the two topmost layers of the slab surface to relax unconstrained until the residual forces were less than 0.05 eV/Å. We did not include symmetry constraints in the structural optimisation. The artificial electric field created by the asymmetry of the system was compensated by a self-consistently determined dipole correction applied in the vacuum region [11, 12].

The irreducible Brillouin zone was sampled by 18 k-points using the Monkhorst-Pack scheme [13]. To reduce the needed number of k-points we employed a Fermi-Dirac smearing

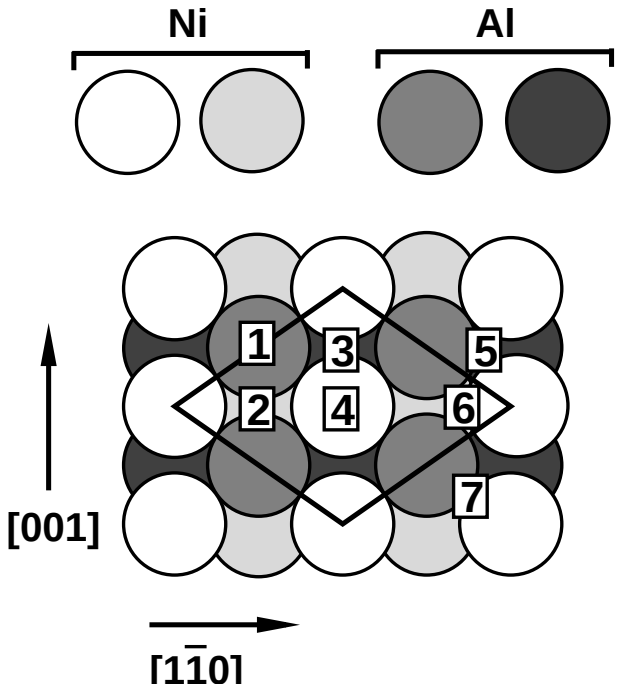

FIG. 1: Top view of the NiAl(110) surface with the $c(2 \times 2)$ surface unit cells indicated. The sites considered for methoxy adsorption are indicated by numbers and is referred to in the text and table I as (1) Al ontop, (2) Al bridge, (3) Ni bridge, (4) Ni ontop, (5) Ni_2Al hollow, (6) Al_2Ni hollow, and (7) AlNi bridge.

of 0.2 eV. The influence of different k-point sampling and plane-wave energy cutoff was explored in a series of test calculations, and we found that our choices (18 k-points and 350 eV) resulted in converged results with errors in the order of 0.01 eV.

The geometry of the isolated methoxy radical was optimized in a large fcc supercell with a lattice constant of 12 Å, and only the Γ-point of the Brillouin zone was sampled. Because of the open-shell nature of methoxy this calculation was spin-polarized. All other parameters were equivalent to those used in the slab calculation. We did additional spin-polarized calculations for the adsorbed methoxy, but found no influence of including spin on the adsorption geometry, nor the adsorption energy.

III. RESULTS AND DISCUSSION

A. The clean NiAl(110) surface

As a first step in our investigation we determined the atomic structure of bulk NiAl and the clean (110) surface. We will briefly comment on the results of these calculations.

NiAl crystallizes in a cubic B2 (CsCl) structure. The calculated bulk lattice constant $a_0 = 2.89$ Å, bulk modulus $B = 161$ GPa, and heat of formation [14] $H_f^0 = -0.67$ eV/atom are in excellent agreement with the reported experimental values $a_0 = 2.8870$ Å [15], $B = 166$ GPa [16], and $H_f^0 = -61.8$ kJ/mol (-0.64 eV/atom) [17], and other theoretical calculations [18].

The ideal NiAl(110) surface is composed of an equal number of Al and Ni atoms. No reconstruction occurs, however the surface is well known for its surface ripple, where the surface layer Al atoms are shifted outwards while the Ni atoms are contracted inwards creating a height difference perpendicular to the surface between the Al and Ni atoms of $\sim$0.22 Å [19]. The surface ripple was well reproduced in our calculation. We found an outward displacement of the Al atoms by 0.09 Å compared to the unrelaxed surface, while the Ni atoms contract inwards by 0.10 Å, creating a surface ripple of 0.20 Å. Other reported theoretical values for the magnitude of the rippling vary between 0.10-0.23 Å [20, 21].

B. Adsorption of methoxy

The adsorption site and the orientation of methoxy with respect to the surface are fundamental aspects of the molecular adsorption. In order to determine the energetically favoured adsorption site and molecular orientation of methoxy on NiAl(110), we performed geometry optimizations from a set of initial structures where methoxy was placed with its O atom in the high-symmetry sites of the surface (Fig. 1). Although initially placed in a high-symmetry site, no symmetry constraints were placed on the molecule during the optimization, thus the methoxy molecule was free to change its orientation and move away from the starting site in the search for the lowest energy structure. These initial configurations included structures where the CO-axis were parallel as well as tilted with respect to the surface normal.

Table I summarizes the main results of the present study. We have included adsorption energies calculated using both the PW91-functional, as well as the RPBE-functional (both

calculated self-consistently). The adsorption energies have been calculated from

$$E_{\mathrm{ads}} = -(E_{\mathrm{SM}} - E_{\mathrm{S}} - E_{\mathrm{M}}) \ , \tag{1}$$

where E_{SM} is the total energy of the NiAl(110) slab with adsorbed methoxy, E_{S} is the energy of a clean slab of NiAl(110), and E_{M} is the energy of an isolated methoxy species. With this definition, a positive adsorption energy indicates stability with respect to the free methoxy species. As can be seen from table I, the most stable adsorption site is found to be the Al bridge site.

Although, as expected [10], PW91 yields a somewhat higher adsorption energies than RPBE, they both predict the Al bridge site to be the energetically preferred adsorption site, and methoxy to bind least strongly to the Ni ontop site. However, the ranking of the Ni_2Al and Al ontop site is reversed, with RPBE placing the Al ontop site second after the Al bridge site. The general observation is a preference for the O atom to have Al rather than Ni as its nearest neighbour, demonstrating that NiAl(110) acts chemically very locally [5]. A similar observation has been made in a study of oxygen adsorption on NiAl(110) [22]. They found, however, the Al_2Ni hollow site to be the preferred adsorption site for O, followed by the Al bridge site. The Al_2Ni hollow site is not a stable site for methoxy adsorption, however. During structure optimization, methoxy initially placed in the Al_2Ni hollow site moves laterally into the Al bridge site.

Fig. 2 illustrates the optimum adsorption geometry found in the present study. Methoxy adsorbs with the O atom in the Al bridge site with the CO-axis essentially perpendicular to the surface plane. The main geometrical changes to methoxy is an elongation of the C–O bond by 0.07 Å, indicating a weakening of the intramolecular C-O bond. The nearest-neighbour O–Al distance of $d_{\mathrm{AlO}} = 1.94$ Å is larger than the value reported for methoxy on the Al(111) surface [23] (1.79 Å), and for O on the NiAl(110) surface [22] (1.81 Å).

The adsorption-induced changes to the surface with methoxy in the Al bridge site is mainly a horizontal, outward relaxation of the surface layer Al atoms, while the outermost Ni atoms are pushed further into the surface, increasing the surface ripple to 0.33 Å. Thus, methoxy adsorption has the opposite effect of hydrogen adsorption, which has been predicted theoretically [21] and shown experimentally [24] to remove the rippling on clean NiAl(110). The in-plane changes to the geometry we found to be negligible.

Having determined the adsorption site and geometry, we turned our attention to the

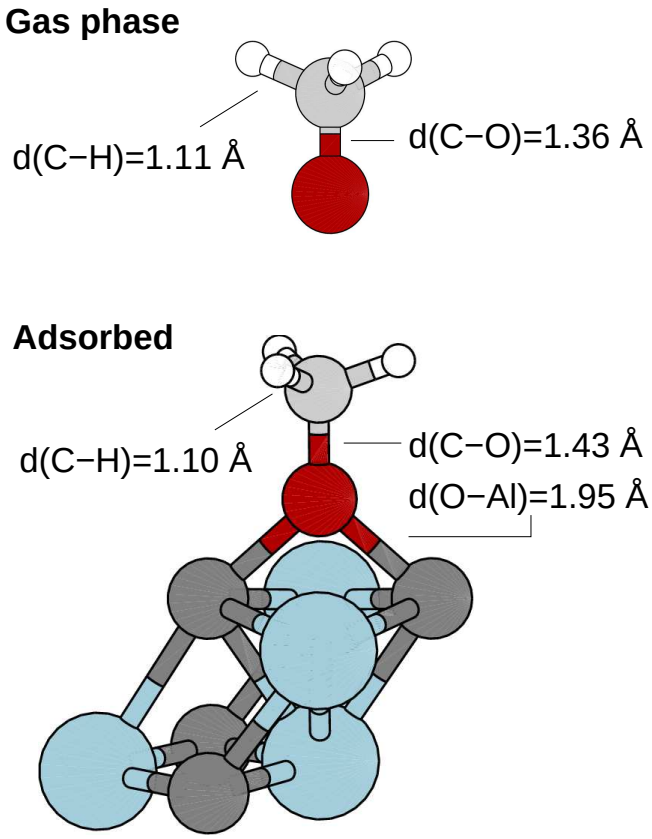

FIG. 2: Schematic illustration of optimized geometries for isolated methoxy and methoxy adsorbed at the NiAl(110) surface.

TABLE I: Adsorption energies for metoxy adsorption on NiAl(110) calculated using the PW91 ($E_{\rm ads}^{\rm PW91}$) and RPBE ($E_{\rm ads}^{\rm RPBE}$) exchange-correlation functional, and selected structural parameters. d are nearest-neighbour distances, z center-of mass interlayer spacings, and $\theta_{\rm CO}$ the tilt angle of the CO-axis away from the surface normal.

Site	$E_{\rm ads}^{\rm PW91}$ [eV]	$E_{\rm ads}^{\rm RPBE}$ [eV]	$d_{\rm AlO}$ [Å]	$d_{\rm NiO}$ [Å]	$z_{\rm AlO}$ [Å]	$z_{\rm NiO}$ [Å]	$d_{\rm CO}$ [Å]	$\theta_{\rm CO}$ [°]
Al bridge	2.73	2.31	1.94	2.68	1.31	1.64	1.43	0.8
Ni_2Al	2.49	2.09	1.80	2.25	1.34	1.48	1.42	1.4
Al ontop	2.42	2.15	1.70	-	1.89	2.27	1.39	0.1
Ni ontop	1.05	0.73	-	1.87	1.92	1.99	1.38	0.1
AlNi bridge	→ Al bridge							
Ni bridge	→ $AlNi_2$ hollow							
Al_2Ni hollow	→ Al bridge							

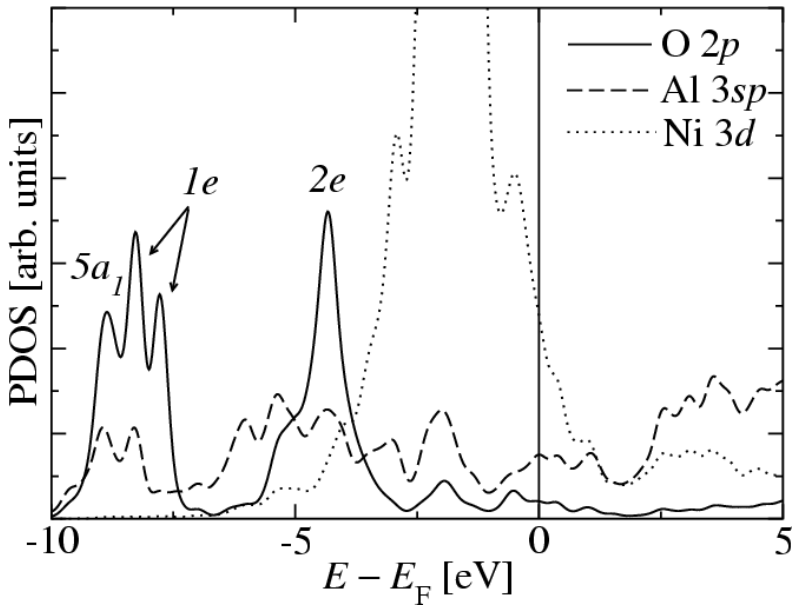

FIG. 3: Projected density of states (PDOS) of the oxygen atom of methoxy when adsorbed in the Al bridge site at the NiAl(110) surface. The dotted vertical line indicate the Fermi level.

nature of bonding to the surface. The isolated methoxy radical belongs to the C_{3v} point group, and the outer valence electron configuration can be expressed as [25]

$$(1\mathrm{e})^4(5\mathrm{a}_1)^2(2\mathrm{e})^3\ , \tag{2}$$

The 2e orbital is a partly filled, anti-bonding C $2\mathrm{p}_x$,p_y, O $2\mathrm{p}_x$,p_y orbital of π-symmetry. The $5\mathrm{a}_1$ is a σ-bonding orbital, and 1e a doubly degenerate (C $2\mathrm{p}_x$,p_y, O $2\mathrm{p}_x$,p_y) π-orbital.

Fig. 3 shows the projected density of states (PDOS) for methoxy adsorbed in the Al bridge site. Upon adsorption, the $2e$ orbital is filled and shifts down in energy below the Fermi level. The order of the $5\mathrm{a}_1$ and the 1e orbitals are reversed compared to gas-phase, indicating a strong interaction of the $5\mathrm{a}_1$ orbital with the substrate states. Furthermore, the 1e orbitals are no longer degenerate. A closer inspection of the PDOS reveals that the 1e peak of lowest energy (furthest form the Fermi level) correspond to an O 2p orbital interacting with the Al 3sp substrate states.

To gain further insight into the bonding, we calculated the electron density difference. The electron density difference was obtained by subtracting from the total electron density of the adsorbate system, the sum of the electron densities of the isolated adsorbate and substrate, where the geometry of the isolated methoxy and NiAl(110) were those of the adsorbate system.

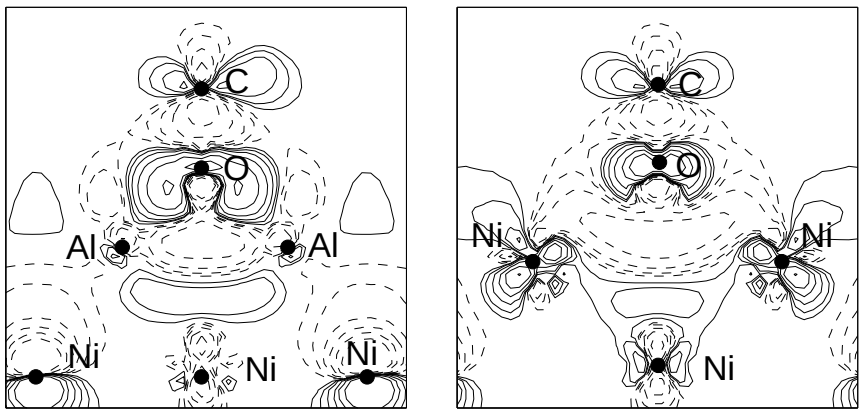

FIG. 4: Contour plots of the electron density difference for methoxy adsorbed on NiAl(110). Panel (a) and (b) displays cuts with horizontal axes along the [001] and $[1\bar{1}0]$ directions respectively and vertical axes along the surface normal. Solid (dashed) lines indicate gain (loss) of electron density. The contours are drawn at densities $\pm 0.005 \times 2^k \ e/\text{Å}^3$ for $k = 0, 1 \ldots, 6$.

Fig. 4 shows contour plots of the electron density difference for cuts perpendicular to the surface and with horizontal axes along the [001] and $[1\bar{1}0]$ directions. There is a gain in electron density into the 2e orbital, in accordance with the PDOS-analysis. Furthermore, there is a loss in electron density from the σ-bonding $5a_1$-orbital, consistent with the elongation of the CO-bond noted above. To quantify the charge transfer between the substrate and the adsorbate we used the space-partitioning scheme of Bader [26]. Based on this analysis, we estimate that a net charge of 0.90 $|e|$ is transfered from the substrate to the adsorbate, thus making the adsorbate more negatively charged. This relatively large charge transfer indicates that the bonding has a significant ionic component. There is also some hybridization of the methoxy orbitals with the Al 3sp states (Fig. 3), and a build-up of electron density between the methoxy O atom and substrate Al atoms (panel (a) of Fig. 4), suggesting some covalent contribution to the bonding. A similar bonding mechanism has been found for methoxy on other metal surfaces [1, 3].

IV. CONCLUSIONS

The adsorption of methoxy on NiAl(110) have been studied using density functional theory within the generalized gradient approximation, and using a slab geometry. We find a

clear preference for the methoxy O atom to have Al as its nearest neighbour rather than Ni. The energetically preferred adsorption site is the Al bridge site, with an O–Al distance of 1.95 Å, and with the methoxy CO-axis perpendicular to the surface. The adsorbate-substrate chemical bond is largely ionic with a covalent contribution.

Acknowledgments

This work was partly carried out within *Light Metal Surface Science*, a joint project between SINTEF and NTNU, financed by the Norwegian Research Council (NFR), Hydro Aluminium, Profillakkering AS, Norsk Industrilakkering AS, Fundamus AS, and Jotun Powder Coating. NFR and NTNU are acknowledged for support through computing time at the Norwegian High Performance Computing Center (NOTUR). Valuable discussions with Ingeborg-Helene Svenum and Anne Borg are gratefully acknowledged.

---

[1] G.-C. Wang, Y.-H. Zhou, and J. Nakamura, J. Chem Phys. **122** (2005) 044707.

[2] W. S. Sim, P. Gardner, and D. A. King, J. Phys. Chem. **99** (1995) 16002.

[3] J. R. B. Gomes and J. A. N. F. Gomes, J. Mol. Structure (Theochem) **503** (2000) 189.

[4] A. T. Hanbicki, P. J. Rous, and E. W. Plummer, Phys. Rev. B **67** (2003) 205405.

[5] B. Hammer and M. Scheffler, Phys. Rev. Lett. **74** (1995) 3487.

[6] I. H. Svenum, Ø. Borck, H. Dalaker, K. Mo, and A. Borg. In preparation.

[7] The DACAPO code can be downloaded at http://www.fysik.dtu.dk/campos.

[8] D. Vanderbilt, Phys. Rev. B **41** (1990) 7892.

[9] J. P. Perdew, J. A. Chevary, S. H. Vosko, K. A. Jackson, M. R. Pederson, D. J. Singh, and C. Fiolhais, Phys. Rev. B **46** (1992) 6671.

[10] B. Hammer, L. B. Hansen, and J. K. Nørskov, Phys. Rev. B **59** (1999) 7413.

[11] J. Neugebauer and M. Scheffler, Phys. Rev. B **46** (1992) 16067.

[12] L. Bengtsson, Phys. Rev. B **59** 12301 (1999) 12301.

[13] H. J. Monkhorst and J. D. Pack, Phys. Rev. B **13** (1976) 5188.

[14] The heat of formation was calulated using $\Delta H_f^0 = (E_{\mathrm{NiAl}} - E_{\mathrm{Ni}} - E_{\mathrm{Al}})$, where E_{X}, X=(NiAl,Ni,Al) is the total energy of bulk NiAl, Ni, and Al respectively.

[15] A. Taylor and N. J. Doyle, J. Appl. Cryst. **5** (1972) 201.

[16] R. J. Wasilewski, Trans. Soc. Min. Eng. AIME **236** (1966) 455.

[17] P. Nash and O. Kleppa, J. Alloys and Compounds **321** (2001) 228.

[18] P. A. Korzhavyi, A. V. Ruban, A. Y. Lozovoi, Yu. Kh. Vekilov, I. A. Abrikosov, and B. Johansson, Phys. Rev. B **61** (2000) 6003.

[19] H. L. Davis and J. R. Noonan, Phys. Rev. Lett.**54**, (1985) 566.

[20] M. Konôpka, I. Štich, and K. Terakura, Phys. Rev. B **65** (2002) 125418

[21] A. T. Hanbicki, A. P. Baddorf, E. W. Plummer, B. Hammer, and M. Scheffler, Surf. Sci. **331-333** (1995) 811.

[22] A. Y. Lozovoi, A. Alavi, and M. W. Finnis, Phys. Rev. Lett. **85** (2000) 610.

[23] M. Kerkar, A. b. Hayden, D. P. Woodruff, M. Kadowala, and R. G. Jones, J. Phys.: Condens. Matter **4** (1992) 5043.

[24] A. T. Hanbicki, H. L. Davis, A. P. Baddorf, D. B. Poker, and E. W. Plummer, Surf. Sci. **365** (1996) L639.

[25] C. F. Jackels, J. Chem. Phys. **82** (1985) 311.

[26] R. F. W. Bader, *Atoms in Molecules - A Quantum Theory* (Oxford University Press, Oxford, 1990).